Journal of Materials Chemistry A

ROYAL SOCIETY OF CHEMISTRY

REVIEW

View Article Online
View Journal | View Issue

Cite this: J. Mater. Chem. A, 2023, 11, 12593

Hybrid polymer gels for energy applications

Arun K. Nandi *[a] and Dhruba P. Chatterjee [b]

Polymer gels, specifically conducting polymer gels, share the benefits of gels, like large specific surface area, excellent flexibility, three-dimensional accommodative framework, elasticity, tunable mechanical strength, and excellent electronic, optoelectronic, and electrochemical properties. Various carbon, metal, and other nanoparticles can be accommodated abruptly changing not only the physical and mechanical properties of the polymer gels but also improving their electronic and electrochemical properties enormously making them suitable for different energy applications. Here, we shall discuss different polymer/conducting polymer hybrid (dihybrid and trihybrid) gels for energy generation (solar cell, fuel cell) and energy storage applications such as supercapacitors and batteries. To make the conducting polymer gels, supramolecular cross-linkers (gelators) such as folic acid, dibenzoyl-L-cystine (DBC), and phytic acid have been used and hybrid hydrogels are constructed by blending conducting polymers such as polyaniline, polythiophene, polypyrrole, and PEDOT:PSS, with graphene oxide (GO), Ag NPs, and molybdenum sulphide quantum dots (MoS_2 QDs). Nanoparticles are tightly bound with fibrils of the network due to large surface forces resulting in a synergic improvement in all the electronic and electrochemical properties. The energy devices such as dye-sensitized solar cells, fuel cells, supercapacitors, batteries, mostly use hybrid xerogels. Apart from conducting polymers, we will highlight the use of other synthetic and natural polymer gels used for energy applications. This review thus embodies the synthetic strategy of producing conducting polymer hybrid gels, presents their properties, illustrates their applications in energy generation and storage, and discusses future opportunities and challenges.

Received 7th December 2022
Accepted 21st February 2023

DOI: 10.1039/d2ta09525d

rsc.li/materials-a

10th anniversary statement

The Journal of Materials Chemistry A is the most important journal publishing top-class articles in the field of energy and sustainability. Green energy is the most important requirement in the place of fossil fuels, which are gradually decreasing, to prevent the carbonaceous gas emission from fossil fuel burning causing damage to the earth's atmosphere. Hence, the challenge of this journal is to record growth in the field of green energy generation and its storage for the fruitful use of energy in need. Hence, the journal is premier in publications in the areas of photovoltaic cells, fuel cells, and energy storage in batteries and supercapacitors dealing with various materials including soft matter. During my association as an editorial board member, I have witnessed tremendous growth in these important fields and have also contributed few important papers. The term sustainability meaning to keep ecological balance is the most important issue in the world for the survival of living beings and the journal has recorded some important studies in this field, where I have also contributed a study on oil spill recovery using supramolecular gels. Thus, this journal is very important to the progress of civilization both from green energy and sustainability points of view and would continue to contribute further.

1 Introduction

In the present century, coping with the overwhelming global energy crisis is the most important challenge for the development of modern civilization, which is stringently dependent on energy resources.[1] However, the huge consumption of non-renewable fossil fuels has not only affected the world with severe energy deficiency but also the corresponding carbon (greenhouse gas) emissions have deteriorated the environment.[2] Hence the need for sustainable and clean energy resources *e.g.* solar, tidal, and wind energy are the alternatives to decrease the burning of fossil fuels. These renewable energies are, however, dependent on external environments such as climate, weather, and geographical position, featuring their collection and storage as intermediate steps for efficient utilization of these eco-friendly energies. An important property of energy is that it can neither be created nor destroyed, but it is inter-convertible. For example, in solar cells, light energy is converted into electrical energy, and in fuel cells chemical energy is converted into electrical energy. To use the energy fruitfully in need it should be stored and it can be stored as chemical energy *via* redox reactions.[3] Such redox reactions can be extended to new reactant materials with convenient electron

[a]*Polymer Science Unit, School of Materials Science, Indian Association for the Cultivation of Science, Jadavpur, Kolkata-700032, India. E-mail: psuakn@iacs.res.in*
[b]*Department of Chemistry, Presidency University, 86/1 College Street, Kolkata-700073, India*

transfer so that the renewable energy can be transformed into electrical energy efficiently and statically stored. Thus, electrochemical energy storage and conversion technologies capable of inter-conversion of chemical and electrical energy with high efficiency have recently drawn significant research interest to alleviate global warming, declining fossil-fuel reserves, and also to cope with the increasing demand for power over the past decade. In this review, we delineate the use of different polymer gels for energy generation and storage.

Presently, research communities show remarkable research interest in the growth of flexible and portable electronics in the fields of flexible displays, electronic papers, micro-robotics, and implantable medical devices.[4,5] Though there is large progress on flexible and wearable electronic devices, there is limited growth for flexible energy generation and storage devices. Soft electronics have the bonafide potential for flexible and stretchable electronic devices and for the development of soft electronics it is essential to tune innovative soft materials.[6] Polymer gels, especially conducting polymer gels, have the benefits of gels, such as excellent flexibility, elasticity, large specific surface area, three-dimensional accommodative framework, tunable mechanical strength, optoelectronic and electrochemical properties. So, polymer gels are ideal materials for developing soft electronics and for these purposes, particularly conducting polymer gels are most important because they possess the properties of semiconductors along with the viscoelastic properties of gels. So, to develop civilization, green energy is the most important requirement, and for making soft energy devices, hybrid polymer gels are important materials. Hence, the importance of the present review is to delineate the use of hybrid polymer gels as energy materials suitable for energy generation (conversion) as well as its efficient storage, mostly for flexible and soft devices. Recently, an enormous amount of literature growth is seen in this field and to keep it concise, the recent and important literature references are cited with a fruitful discussion.

1.1 Gels and their physical characteristics

Gels are easy to recognize than to define as they are visibly characterized by the "inversion test" (turning upside down a gel pot whether it can bear its own weight). The most accepted definition of gels is given by P. J. Flory "a gel has a continuous structure that is permanent on the analytical time scale and is solid-like in its rheological behavior".[7] The most important characteristics of gels are: (i) fibrillar network structure, (ii) invariant storage modulus with frequency and higher than loss modulus, and (iii) reversibly compressible.[8] The 'solid-like' rheological behavior arises from the 3-dimensional fibrous network encapsulating the liquid from where the gel is produced thereby preventing its flow, causing its semisolid nature. The gels behave intermediately between liquid and solid, and are produced from physical or chemical interactions between the building blocks and sometimes chemical or physical cross-linking agents are also used between the building blocks. Gels produced by chemical forces (covalent bonds) are called chemical (irreversible) gels and gels produced by physical forces (non-covalent interactions) such as coulombic, hydrogen bonding, π-stacking, hydrophobic interactions between the building blocks are called physical (thermo-reversible) gels. The fibrils in a three-dimensional network mostly have nano-dimension and only 1–2 wt% of the solid encompasses the entire space, though the surface forces of the nano-fiber

Prof. Arun K. Nandi obtained his PhD degree on "Thermodynamics of Polymer–Polymer and Polymer–Solvent Mixing" by working at Indian Association for the Cultivation of Science (IACS) and joined the Chemistry Department, North Bengal University, Darjeeling. He did post-doctoral work at the Florida State University with Prof. L. Mandelkern in the crystallization of polymers. In 1992, he joined the Polymer Science Unit of IACS and he retired from the senior Professor position in February, 2019. Presently, he is Emeritus Scientist (CSIR) at IACS. His research interests focus on polymer blends, polymer crystallization, polymer and supramolecular gels, polymer nanocomposites, polymer synthesis, biomolecular hybrids, supercapacitors, polymer photovoltaics and fuel cells. He is the author of 247 papers, 5 book chapters and a text book "Polymer Functionalized Graphene" (RSC, 2021; Doi ***https://doi.org/10.1039/9781788019675****) and has supervised 37 PhD students to date.*

Dr Dhruba P. Chatterjee is presently working as an Assistant Professor in the Department of Chemistry Presidency University, Kolkata, West Bengal, India. He received his PhD from Jadavpur University in 2006 working at the Indian Association for the Cultivation of Science, Jadavpur, Kolkata in the field of controlled polymer synthesis and characterization. His present research interest includes the design and controlled synthesis of vinyl polymers and conducting polymers for the preparation of hybrid materials with inorganic/organic quantum dots for energy-related applications, bio-applications and membrane applications. He has authored 43 publications and supervised a couple of PhD students to date.

encapsulate a large volume of solvent. This imparts elasticity, tunable mechanical strength, and excellent electronic, optoelectronic, and electrochemical properties depending on the building blocks and the concentration producing the gel fiber. In the polymer gels, the building block may be a natural polymer such as gelatin, chitosan, and agarose or synthetic non-conducting polymers such as poly(ethylene glycol), poly(acrylic acid), and poly(vinyl alcohol) or synthetic conducting polymers such as polyaniline, polypyrol, and polythiophene. These building blocks influence the gel properties and for energy applications conducting polymer gels are mostly used because the conjugated chains are very much sensitive to any external stress such as light, voltage, and pH to fabricate the device. Apart from the conducting polymer gels, the ion-conducting gels are important for the fabrication of energy devices, and the mobility of ions accounts for the conductivity. Supramolecular gels showing conductivity are also very important in fabricating energy materials and they include carbon nanomaterial gel, metallo gel, and π-conducting gels. It is necessary to mention here that conducting polymers are difficult to dissolve and as such to prepare their gels sometimes supramolecular crosslinkers are used, *e.g.*, to prepare polyaniline gels phytic acid, folic acid, *etc.* are used. These gelators not only act as cross-linkers but also act as dopants for the conducting polymer producing 3D network structures, yielding large surface area, high electrical conductivity, and hierarchical porosity for rapid mass/charge transport. Through the hierarchical pores of the gels, there is interconnectivity between the pores[9,10] through which ion transport can occur easily under electrical bias. In the electrochemical process during the flow of ions, there may arise interactions of ions with the neighboring chains and it becomes shared through the inter-connected fibrillar network structure. In the electrochemical process due to the flow of mass(ions) volume changes can occur, but the interconnectivity between the hierarchical pores of the gels can cause a decrease in the damage to transport paths through the pores due to the elastic nature of the gel.

1.2 Hybrid gels

It is apparent from the above discussion that conducting property of the gel fiber is very much necessary to prepare the energy materials but it is not the only criterion for it. For solar cell applications, some photosensitizers should be used, for fuel cells, some catalysts for hydrogen reduction should be present, for battery applications some conducting ions are required and for supercapacitors some redox system is necessary. Hence, the concept of hybrid gels can be used to prepare efficient energy materials and in the three-dimensional network, it is easier to accommodate various carbon, metal, and other nanoparticles, which can abruptly change not only the physical and mechanical properties of the gels but can also improve their optoelectronic and electrochemical properties making them suitable for different energy applications. These hybrid gels retain the properties of the components and facilitate synergic effects from the large surface forces between the gel fibers and the nanoparticles increasing enormously the mechanical and electrical properties of gels. The physical and chemical properties of the dopant cross-linked hybrid gels may be modulated by changing the cross-linker structure and its amount. Apart from the above hybrid gels, interpenetrating double network gels provide multifunctional properties as they enjoy the benefits from each component and also tender new exciting features from the synergic effects present among the two polymeric networks.[11]

For preparing the soft devices, the molecular tailoring of gel networks is very much necessary to interact with environments in an intelligent fashion. Various intelligent gels, which are sensitive to external stimuli, such as light, pH, temperature, and mechanical stress demonstrated applications not only in energy conversion and storage but also in biotechnology. In energy devices, the transport of both ions and electrons is crucial and the 3D fibrillar network facilitates the transport of electrons along the fibers while the diffusion of ions is facilitated through the hierarchical pores of the network.[12] Physical or chemical interactions are required at surfaces and interfaces for energy conversion and storage so the surface area of gel material plays a very important role in these processes.[13] In soft high-performance energy devices, hybrid gel materials play important roles where the gel network supports other active materials as well as the introduction of a second gel network. Finally, the mechanical, chemical and electrochemical properties of hybrid gels can be tuned by introducing different functional materials/cross-linkers, thereby expanding their applications and improving their performance.[12]

Due to the increasing demand for soft energy devices with long stability, the applications of hybrid gels in energy conversion (loosely termed as energy generation in this review *e.g.*, in solar cells and fuel cells) and energy storage (battery and supercapacitors) are shown in Scheme 1. However, it should be mentioned that in all the generation and storage devices, the interconversion of energy from one form to the other occurs. The main difference between the generation and storage devices is that in the former type, the outcome electrical energy (from light/chemical energy) should be used immediately whereas in the storage systems (*e.g.* battery and supercapacitors) during charging, the energy is stored as chemical energy while during discharging electrical energy is produced from chemical energy for the external work. In the following sections, a brief overview of different hybrid gels in making energy generation and storage devices using conducting polymers, graphene oxide (GO), Ag NPs, molybdenum sulphide quantum dots (MoS_2 QDs), *etc.* with supramolecular cross-linkers such as dibenzoyl-L-cystine (DBC), folic acid, and phytic acid are presented.

2 Energy generation

In this section, we will delineate the use of gel materials for the fabrication of solar cells and fuel cells using polymers, especially conducting polymers.

2.1 Solar cell

A solar cell is a device that converts sunlight into electric energy using the photovoltaic cell, which is generally made of silicon

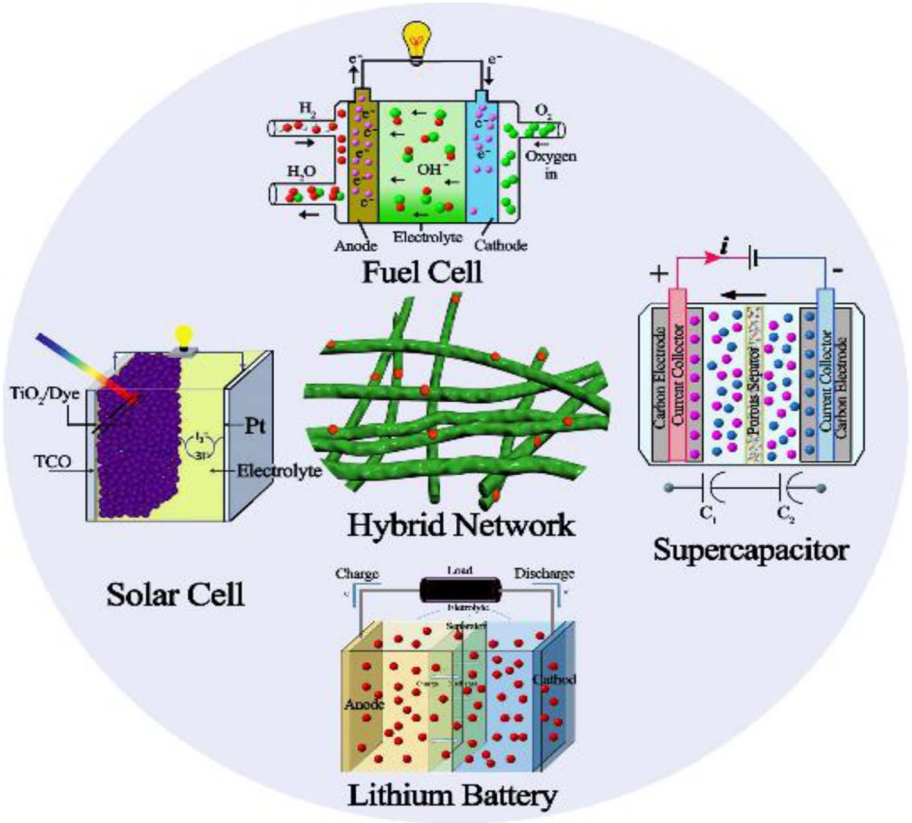

Scheme 1 Illustration of hybrid gel network in solar cell, fuel cell, battery and supercapacitor.

(Si), cadmium telluride (CdTe), bulk heterojunction (BHJ), perovskite and dye-sensitized solar cells (DSSC). The polymer gels are most relevant for application in DSSCs as the membranes made from polymer gels have pores giving transparency to sunlight, also facilitating charge conduction in DSSCs. Although there are some reviews on polymer gels used in DSSCs,[12,14,15] they should be updated as lot of works in this field are recently reported purporting the purpose of the present review that highlight mostly recent works.

A schematic presentation of a DSSC is shown in Fig. 1a and b[16] which basically mimics photosynthesis by plants from the Sun. The device has four vital components: (i) a transparent photo-electrode with an active layer of mesoporous TiO_2, (ii) a counter electrode of high-catalytic-activity promoting redox reactions, (iii) a photosensitizer dye adsorbed onto the photo-electrode, (iv) a redox electrolyte couple [iodide (I^-)/triiodide (I_3^-)] dispersed in a liquid. The principle includes photo-excitation of electrons of dye from HOMO to LUMO pursuing its injection to the conduction band of TiO_2 photoanode, keeping the dye in an oxidized state, which returns to its pristine form by the exchange of electrons from the electrolyte. The I_3^- ions produced from the oxidation of I^- diffuse through the counter electrode satisfying the regenerative cycle and the electrical circuit becomes complete by the flow of electrons to the external circuit.[17,18]

2.1.1 Hybrid polymer gel replacing TiO_2 active-layer in the photoelectrode. Due to the porous nature of the xerogel, an idea was proposed that the xerogels of the conducting polymers are likely to be transparent to sunlight and could replace the active layer of TiO_2 NPs, provided the gels are mechanically strong. Based on this idea we prepared a hybrid hydrogel taking polyaniline (PANI) as a donor and 5,5′-(1,3,5,7-tetraoxopyrrolo[3,4-*f*] isoindole-2,6-diyl)diisophthalic acid (P) as an acceptor cum gelator.[17] P was intimately mixed with PANI in the gel state and a dye-sensitized solar cell (DSSC) was constructed by coating the hydrogel as the active layer on the indium-tin-oxide (ITO) anode yielding a power conversion efficiency (PCE) of only 0.1%.[19] In order to improve the PCE, Das *et al.*[20] produced xerogels of hybrid hydrogels comprising a conducting polymer, GO, and a gelator P, to replace the active layer of TiO_2 NPs. Using poly(3,4-ethylenedioxythiophene) poly(styrene sulfonate) (PEDOT:PSS), instead of PANI, the dihybrid xerogel of PEDOT:PSS/P showed a higher PCE value of 0.27%. With graphene oxide (GO) as a gelator cum acceptor, the DSSC of GO-PEDOT:PSS dihybrid gel exhibited PCE of 3.25%. They extended it to a trihybrid conducting hydrogel consisting of GO, P, and PEDOT:PSS (GPPS) to fabricate a DSSC and observed a maximum PCE of 4.5%. The *J–V* characteristic curves of GPPS hybrids (Fig. 2a) showed the highest short circuit current ($J_{SC,}$ 10.2 mA cm^{-2}), open circuit voltage ($V_{OC,}$ 0.73 V), fill-factor (0.59) and the highest PCE of 4.5%.

The incident photon to current conversion efficiency (IPCE) curve of the system showed a wide absorption range (360–700 nm) with a maximum absorbance value of ~57%.[20] Here, P and

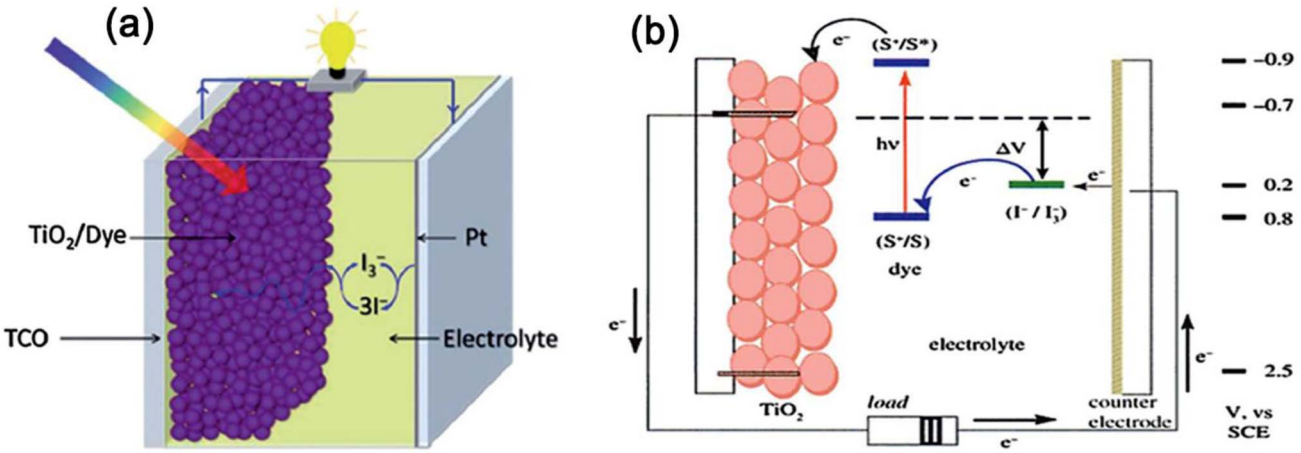

Fig. 1 (a) A schematic diagram of a DSSC device, (b) working principle of a DSSC showing the sequence of electron transfer. Reproduced from ref. 16 with permission from the Royal Society of Chemistry.

GO acted as the joint acceptor but adding the PCE of both individual acceptors with PEDOT:PSS total PCE of the trihybrid system became 3.52%. Thus, in the trihybrid gel (GPPS3), the PCE was 1.0% higher and probably PEDOT:PSS in the co-assembled xerogel showed better organic mixed electronic and ionic conductivity (OMEIC), properties facilitating easier transport of charges resulting in improved PCE. Impedance spectroscopy of the DSSC yielded the Nyquist plot containing three semicircles and the equivalent resistance–capacitance (*R*–*C*) circuit yielded the highest lifetime values (3.2 ms) of the photo-injected electrons attributed to the highest PCE value of the GPPS3 hybrid. The mechanism of photoconduction is presented in (Fig. 2b) taking the lowest unoccupied molecular orbital (LUMO) energy of GO (−3.5 eV), PEDOT:PSS (−2.4 eV), and P (−4.25 eV). The N-719 dye absorbs light promoting its electrons to the excited state, then enter into the LUMO of PEDOT:PSS and flows through the LUMO of GO, and finally flows into the LUMO of P causing charge flow through an external circuit (Fig. 2b).[21] The intimate mixing of P, GO, and PEDOT:PSS in the xerogel promotes the charge flow, yielding a high value of PCE.

2.1.2 Hybrid polymer gel electrolyte (HPGE) for the dispersion of redox electrolyte couple. In order to impart long-term stability of DSSCs, substantial efforts were made to substitute the liquid electrolyte (LE) with a solid-state electrolyte and polymer electrolytes, formed by dispersing alkali metal salts into the polymer matrix. However, the device performance was hampered in the polymer electrolytes for low ionic diffusion due to the high viscosity of the medium in the polymer matrix. So, quasi-solid-state (QSS) electrolyte, *e.g.*, the polymer gel electrolyte (PGE), formed by entrapping liquid electrolyte into polymer networks, is the best choice in DSSCs as it can afford the advantages of liquid and solid electrolytes, *e.g.* superior ionic diffusion enabling the infiltration of electrolyte into the active layer of the mesoporous TiO_2 film and also yields high stability.

2.1.2.1 Iodide (I^-)/triiodide (I_3^-) redox couple. The iodide/triiodide (I^-/I_3^-) redox couple in DSSC is the mostly used

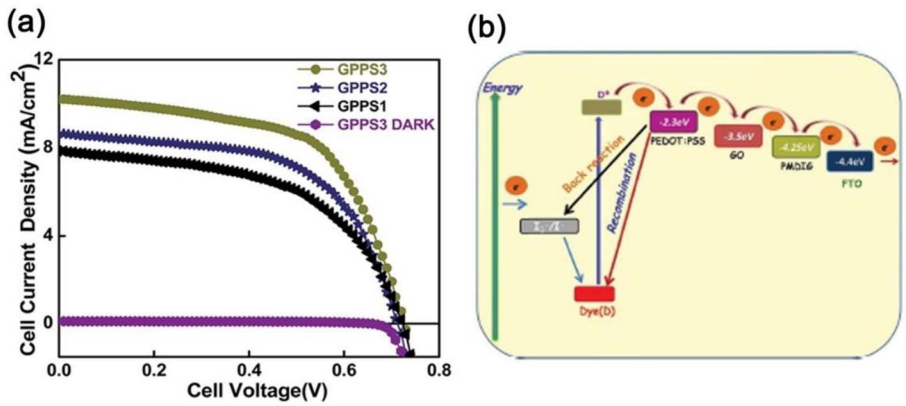

Fig. 2 (a) Plot of *J*–*V* characteristics of GPPS1, GPPS2 and GPPS3 under AM 1.5G light illumination of 100 mW cm^{-2}. (b) Energy level diagram of the components of GPPS gels explaining the photocurrent behavior of the FTO/GPPS gel/graphite DSSC with the N719 dye. Reproduced from ref. 20 with permission from the Royal Society of Chemistry.

redox couple from the beginning of DSSC development as it yields efficient PCE values of DSSCs. Overall, the I^-/I_3^- couple has good solubility, appropriate redox potential, does not absorb much light, and facilitates quick dye regeneration. For outdoor application of the DSSC, a major challenge is the lack of long-term stability for temperatures at ~80–85 °C, though a respectable 10.4% power conversion efficiency (PCE) at 1.5 AM solar irradiation was achieved for photovoltaic devices with a panchromatic dye and a liquid electrolyte (LE) having the I^-/I_3^- couple.[22,23] At high temperatures, the leakage of liquid electrolytes occurs from the device, causing the desorption of the loosely bound dyes resulting in its photo-degradation. The I^-/I_3^- couple also causes corrosion of the Pt counter electrode and all the above factors limit the long-term performance of DSSC at the outdoor high temperature. Hence, substantial efforts were made by scientists and technologists to comprehend devices with high performances and long-term stability for outdoor use. For this purpose, new counter-electrodes, other sensitizers, and redox couples were employed[23] and importantly, polymeric gel materials entrapping I^-/I_3^- redox couple were fruitfully used to replace LEs. The polymer gels mitigate the potential instability of the DSSC from solvent evaporation at high temperatures. The additional benefits are that the PGEs have good interfacial filling properties, high ionic conductivity, and long-term stability, for their ability to absorb and retain a large amount of the solvent.

Grätzel and his coworkers[23] used photo-chemically stable poly(vinylidenefluoride-*co*-hexafluoro propylene) (PVDF-HFP), to immobilize a 3-methoxypropionitrile (MPN)-based liquid electrolyte yielding a semisolid PGE entrapping the I^-/I_3^- redox couple inside the gel network. The DSSC fabricated with amphiphilic polypyridyl ruthenium dye showed 6.1% PCE under the exposure to light (one sun). The DSSC exhibited amazingly high stabilities for thermal stress at 80 °C and also for prolonged irradiation with light, thus, the durability criteria match well for outdoor applications. Conducting polymers are important candidates for developing gel electrolytes in DSSC for high conductivity, good stabilities, low cost, and good catalytic activity for I^-/I_3^- reaction. Liu *et al.*[24] used (PAA-*g*-PEG/PANI) (poly(acrylic acid)-*g*-poly(ethylene glycol)/polyaniline) hybrid gel as a semisolid electrolyte for DSSC. The hybrid conducting polymer gel has a porous network structure that can entrap a large quantity of liquid. PANI improved the conductivity of PGE, as an interpenetrated conductive network was formed when a second PANI chain was produced. The outstanding conductivity of PAA-*g*-PEG/PANI significantly improved the PCE of the DSSC to 6.38%. Apart from PANI, for fabrication of PGE polypyrrole (PPy) was also used by Li *et al.*[25] using poly(-hydroxyethyl methacrylate/glycerol) [poly-(HEMA/GR)] gel 3D network. The PPy-based gel electrolyte showed highly improved transport kinetics, ionic conductivity, and electro-catalytic activity for the I^-/I_3^- redox couple yielding a reasonable PCE of 6.63%. Apart from the conductive polymer hybrid gels, the dopant molecules cross-linked HPGE can also be used in DSSCs showing improved mechanical properties, good catalytic activity, high conductivity, and good porous structure facilitating ion transport.

The most common polymer electrolyte is poly(ethylene oxide) (PEO) and Wu *et al.*[26] applied PEO to solidify the liquid phase containing LiI, I_2, and 4-*tert*-butylpyridine (4-TBP) into the organic solvent mixture of propylene carbonate (PC) and ethylene carbonate (EC) with a 1 : 1 volume ratio. The mixture was stirred till solidification, and they made PEO gel electrolytes by dissolving various amounts of PEO into the mixed LE. They focused on the open circuit voltage (V_{oc}) of DSSC, which increases with the increase of PGE. The origin of the increased V_{oc} was analyzed from the interfacial charge-transfer processes from the dark-current characteristics measurement of DSSCs with different electrolytes. The reaction kinetics of the injected electrons with triiodide in the electrolyte is evident from the dark current, indicating suppression of electron recombination at the TiO_2/electrolyte interface. In addition, the stability of the DSSC using different amounts of PEO gel electrolyte was tested, and no degradation of cell performance was noticed for DSSC containing 30% gelator after 1100 h testing. DSSCs with different electrolytes do not exhibit any change in V_{oc} values with time. The results indicate that the polymer gel electrolyte can restrain the leakage of solvent, increasing the durability of the device. Thus, the hybrid polymer gel electrolyte (HPGE) plays a dual role in controlling the interfacial charge-transfer kinetics and improving the long-term stability of the DSSC.

The organic dye used in DSSC also plays an important role in the performance of DSSC and recently, Ji *et al.*[27] used a D–π–A structure-organic dye, *e.g.*, thieno[3,2-*b*] indole-based organic dyes with porphyrin sensitizer and a high PCE of 11.6% was achieved using I^-/I_3^- redox LEs, however, using ruthenium-based N719 dye and I^-/I_3^- LEs, the highest PCE 11.1% was reported by the Gratzel group.[28] Not only the dye but also the use of different redox couples also influences the cell performance, *e.g.*, using $[Co(bpy)_3]^{2+/3+}$ redox LEs with the same dye Ji *et al.* achieved a PCE = 14.2% under 1 sun.[27] The LEs in these highly efficient DSSCs comprise volatile organic solvents causing instability in long-term applications for outdoor conditions. To overcome this drawback, polymeric gels or quasi-solid-state (QSS) electrolytes carrying the I^-/I_3^- redox couple were used. However, poor penetration and low ionic conductivity of these materials into mesoporous TiO_2 photoanode, reduce the PCE values compared to those in the liquid-state DSSCs. A non-ionic polysaccharide biopolymer extracted from guar beans (guar gum, GG), was used to prepare a cost-effective PGE for the fabrication of DSSC by Gunasekaran *et al.*[29] A redox PGE was prepared by mixing guar gum, LiI/I_2, 1-methyl-3-propylimidazolium iodide, 4-*tert*-butyl pyridine and poly-ethylene glycol for 24 h. With this PGE they fabricated DSSC by inserting a Pt counter electrode and TiO_2 photoanode coated with metal-free organic MK-2 dye. The device exhibited a maximum PCE of 4.96% instead of 2.13% obtained with LE without guar gum.

Tang and coworkers[30] fabricated a PGE using 1-butyl-3-methylimidazolium chloride ([BMIM]Cl) ionic liquid, poly(-hydroxyethyl methacrylate/glycerol) [poly(HEMA/GR)] as a polymeric gel and 1-methyl-3-propylimidazolium iodide (MPII) as the iodine source. In an ionic liquid, poly(HEMA/GR) can swell to form a stable gel, and the imbibed ionic liquid is present in

the poly(HEMA/GR) framework. The cross-sectional SEM image of poly(HEMA/GR) (Fig. 3a), shows a three-dimensional microporous fibrillar network capable of entrapping a large amount of ionic liquid into the network. Thus, poly(HEMA/GR) acted as an anionic liquid electrolyte supporter producing robust PGE. A QSS-DSSC was fabricated from ionic liquid-imbibed poly(HEMA/GR) gel electrolyte by inserting a PGE slice between a Pt counter electrode and N719 dye-sensitized TiO_2 anode. The photocurrent behavior of the above PGE-based DSSC is much better than that of acetonitrile-based LE, as shown in Fig. 3b.

The PCE of QSS-DSSC made with poly(HEMA/GR) embedded ionic liquid was 7.15% compared to 6.10% from the acetonitrile electrolyte. The enhanced PCE in PGE was attributed to the increased ionic conductivity (14.29 mS cm^{-1}) and good retention of ionic liquid. As evidenced from the Impedance Spectral (IS) analysis, the interfacial resistance of the Pt counter electrode/electrolyte interface (R_{ct1}) of acetonitrile-based LE and ionic liquid embedded poly(HEMA/GR) PGE were 6.3 and 3.1 Ω cm^2, respectively, whereas, the interfacial charge-transfer resistance (R_{ct2}) of the TiO_2 anode/electrolyte interfaces were 14.3 and 10.6 Ω cm^2, respectively. The lower R_{ct1} and R_{ct2} values in ionic liquid-embedded poly(HEMA/GR) compared to acetonitrile-based liquid electrolyte embedded poly(HEMA/GR), causes an augmented charge-transfer between the anode/gel electrolyte and counter electrode/gel electrolyte interfaces. Better contact and greater ionic conductivity caused slower diffusion of the I^-/I_3^- redox species in the ionic liquid-embedded poly(HEMA/GR) gel electrolyte. Hence, ionic conduction is favored in the microporous 3D poly(HEMA/GR) PGE network increasing the PCE of the DSSC.

There are many reports for the I^-/I_3^- redox system[31–39] that the PCE of gel-state DSSCs can be improved by inserting TiO_2 nanofillers (NFs), where TiO_2 NFs could enhance the conductivity of PGEs due to lower charge-transfer resistance at Pt/electrolyte interface. The PGE produced from *in situ* gelation of poly(acrylonitrile-*co*-vinyl acetate) (PAN-VA), exhibited a PCE of 9.03% as high as that obtained from the LE due to good infiltration of the gel-electrolyte into TiO_2 film. Also, adding TiO_2 NFs into the PGE can increase the PCE up to 9.46% even

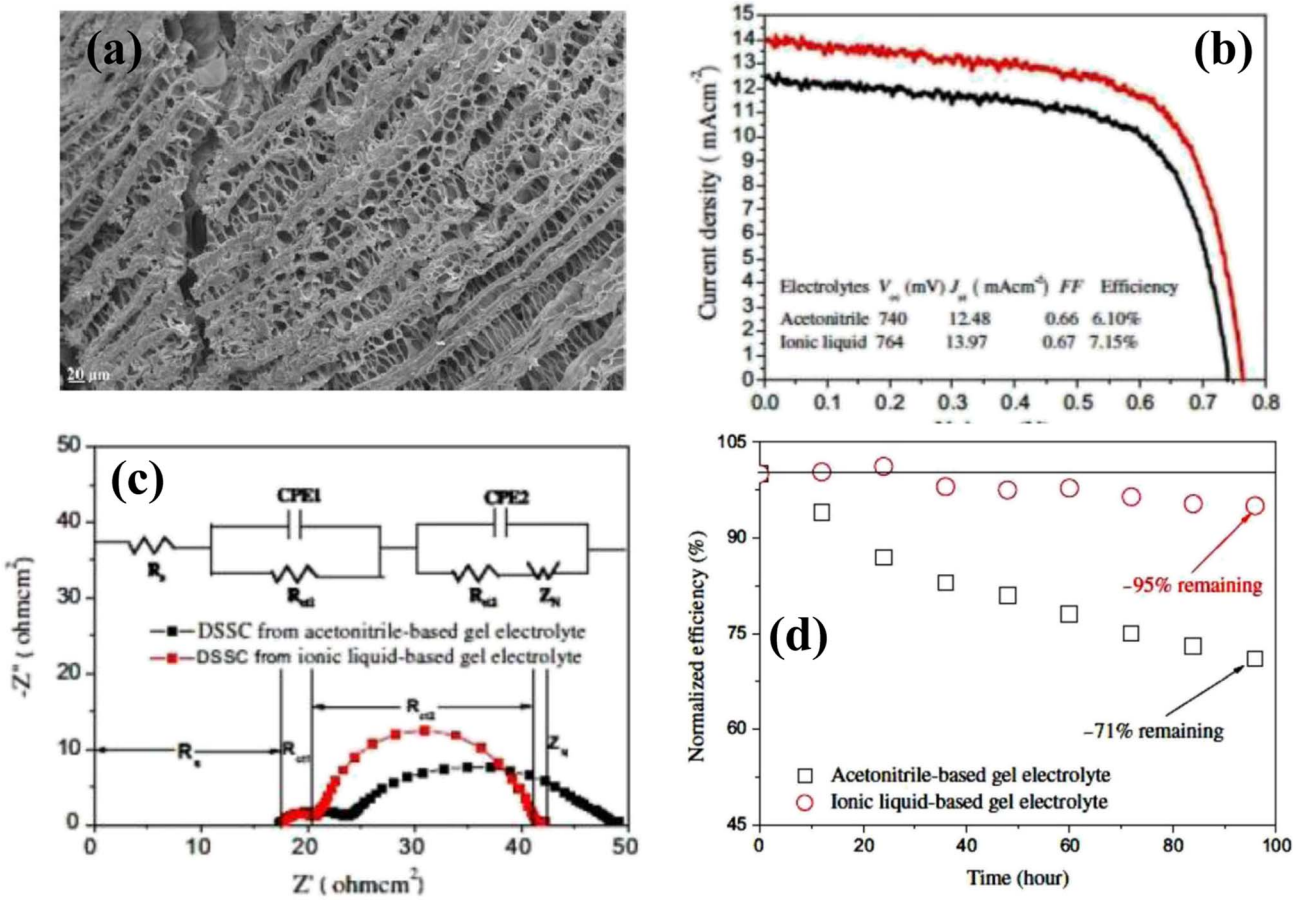

Fig. 3 (a) Cross-sectional SEM image of pure poly(HEMA/GR) matrix (b) photovoltaic performance of the DSSCs. The ionic liquid electrolyte contains: 0.5 M I_2, 0.01 M LiI, 40 vol% MPII, 50 vol% [BMIM]Cl, and 10 vol% *N*-methyl pyrrolidone, (c) Nyquist plots of DSSCs from acetonitrile-based liquid electrolyte-imbibed and ionic liquid-imbibed poly(HEMA/GR) gel electrolytes and equivalent circuit models for the I^-/I_3^-reaction: R_s, ohmic serial resistance of Pt counter electrode; R_{ct1}, charge-transfer resistance between Pt counter electrode and gel electrolyte; R_{ct2}, charge-transfer resistance between dye-sensitized TiO_2 anode and gel electrolyte; Z_N, diffusion impedance, (d) *N*ormalized power conversion efficiencies of DSSCs from acetonitrile-based liquid electrolyte-imbibed and ionic liquid-imbibed poly(HEMA/GR) gel electrolytes. (Reprinted from ref. 30 with permission from Elsevier).

higher than the value of LE. It also greatly improved the stability of a cell from the cell of acetonitrile (AN) electrolytes.[35] This high efficiency was noticed only for the I^-/I_3^- redox system in the AN system. Mohon *et al.*[37] produced poly(acrylonitrile)(PAcN)/LiI/activated carbon composite PGE to explore the working mechanism of DSSCs. The PGE consisted of PAcN as a gelator, propylene carbonate (PC), ethylene carbonate (EC) solvents, I_2, 1-*N*-butyl-3-hexyl imidazolium iodide ionic liquid, and 4-*tert*butylpyridine as the solvent. PGEs were synthesized at different concentrations of activated carbon and the TiO_2 photoelectrode films were prepared by the hand spray technique. For comparison purposes, PAcN/SiO_2 NP (~20 nm) based gel electrolytes using the same procedure without activated carbon were also produced. The PAcN/activated carbon PGE showed the best electrical conductivity of 8.67×10^{-3} S cm^{-1} and PAcN/SiO_2 HPGE exhibited a maximum conductivity of 1.32×10^{-3} S cm^{-1}. The composite gel electrolyte exhibited some catalytic behavior, which increased its photovoltaic performance. The PCE of the DSSC with this PGE showed the highest value of 8.42%, which was 1% lower than that of the DSSC made from the LE (9.5%). For the DSSCs based on PAcN/SiO_2 composite PGEs exhibit a maximum PCE of 7.51%, indicating that the high PCE was due to higher conductivity and catalytic activity.

In DSSCs, PGEs are a good substitute for LEs as they have better thermal stability and good ionic conductivity but, the PCE of PGE-DSSCs are lower than the corresponding LE-DSSCs. However, the evaporation of iodine, substantially decreases the long-term durability and stability of the devices. The major drawback of the I^-/I_3^- redox couple is that iodine corrodes the working electrode and in comparison with I^-/I_3^-, the cobalt(II)/(III) redox couples have advantages of insignificant visible absorption and non-corrosiveness. As such, in the following section, we will discuss DSSCs with iodine-free PGEs.

2.1.2.2 DSSCs based on iodine-free polymer gel electrolyte. In polymer gel electrolytes (PGEs) the structural properties and molecular weights of polymers play important roles in the gelator efficiency of quasi-solid state (QSS) DSSCs. To find an appropriate gelator, Kim and co-workers[40] synthesized an ABA triblock copolymer, poly(acrylonitrile-*co*-*N*,*N*-dimethylacrylamide)-block-poly(ethyleneglycol)-block-poly(acrylonitrile-*co*-*N*,*N*-dimethyl acryl amide) (SGT) with various molecular weights and copolymer compositions. The solubility and thermal stability depended on the ratio of *N*,*N*-dimethyl acrylamide (DMAA)/acrylonitrile (AcN) in the triblock copolymers. Both the AcN/DMAA ratios and the molecular weights facilitated the gel formation by regulating the polymer amount, hence, influencing diffusion and ionic conductivity. PGEs polymers having molecular weights >100 kg $mole^{-1}$ were effective for QSS-DSSCs as evident by electrochemical properties. The overall PCE in PGE-based QSS-DSSCs with $[Co(bpy)_3]^{2+/3+}$ redox system was reduced to 9.72% from 14.2% in LE under 1 sun (AM 1.5G) illumination. The SGTPGE-based QSS-DSSC when tested with indoor white LED light of 1000 lx gave the best PCE of 21.26%, which was higher than the 19.94% PCE of the LE DSSC. The long-term stability of the device at 50 °C and 1 sun illumination indicate much-improved stability of the PGE-based QSS-DSSCs (retaining 70% for 800 h) over LE-DSSCs. In terms of device stability and PCE, these PGE QSS-DSSCs exhibited good potential over LE-DSSCs for both outdoor and indoor applications. In another work, Rong *et al.*[41] reported an efficient monolithic QSS-DSSC assembled with a mesoscopic carbon counter electrode and an iodine-free polymer gel electrolyte (IFPGE). In IFPGE, the ionic liquid (1,2-dimethyl-3-propylimidazolium iodide, DMPII) acts as a source of redox couple and a charge transfer intermediate where a composite of PVDF-HFP/poly(ethylene oxide) (PEO/PVDF-HFP) act as host and acetonitrile as the solvent. It is important to note that the ionic liquid act as the source of redox couple and a PCE of 4.94% was obtained with the IFGE. To improve the performance, they also incorporated lithium iodide (LiI) and *N*-methyl benzimidazole (NMBI) into the IFGE, resulting in significant improvement in J_{sc} and V_{oc}, and achieved an optimal PCE of 6.97%. A good synergistic effect was noticed when LiI and NMBI were used together in the electrolyte causing an increase in J_{sc} for the addition of LiI facilitating higher electron injection efficiency of the excited dye. The addition of NMBI causes improvement of V_{oc} and fill factor due to the longer electron lifetime in the TiO_2 film at the open-circuit conditions. The monolithic structure and IFPGE recommend the practical applications of DSSCs.

Chen *et al.*[35] fabricated DSSCs with an efficient PGE of poly(acrylonitrile-*co*-vinyl acetate) (PAcN-VA) gelator using 3-methoxypropionitrile (MPN) liquid electrolyte. The dissolution of the copolymer in MPN was enhanced by VA segments, also AcN segments enhanced the mechanical strength of a gel. The conductivity of the gel electrolyte was similar with the liquid electrolyte, due to the increase of dissociation of 1-propyl-2,3-dimethylimidazolium iodide (DMPII) and LiI by the AcN segment of the copolymer. The PCE of DSSC using this gel-electrolyte was 8.23%, which was nearly equal to that of the liquid-state cell (8.36%). For cobalt(II/III) redox couple, an *in situ* gelation of PVDF-HFP in AN solvent showed a PCE of 8.7%,[42] but the PCE with cobalt PGE was 3% lower from the respective liquid cell. In a seminal paper, Venkatesan *et al.*[43] reported a DSSC with PGEs of the cobalt redox system using N719 dye. PVDF-HFP was utilized as a gelator of acetonitrile (AN) solvent containing the tris(2,2′-bipyridine) cobalt(II/III) redox couple. Here, TiO_2 and titanium carbide (TiC) NPs were used as nano-fillers (NFs), and the effects of the two NFs on the PCE of the gel-state DSSCs were compared. The conductivity of PGE increased in the presence of TiC NFs, which lowered the charge transfer resistance at the interface of the Pt counter-electrode. So, utilizing TiC NFs in the gel state, DSSC could achieve a PCE of 6.29%, which was close to its liquid counterpart (6.30%), and a stability test at 50 °C showed that the PCE could retain up to 94% after 1000 h duration. However, introducing TiO_2 NFs in the PGE caused a lowering of cell performances due to the increase in the charge-transfer resistance at the Pt cobalt electrolyte/PGE interface. These results are quite dissimilar from the iodide redox system and are attributed to an interaction between cobalt redox ions and TiO_2.

Recently, Lim *et al.*[44] fabricated DSSCs with poly(ethylene glycol) based PGEs incorporating surface carbon shell-

functionalized ZrO_2 nanoparticles (ZrO_2–C). ZrO_2 is polymerized with poly(ethylene glycol) methyl ether methacrylate (POEM) by ATRP technique and the ZrO_2-*g*-POEM was used as a template to obtain ZrO_2–C *via* carbonization. The PCE of DSSC was 5.6% with 12 wt% ZrO_2–C/PGEs and it was higher than that of pure PGEs (4.4%). The increased PCE was for the Lewis acid–base interactions of ZrO_2–C and poly (ethylene glycol), resulting in reduced crystallinity, improved ion conductivity, and lower electrolyte/counter electrode interfacial resistance, thus improving the charge transfer rate. These results demonstrate the role of ZrO_2–C in PGEs, effectively improving the performance, and highlighting the importance of carbon shell-functionalized nanomaterials for enhancing the PCE of DSSCs. Dong *et al.*[45] prepared a structurally interconnected block copolymer of poly(oxyethylene) (POE)-segmented diamine and a dianhydride to prepare the POE-PAI amide-imide copolymer, which could absorb the liquid electrolyte-producing PGE with well-defined nanochannel structure. DSSC fabricated with this PGE containing 76.8 wt% liquid electrolyte exhibited the PCE of 9.48% DSSC, with J_{sc} of 19.50 mA cm^{-2}, fill factor of 0.64, and V_{oc} of 0.76 V. The excellent efficiency of the gel-state DSSC, higher than that of the DSSC with the LE (8.84%), was due to the decrease of back electron transfer in the PGE as evident from dark current and impedance spectra analysis. This result shows an important advancement in DSSC for higher PCE, along with the higher longevity of cells avoiding the leakage problem of common liquid-state DSSC.

To overcome the long-term device stability problem of LE DSSCs, Subramaniam and his coworkers[46] made QSS electrolytes using Co_3O_4 additives to augment ionic conductivity. The sono-chemical process was applied successfully to generate fine Co_3O_4 nanoparticles, which were highly dispersible in polyacrylonitrile:poly(vinylpyrrolidone-*co*-vinylacetate) [PAN:P(VP-*co*-VAc); PVVA], even after calcination. The sonicated Co_3O_4 nanoparticles exhibited high dispersibility in a PVVA matrix resulting in homogenous QSS PGEs with highly amorphous phases. A nanocomposite PGE with 3 wt% Co_3O_4 nanoparticles (PVVA-3) exhibited the highest ionic conductivity (4.62×10^{-3} S cm^{-1}). A 51% increase in the diffusion coefficient of triiodide occurred compared to that with the unmodified un-sonicated electrolyte. The DSSC based on PVVA-3 displayed a PCE of 6.46% under AM 1.5G, 100 mW cm^{-2}. This effect is apparent in a selective 51% enhancement of photocurrent density ($J_{SC} = 16.2$ mA cm^{-2}) and a lowered barrier to N719 dye regeneration than an unmodified solar cell. The device stability in sonochemical Co_3O_4 PGE-DSSC of PVVA-3 was monitored over seven days and retained 83% of its original efficiency, whereas un-sonicated Co_3O_4 NPs retained only 13% of their initial efficiency. This remarkable stability for sonochemical Co_3O_4 NPs of PVVA-3 was attributed to the higher surface area and porous structure of the nanoparticle preventing the PGE collapse, originating from the evaporation of the solvent from the device.

To operate DSSCs with low-light illuminations, the optimal conditions differ from those under sunlight conditions. Since relatively few electrons are excited, the V_{oc} is strongly affected and for the prominent reduction in excited holes, lower iodide ions are needed to reduce the holes decreasing the optimal concentration of the redox couple to obtain good PCE at room light illumination. With this objective, Venkatesan *et al.*[47] prepared cobalt nanoparticle HPGEs, which acted as an effective electrolyte for QS-DSSCs under room-light conditions. The cobalt-based PGE was produced using PVDF-HFP as a gelator and ZnO NPs as a nanofiller using AN and 3-methoxypropionitrile (MPN) liquids. Interestingly the PCEs of the gel state cells with different ZnO nanofiller concentrations were higher than those of LE under room light conditions (200 lx). To obtain a high PCE of QS-DSSCs, optimization of the important components of DSSC was performed from the PCE values of liquid-state DSSCs. The liquid cell of the MPN-based cobalt electrolyte showed greater efficiency (18.91%) than the AN-based electrolyte (17.82%) at 200 lx illumination. Further, to improve the PCE of the QS-DSSCs, metal oxide nanoparticles were incorporated into the PGEs, and ZnO nanofillers have a superior performance in increasing the PCE of QS-DSSCs, even higher than the respective liquid cells. By tunning the ZnO nanofillers concentration, the PCE of MPN-based QS-DSSC exhibited a value of 20.11% at 200 lx illumination (Fig. 4a and b) with long-term stability of 1044 h at 35 °C. The gel-state cell without ZnO had high stability under room light conditions retaining 98% efficiency, and for the cell with 4 wt% ZnO, a gradual increase of the efficiency with time in the early testing period occurred, and the 100% PCE obtained after 1044 h is promising for indoor applications. The MPN-based DSSC containing a 90 nm PEDOT layer showed a very high PCE of 26.93% under 1000 lx illumination.[47]

Usually, inside an assembled DSSC, electrolytes are injected into a fixed space, causing the electrolyte layer in good touch with the photo-electrode and counter electrode. For the printing process, the electrolytes are to be coated on a photo-electrode before the heating step of sticking the two electrodes and the contact of the counter electrode with the electrolyte layer is a matter of apprehension. To overcome this problem, Liu *et al.*[48] made a new solar cell device *i.e.*, a double-layered electrolyte in a DSSC. Before the device assembly, electrolytes were separately coated onto the counter electrode and photo-electrode by doctor blading, confirming the close contact between electrodes and the electrolytes. The benefit of this architecture is that the coexistence of two kinds of electrolytes in a single DSSC is completely new. Here, the PEO/PVDF blend HPGEs are successfully fabricated, and ZnO nanoparticles were added as an electrolyte additive to improve the PCE. The electrolyte made with 9 wt% polymer blends has rheological characteristics benign for printing, and the respective DSSC with a double-layered electrolyte architecture exhibited PCE 7.99% similar to that of a normal liquid-state cell under 1 sun irradiation. Moreover, the V_{oc} increases when ZnO NPs are introduced as fillers, whereas the J_{sc} decreases as ZnO affects two electrodes differently, *i.e.*, at the photoelectrode upward shift of TiO_2 conduction band and the counter electrode decrease of interfacial charge transfer occurs. The double-layered architecture (Fig. 5a) overcomes the dilemma. Electrolytes with and without ZnO are printed on photo-electrode and counter electrode, respectively. The new DSSC device maintains high V_{oc}, and the

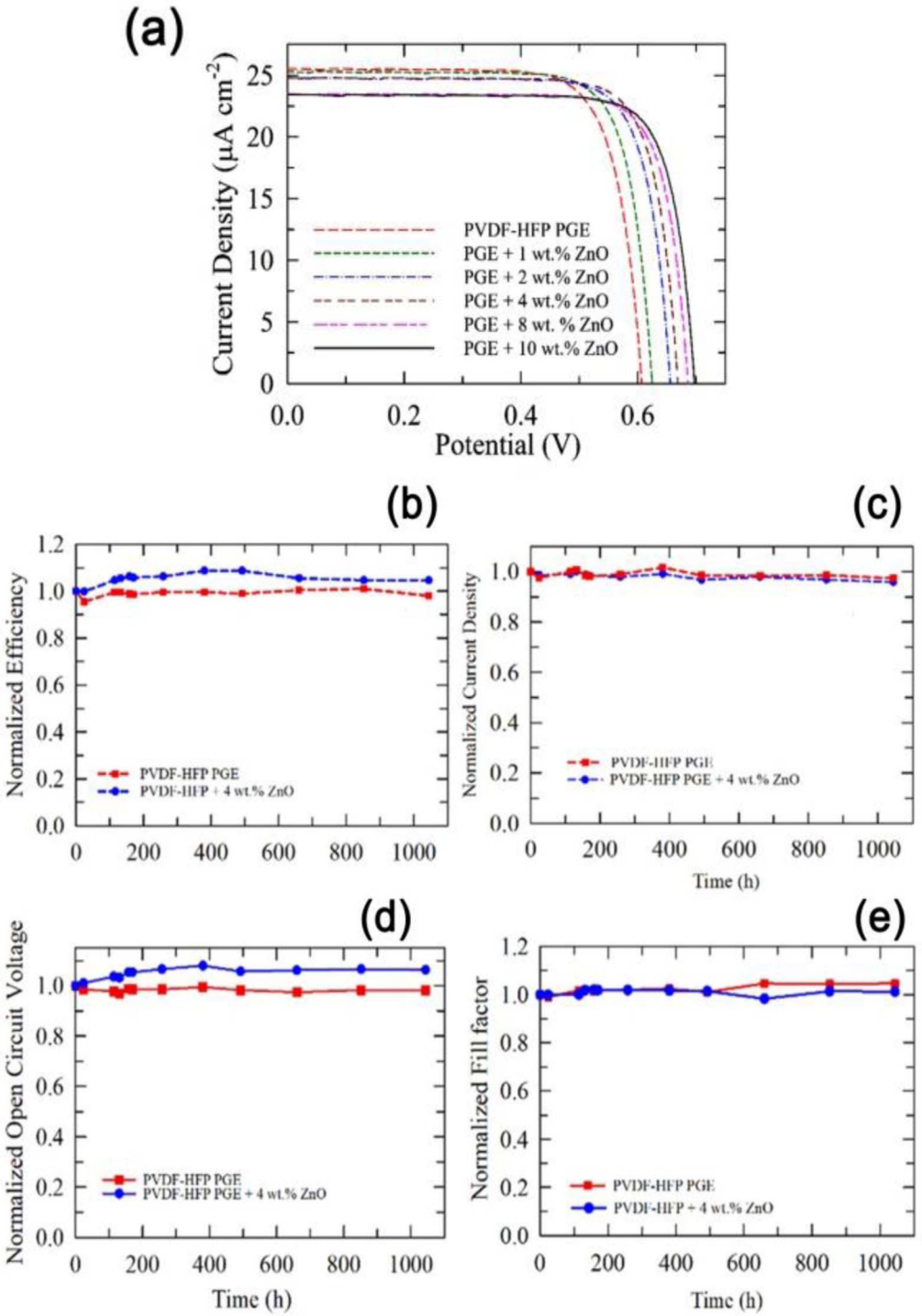

Fig. 4 (a) *J*–*V* curves of the QS-DSSCs using PVDF-HFP PGEs with and without various concentrations of ZnO nanofillers. (b) Normalized efficiency, (c) J_{sc}, (d) V_{oc}, and (e) FF of the QS-DSSC with and without 4 wt% ZnO nanofillers under continuous light illumination of 200 lx at 35 °C. (Reprinted from ref. 47 with permission from American Chemical Society).

J_{sc} increases, showing an improved PCE of 8.50% (Fig. 5b). At indoor fluorescent-light conditions, the same QSS DSSC outperforms its liquid-state counterpart, demonstrating a 15% higher PCE.

Thus, modern research on DSSCs using the hybrid polymer gel consists of using the xerogel to replace the TiO_2 active layer and also to use the polymer gel electrolyte, to achieve long-term stability. Various works are in progress by introducing different nanoparticles in the PGEs to improve both the cell performance and durability of the DSSCs. Developing PGE can improve safety issues occurring in liquid electrolytes thus facilitating the fabrication of DSSC in an easier way. To improve PCE in PGEs

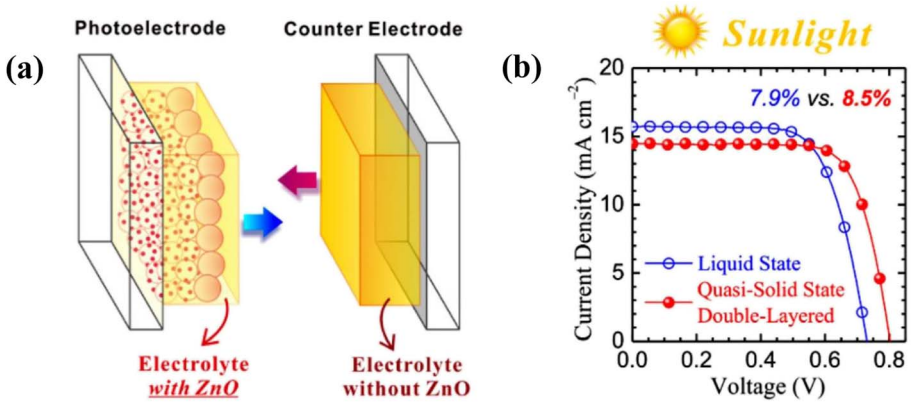

Fig. 5 (a) Schematic illustration of a DSSC featuring a "modified double-layered" electrolyte architecture. (b) Photovoltaic J–V curves related to the N719 DSSCs using modified double-layered electrolytes (under 1 sun). (Reprinted from ref. 48 with permission from Elsevier).

there is a problem and Saidi *et al.* used, 4-*tert*-butyl-pyridine (TBP) as an additive at different concentrations,[49] in the blend of poly(1-vinylpyrrolidone-*co*-vinyl acetate), P(VP-*co*-VAc) and PAcN, NaI, iodine and Co_3O_4 NPs in EC/PC PGE. The addition of TBP is beneficial as it can effectively adsorb on the TiO_2 photoanode surface, which shifts the quasi-fermi level of TiO_2 to a higher potential. It causes the V_{OC} of DSSC to increase and the PGE sample containing 3 wt% of TBP shows the highest PCE of 8.11% under light illumination of 100 mW cm^{-2}. The low efficiency in PGEs probably causes difficulty in the segmental motion of the polymer and introducing metal oxide nanofiller can enhance the PCE for its cross-linking centers, which coordinate with polymer segments. In this context, Farhana *et al.*[50], used an HPGE of a terpolymer poly(vinyl butyral-*co*-vinyl alcohol-*co*-vinyl acetate) (P(VB-*co*-VA-*co*-VAc)), tetrapropylammonium iodide (TPAI), and copper oxide (CuO) NPs where NPs becomes connected in the chain altering the amorphous phase and roughness of the surface disrupting the structural order of polymer chain, thus enabling easy redox couple transportation showing highest PCE 7.05%. Very recently Jana and coworkers published a review article on DSSCs highlighting some uses of GPE increasing the stability of the devices along with polymer and semiconductor electrolytes.[51]

It is necessary to mention the merits and demerits of PGEs compared to the use of LEs in DSSC. As discussed above, the LEs exhibit higher PCE values compared to those of PGEs due to the lower diffusion rate of charges in PGEs for the high viscosity of the medium, through which charges do not easily come in contact with the electrodes. To rectify this problem, PGEs are mixed with metal nanoparticles such as TiO_2, Co_3O_4, and TiC to make HPGE where the higher surface area of the nanoparticle improves ionic conductivity, reduces crystallinity and decreases activation energy of HGPEs, facilitating the charge flow, hence PCE increases to a reasonable value. The important benefit of PGEs are longer durability of the cell as the evaporation loss of the electrolyte medium is very low, making the cell stable. Further, another important use of PGEs is for making the cell in printable form. Also, the PGEs provide flexibility to the cell that is suitable for application in soft devices.

2.2 Fuel cell

2.2.1 Introduction. A fuel cell possesses two electrodes, *e.g.*, anode and cathode, where electrochemical reactions occur creating electricity. Apart from the electrodes, an electrolyte facilitates the flow of charged ions from one electrode to other electrodes, and also possesses a catalyst, accelerating the reactions at the surface of electrodes. Here, the basic fuel is hydrogen and also needs oxygen/air. The most important advantage of fuel cells is the generation of electricity with very little pollution as the hydrogen and oxygen used in generating electricity mostly combine to form water as a byproduct. Since a single fuel cell yields a small amount of dc-current, for practical application many fuel cells are assembled together to produce and drive current outside the cell to do work, *e.g.*, powering an electric motor or illuminating a light, *etc.* The main building block of fuel cells has an electrolyte layer in touch with a porous cathode and anode on either side.[52] In a dual chamber fuel cell, the fuel enters the anode and an oxidant enters the cathode and they are separated selectively by an electrolyte, through which the charge carriers, *e.g.*, H^+, CO_3^{2-}, O^{2-}, OH^- conduction can occur in any direction, *i.e.*, anode to cathode or cathode to anode. The following are the five different types of fuel cells, and their applications are mentioned in parenthesis:

(i) Proton exchange membrane fuel cells (PEMFCs) (transportation, portable power).

(ii) Alkaline fuel cells (AFCs) (military, space).

(iii) Phosphoric acid fuel cells (PAFCs) (distributed generation).

(iv) Solid oxide fuel cells (SOFCs) (auxiliary power, electric utility, distributed generation).

(v) Molten carbonate fuel cells (MCFCs) (electric utility, distributed generation).

(vi) Direct alcohol fuel cell (DAFC) (portable power).

In a typical proton-conducting fuel cell, gaseous hydrogen is fed into the anode (negative electrode) where the hydrogen atom is oxidized into a proton and an oxidant (*e.g.*, O_2) is fed into the cathode (positive electrode). Here the protons pass through the electrolyte and the electrons return to the cathode producing O_2^-, which unites with the proton to produce water.

In an alkali fuel cell, compressed hydrogen and oxygen and a solution of potassium hydroxide in water are generally used. A solid oxide fuel cell (SOFC) is an oxygen anion conductor, which flows from the cathode to the anode where it electrochemically combines with a fuel, *e.g.*, H_2 or CO, forming H_2O and CO_2, respectively. In PAFCs, phosphoric acid in the SiC matrix is used as an electrolyte, and hydrogen and oxygen are used as cathode and anode feed, respectively. In MCFCs, molten $LiCO_3$ in $LiAlO_2$ is used as an electrolyte and the feed gases in the cathode and anode are the same as the other type of fuel cells. In the DAFCs, methanol or ethanol are used as feed fuels and hybrid Nafion membranes are used as the fuel cell membrane.

2.2.2 Membranes of fuel cells. In polymer electrolyte membrane fuel cells (PEMFC, also called the proton exchange membrane fuel cell), Nafion (sulfonated tetrafluoroethylene based fluoropolymer-copolymer) membranes used as the electrolyte operating usually in 60–100 °C range is suitable not only for transport and for portable applications, but also for power generation in buildings.[53] The PEMFCs find use in power generation to generate peak power escaping the grid reinforcement and are tested on a 250 kW scale using hydrogen as the fuel. The main component of PEMFCs is the polymer electrolyte membrane (PEM), acting as an electrolyte for the transport of protons from anode to cathode, and also providing a fence to the channel of electrons and fuel. The principle of operation of PEMFCs is presented in Fig. 6a.[54]

Hence, most studies on fuel cells are focused on developing high-performance PEM with high proton conductivity, high oxidative stability, low fuel permeability, good mechanical stability, and low cost of fabrication. Proton conductivity is essential for high current density, occurring in the electrolyte membrane of PEMFCs. In hydrated polymeric matrices, proton transport occurs through two principal mechanisms: ''hopping'' and ''vehicular''. The protons transfer occurs from H^+ and H_3O^+, and even NH_4^+ species, to other protonic sites in the membrane. The schemes of the vehicular and hopping mechanisms are shown in Fig. 6b and c; the former occurs when the hydrated proton passes through the medium in response to an electrochemical difference when protons attach to a vehicle site such as water and diffuse through the medium conveying the protons.

In 1966, Nafion, membranes with good thermal and chemical stability, was first developed by DuPont and the high chemical stability, thermal stability, and proton conductivity of Nafion are due to the strong tetrafluoroethylene backbone, and high acidity of the sulfonic acid groups at the side chain.[55] The Nafion membrane acts as a standard membrane for PEMFCs for its chemical and thermal stability and high ionic conductivity ($\sim$0.1 S cm^{-1}) at completely hydrated conditions. Despite the low water uptake, Nafion membranes have effective uniform water channels showing high electric properties facilitating to act as proton conductors in PEMFCs for their exceptional electrochemical properties and durability under unkind conditions. A drawback of these polymers is the high manufacturing cost, hence hydrocarbon-based polymeric membranes with various kinds of monomers are used to tune the reaction conditions of the fuel cell. To enhance the properties and stability of the membranes, rigid aromatic structures are introduced into the polymer backbone yielding thermal and mechanical stability. For automotive applications, the U.S. Department of Energy (DoE) made guidelines with a target conductivity value of 0.1 S cm^{-1}, at 120 °C and 50% relative humidity (RH) taking Nafion as the standard.

For commercialization, Nafion membranes have many disadvantages such as a decrease in ionic conductivity and humidity at high temperatures, and a high cost of preparation. As such, modulation of PEMs is the peak area of research for improving the fuel cell performance and new polymers, such as sulfonated poly(ether ketone) (SPEEK), poly(ether sulfone) (PES), and polybenzimidazole (PBI), are the most important in this regard.[54] For fabricating fuel cell membranes, inorganic NPs are usually mixed with the polymer matrix using the conventional solution blending technique but the sol–gel method is the most elegant technique for producing hybrid fuel cell membranes. Here, inorganic nanoparticles are *in situ* produced by hydrolysis and condensation of inorganic alkoxide precursors inside the polymer matrix. Another important method to prepare hybrid polymer gel membranes is infiltration, where after the polymer membrane formation, the inorganic particle infiltrates into a hydrogel-like or swollen polymer matrix. Finally, the organic–inorganic hybrid membranes are produced from nanoparticle growth, removal of impurities, and polymer curing.[56] In this review, we will discuss the PEM membranes made from hybrid polymeric gels or hybrid polymer membranes made by sol–gel techniques. There are few reviews in this regard[12,54,57–62] and to keep updated the rapid growth *in situ* sol–gel template strategy facilitating the fabrication of new organic–inorganic hybrid proton exchange membranes showing outstanding properties would be discussed here.

2.2.3 Hybrid polymer gels as fuel cell membrane material. Joseph *et al.*[57] prepared Nafion–silica membranes using silica precursors with various functionalized silicate materials by the sol–gel reaction and implantation of silica compounds with polymeric membranes. The homogeneous dispersion of SiO_2 NPs in the polymer matrix occurred and the mesoporous inorganic network formed in the polymer matrix did not hamper the proton transport pathways. Rather, the composite Nafion membranes with functionalized silica have higher proton conductivity from pure Nafion and normal Nafion/silica composites, over a large temperature range and relative humidity. At low humidity conditions, the phosphonate functionalization of SiO_2 NPs played a dominant role in retaining water.

To understand the role of oxide particles in improving the performance of Nafion membrane in fuel cells, Santiago *et al.*[63] produced TiO_2–Nafion hybrids by non-conventional *in situ* sol–gel process where a low-temperature sol–gel synthesis, from a sol of titanium tetra isopropoxide (TiP), was used to introduce anatase TiO_2 NPs into the Nafion matrix. From the gravimetric analysis, the degree of TiO_2 incorporation into PEM as a function of TIP concentration was determined. XRD analysis indicated that the intensity of anatase TiO_2 diffraction peaks increases with increasing TIP concentration and the crystallite

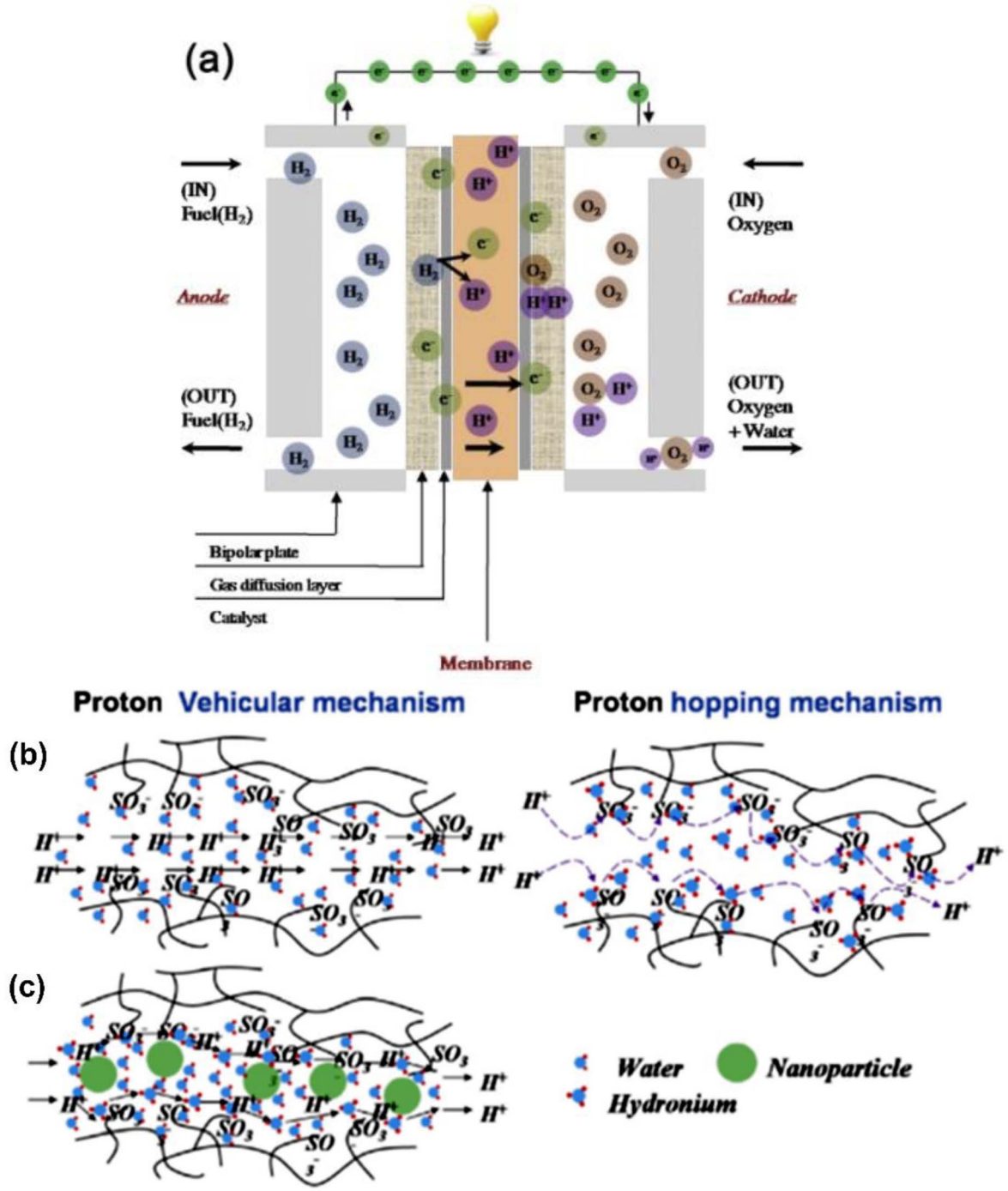

Fig. 6 (a) Principle of polymer electrolyte membrane fuel cell. Schematic design of vehicular mechanism and hopping mechanism as proton conduction in (b) pristine membranes and (c) polymer/nano-particle composite membranes reproduced from ref. 54 with permission from Elsevier.

sizes are in the range of 4–6 nm. The proton conductivity of Nafion and Nafion–TiO_2 are compared in Fig. 7 for different TIP concentrations and the membranes' conductivity decreases with increasing TIP concentration (Fig. 7a), suggesting that TiO_2NPs are localized at the hydrophilic sites, *i.e.*, at the paths for proton transport. The data in Fig. 7a demonstrated that the conductivity of Nafion at 23 wt% of TiO_2 became lower by one order, indicating that the membrane has the percolating path for conductance. This was confirmed by Arrhenius plots shown in Fig. 7b, suggesting that conductivity in the hybrid membranes follows a thermally activated process of nearly the same activation energies (E_a), which are very close to that of Nafion (~10 kJ mol^{-1}). Testing of fuel cells up to 130 °C indicated that the hybrid membranes showed higher ohmic drop

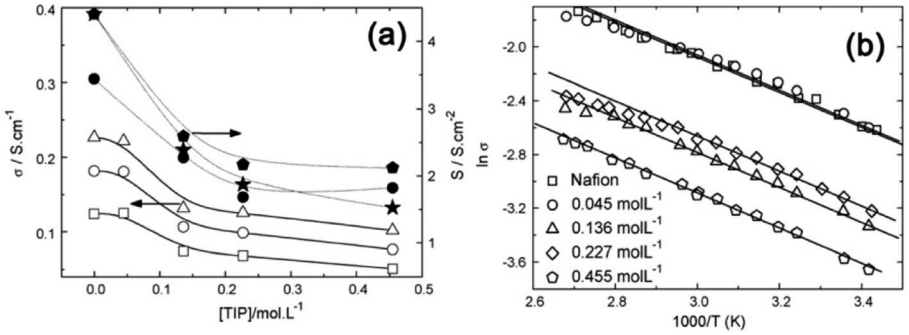

Fig. 7 (a) Electrical conductivity of Nafion and hybrids as a function of the TIP concentration measured at (□) 25 °C, (○) 60 °C, and (Δ) 90 °C (left *Y*-axis). The right *Y*-axis shows the conductance determined from the polarization curves measured at (*) 80 °C, (◆) 120 °C, and (●) 130 °C; (b) the Arrhenius plot for Nafion and hybrids obtained with different TIP concentrations. The straight lines are the best linear fittings. Reproduced from ref. 63 with permission from Elsevier.

with the amount of TiO_2 content incorporated into Nafion. At low relative humidity and at high temperatures, the performance of fuel cells using hybrid membranes surpasses that of Nafion. Further, the inorganic phase confers stability to the polymer, permitting the operation at high temperatures and at reduced RH.

In another work to improve the performance of PEM fuel cells at high temperatures, Amjadi *et al.*[64] used *in situ* sol–gel reaction to dope SiO_2 into the Nafion membrane, thus minimizing the leaching of doped particles. The membranes were characterized for thermal stability, water uptake, proton conductivity, and cell performance. The membranes of the Nafion/SiO_2 composite exhibited low hydrogen permeability, and water uptake of Nafion/SiO_2 membrane with 7% doping increased up to 43%, *i.e.*, 30% higher than that of pure Nafion membrane The proton conductivities of the hybridized membranes at ambient temperature are lower from that of the pure membrane but at low humid conditions and at 110 °C, the modified membranes show higher fuel cell performance from pure Nafion. The membrane with 5–7% SiO_2 content exhibits good water uptake and improved fuel cell efficiency among other membranes.

Jamaludin, *et al.*[65] made an electrochemical study of a direct borohydride fuel cell (DBFC) based on a PGE of sago, which is a natural polymer. To apply in fuel cells, PGEs should have high ionic conductivity and should sustain high electrochemical activities as an electrolyte with a composition of sago, 6 M KOH, and 2 M $NaBH_4$, which was prepared and evaluated as a novel PGE for a DBFC fuel cell because of its high electrical conductivity (0.27 S cm^{-1}). As the $NaBH_4$ solution was directly added, H_2 gas would be readily available for the hydrogen oxidation reaction at the anode without an external supply. At the cathode, the rate of oxygen consumption was associated with the current from the number of electrons that reacted per oxygen molecule and four electrons reacted per oxygen molecule. The fuel cell performance was measured in terms of open circuit voltage and its current–voltage, properties. The highest power density observed was 8.818 mW cm^{-2} at a discharge performance of 230 mA h at a voltage of 0.806 V. The open circuit voltage of cells was ~0.900 V, which was retained for 23 h.

In order to obtain a strong interaction between the sulfonated polyimide (SPI) matrix and mesoporous SiO_2 nanofillers of the composite membranes improving properties of the membranes, Geng *et al.*[66] prepared membranes of SPI/mesoporous silica hybrid by sol–gel and self-assembly process of tetraethoxysilane (TEOS) within the SPI without the phase separation in surfactant (CTAB) templates. Inorganic domains have negative effects on proton conducting properties because high water activity does not occur in these hybrids and the *in situ* formed mesoporous silica remained uniformly dispersed in the entire organic matrix avoiding aggregation. The hybrid membranes exhibited good water-uptake, and thermal properties, and also exhibited intense methanol resistance and proton conductivity. The domains of the hydrophilic mesoporous silica increase the water storage sites thus increasing the uninterrupted proton conductive pathway, facilitating the ability of proton transport into the mesoporous structure.

Jana and his coworkers[67] reported thermoreversible gelation of polybenzimidazole (PBI) in phosphoric acid (PA). The gels exhibited highly dense fibrillar network morphology with a large number of thinner and longer fibrils for higher gel concentration. There is strong hydrogen bonding interaction between PA and PBI molecules; also, free PA molecules are present in the gel network. The PBI gel membrane exhibits very high mechanical and thermal stabilities. High acid loading and high thermo-mechanical stability of the membrane are for the gel network structure, which influences proton conductivity of the membrane showing high conductivity of 0.1 S cm^{-1} at 160 °C and 0% relative humidity and it is higher than the reported values for the PBI in the literature. The activation energy of 14–15 kJ mol^{-1} pointed out rapid proton transfer by hopping in the gel network. Mader and Benicewicz[68] developed a sulfonated PBI (s-PBI) gel membrane using polyphosphoric acid (PPA) as the polymerization solvent, polycondensation agent and casting solvent. Under suitable hydrolysis conditions, gelation took place, yielding a robust PA-doped polymer gel film showing brilliant physicochemical properties that do not arise from the general membrane preparation process. The PPA process

produced membranes with high acid doping levels, excellent mechanical properties, high conductivity, and healthy fuel cell performance. These membranes possess high PA loadings of 30–35 mol PA/PBI, an average tensile stress of 0.804 MPa, and an average tensile strain of 69.64%. Proton conductivities measured have values in the range 0.1–0.25 S cm^{-1} at 180 °C, and were dependent on the acid doping level. The fuel cell testing with hydrogen fuel and air or oxygen as oxidants without external humidification of feed gas exhibited excellent performance. The highest performance at the current density of 0.2 A cm^{-2} and 160 °C is 0.679 V was noted from an s-PBI membrane for the highest PA doping with oxygen as oxidant, while the lowest performance noticed was 0.617 V from the membrane with the lowest acid loading indicating a correlation between phosphoric acid loading and fuel cell performance. There was a ~67–77 mV lowering in performance when air is used as an oxidant instead of oxygen. The cell performance durability test conducted at 160 °C for ~3000 h indicated great promise showing a very low degradation rate of 30 μV h^{-1}.

Choudhury *et al.*[69] synthesized novel environmentally benign PEMs consisting of ionically cross-linked chitosan (CS) hydrogels for direct borohydride fuel cells (DBFCs). Ionic cross-linking of CS membranes was made with sulfate and hydrogen phosphate salts of sodium and the CS hydrogel membrane electrolytes (ICCSHMEs) enhancing the environmental friendliness and cost-effectiveness of fuel cell technologies. The DBFCs were assembled with an anode catalyst containing a composite of carbon-supported palladium and nickel, with a cathode of carbon-supported platinum and ICCSHMEs as electrolytes-cum-separators. An alkaline solution of $NaBH_4$ was used as a fuel in the DBFCs in flowing mode and oxygen as an oxidant. The DBFCs employing Na_2SO_4 ICCSHMEs exhibited a peak power density of ~750 mW cm^{-2} at a current density of ~1.560 A cm^{-2} and Na_2HPO_4-based ICCSHMEs showed a somewhat higher power density of 810 mW cm^{-2} at 1.680 A cm^{-2} current density, at 70 °C operating cell temperatures (Fig. 8a). The durability of the later DBFC exhibited a stable cell performance with a cell voltage loss of only 100 mV during an operation period of 100 h (Fig. 8b).

PEM fuel cells operating above 100 °C at low humid conditions are attractive to replace the most expensive platinum catalysts with oxide-based catalysts and eliminating cumbersome water management systems. Great efforts were made to develop novel PEMs for fuel cells operating in low humidity at high temperatures (above 100 °C), including modified Nafion, heterocycle-based polymers, and alternative sulfonated polymers. Among them, polybenzimidazole (PBI)-phosphoric acid (PA) based membranes have good success for their good proton conductivity at high temperatures but due to their very low proton conductivity at room temperature, it finds difficulties for applications in automotive and microelectronic devices. In an attempt, Song *et al.*[70] reported tetrazole-based PEM fuel cells functioning at low humid conditions at 20 to 120 °C. This tetrazole-based PEM exhibited little dependence on proton conductivity with temperature and humidity. At 120 °C, these membranes exhibit a good proton conductivity value of 0.041 S cm^{-1} with 1.2% relative humidity and it decreased slightly with the lowering of temperature showing greater than 0.03 S cm^{-1} at 40 °C and 31.7% humidity. These tetrazole-based fuel cells exhibited good fuel cell performance for a wide temperature range at low humidity, showing short-circuit current density (770 mA cm^{-2}) and peak power density (120 mW cm^{-2}) at 20 °C. The system showed a higher power density of 190 mW cm^{-2} at 120 °C, indicating improved performance with the increase in temperature. This is sufficient for many microelectronic devices and this novel membrane can spectacularly simplify fuel cell systems making them suitable for commercialization for zero-emission vehicles and microelectronics.

2.2.4 Hybrid polymer gels for electrocatalysis. Electrocatalysis is an electricity-driven process that can reduce the activation energy of chemical reactions occurring on the electrode surface of fuel cells and has played a pivotal role in global warming issues.[71] The 3D network structural advantages and the interesting physicochemical properties of hybrid polymer hydrogels have attracted major research interests in electrocatalysis in oxygen reduction reaction (ORR), hydrogen evolution reaction (HER), and oxygen evolution reaction (OER), *etc.*[72] In the hybrid hydrogel, the high compositional tunability and uniform distribution of hybrid components, facilitate their extensive use as active materials for electrocatalysis.[73] Apart from noble metals, transition metals (*e.g.* Fe, Co, Ni) have received great research attention as alternatives to noble metal electrocatalysts. Among them, the metal and nitrogen-*co*-doped carbon (M–N/C) catalysts have emerged as new-generation catalysts for ORR. As an example, uniformly distributed M–N–C active sites anchored on carbon frameworks (Fig. 9), serve as a substitute strategy for producing large-scale single-atom catalysts.[74,75] Using supramolecular hydrogels, Cu-atoms attached to interconnected carbon fibers were produced with high atom utilization (96%) of Cu(I)–N_2 sites for ORR.

Apart from the metals, metal sulphide, metal oxide, *etc.* nanoparticles/quantum dots embedded in polymer gel matrices can behave as electrode catalysts in fuel cells. For example, Nandi and coworkers[76] synthesized *N*,*N*-dibenzoyl-L-cystine(DBC)–polyaniline (PANI) aerogel framework (Fig. 10a) and dispersed molybdenum disulphide QDs (MoS_2-QDs) made by solvent exfoliation strategy as an electrocatalyst material. DBC-PANI aerogels made from the polymerization of aniline taking DBC as a cross-linker as well as dopant and at different amounts of aniline (1.5 ml and 2 ml), named DBC-PANI1 and DBC-PANI2, were highly conducting. The hybrid xerogels were prepared in a similar way with the addition of 5 mg of MoS_2 QDs and the aniline solution, followed by polymerization of aniline at 5 °C for 24 h with ammonium persulphate when light yellow hydrogel transformed to green colored-DBC-MoS_2-PANI2 gel followed by freeze-drying. Storage and loss moduli (G', G'') showed that in all cases, $G' > G''$ indicating gel nature (Fig. 10b). The DBC-MoS_2-PANI2 gel showed a higher G' value than that of DBC-PANI2 gel for reinforcing the effect of MoS_2 QDs causing better energy storage, indicating better elastic properties. Compressive stress–strain experiments showed higher mechanical properties of DBC-PANI2 and DBC-MoS_2-PANI2 than DBC-Ani2 aerogel (Fig. 10c). The reinforcing effect of MoS_2 QDs yielded greater stress for each strain in DBC-MoS_2-PANI2

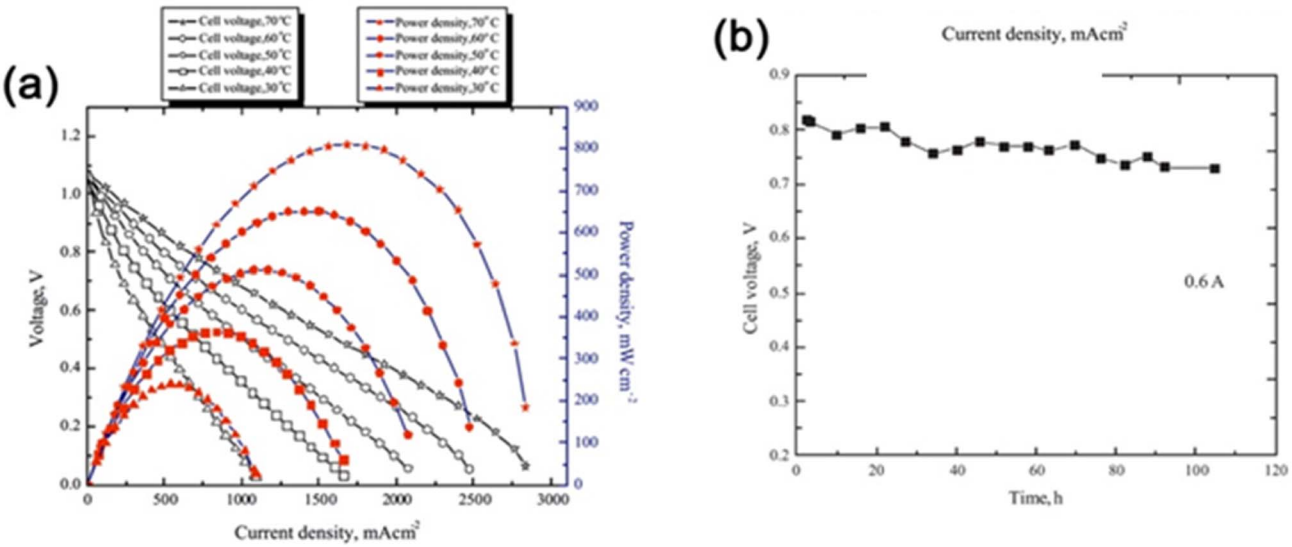

Fig. 8 (a) Cell polarization and power density plots for DBFC employing ICCSHME prepared by ionic cross-linking of CS with sodium sulfate and operating at different cell temperatures (b) electrochemical performance durability data for DBFC employing ICCSHME prepared by ionic cross-linking of CS with sodium hydrogen phosphate and operating at ambient temperature reprinted with permission from ref. 69, Elsevier.

aerogel from that of DBC-PANI2 aerogel it is important to note that DBC-Ani2 gel, has lower modulus and lower stress values than those of DBC-PANI2, indicating that the polymerization improves the modulus and mechanical properties values. Exfoliated MoS_2 sheets, and DBC-PANI1, MoS_2 QDs, DBC-PANI2, DBC-MoS_2-PANI2, and DBC-MoS_2-PANI1, aerogels were used for hydrogen evolution reaction (HER) in 0.5 M H_2SO_4 solution at a 0.5 mV s^{-1} scan rate (Fig. 11a). As evident from the figure, the MoS_2 sheets behaved as a poor HER catalyst for its low conductivity and lower availability of active edge sites, but, MoS_2 QD is an active material for HER as it has greater active edge sites.[77] Fig. 11b exhibits the onset potentials and the potentials at 10 mA cm^{-2} current density where DBC-MoS_2-PANI1, MoS_2 QDs, and DBC-MoS_2-PANI2 aerogel exhibited better catalytic properties with significantly lower overpotential (262, 223, and 196 mV). The kinetics of the HER process were studied to obtain Tafel slopes from the Tafel equation $\eta = b \times \log j + a$, where b is the Tafel slope, η is the overpotential, j is the current density and a is the intercept. The Tafel slope of MoS_2 QDs was 69 $\pm$ 1.2 mV per decade (Fig. 11c), which was significantly lower than that of the MoS_2 sheet (152 $\pm$ 1.6 mV per decade) at 10 mA cm^{-2}. Moreover, DBC-MoS_2-PANI1 and DBC-MoS_2-PANI2 aerogels having Tafel slope values 64 and 58 mV per decade, respectively, exhibited good HER catalytic activity, closer to that of the commercial Pt catalyst (32 mV per decade). The low Tafel slope values of DBC-MoS_2-PANI aerogel catalysts arose from the synergistic coupling at the interface of MoS_2 QDs and PANI fibres of the aerogels, improving the reaction speed considerably. From a comparison of the sensitivity of HER using the Tafel slope for different composites, the DBC-MoS_2-PANI aerogel showed very good activity (Fig. 11d).[76] As such, the present DBC-MoS_2-PANI aerogel is a practically active material for HER catalysis. The PANI network enhanced the catalytic activity of MoS_2 QDs for the conducting nature, facilitating the

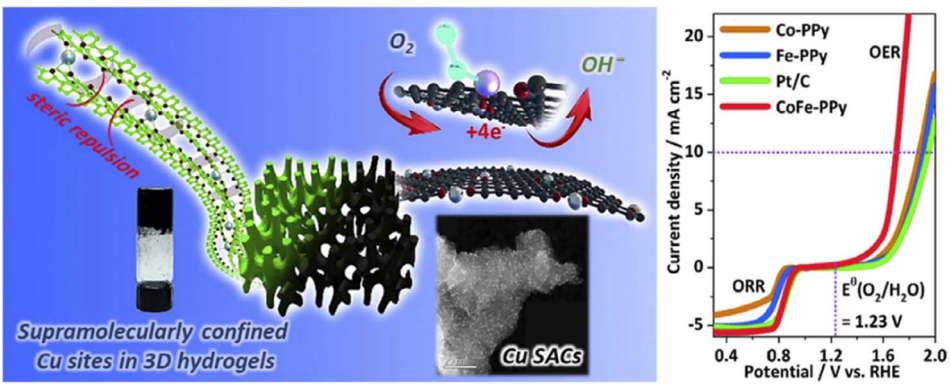

Fig. 9 Hydrogels for electrocatalysis. (a) Hydrogel-derived confined atomic Cu(I)–N sites and (b) Co/Fe-PPy for electrocatalytic OER and ORR. (Reproduced with from ref. 74 and 75 with permission from Elsevier and American Chemical Society).

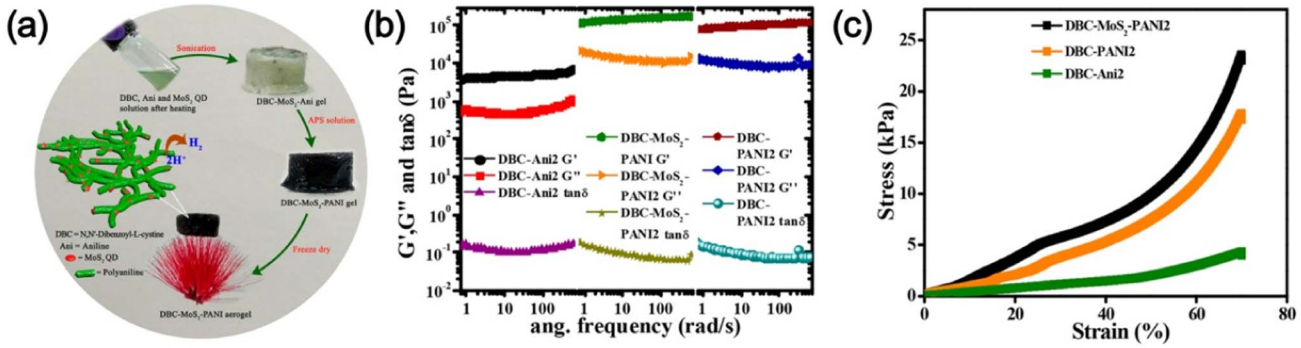

Fig. 10 (a) Schematic illustration of DBC-MoS_2-PANI aerogel preparation and their electrocatalytic properties showing the hydrogen evaluation reaction. (b) Plots of storage modulus (G) loss modulus (G) and tan δ *vs.* angular frequency of the DBC-Ani2, DBC-PANI2, and DBC-MoS_2-PANI2 hydrogels. (c) Corresponding compressive stress *vs.* strain plot of DBC-Ani2, DBC-PANI2, and DBC-MoS_2-PANI2 aerogels reproduced from ref. 76 with permission from American Chemical Society.

easier flow of electrons necessary for the HER process. It is important to note that a Tafel slope of 36 mV per decade was observed for MoS_2-CNT indicating that the catalytic power was very similar to that of the commercial PT electrode (32 mV per decade).[78] The higher catalytic activity for MoS_2-CNT from the present work was for higher conductivity of CNT (10^4 S cm^{-1})[79] than that of the DBC-PANI2 aerogel (0.02 S cm^{-1}).

To understand the long-term operating stability of DBC-MoS_2-PANI2 aerogel, the cyclic stability of the electrocatalyst was tested using cyclic voltammetry at a scan rate of 50 mV s^{-1} over 1000 cycles (Fig. 11e) and here the lowering of current density was negligible, indicating that the DBC-MoS_2-PANI2 aerogel is a steady electrocatalyst for HER for long-term repeated cycling in acidic electrolyte. The fast charge transfer from the conducting PANI (ES) nanofibers to active spots of MoS_2 QDs was also recognized from the electrochemical impedance spectroscopy (Fig. 11f). At higher frequency regions, the Nyquist plot exhibited a smaller radius of curvature (Fig. 11f, inset) qualitatively suggesting that the DBC-MoS_2-PANI2 aerogel has lower charge transfer resistance (R_{ct}) from those of MoS_2 sheets and MoS_2 QDs. The HER catalyst performance was evident from the lower R_{ct} value of DBC-MoS_2-PANI2 aerogel, affording markedly faster HER kinetics. The Tafel slope of 58 mV dec^{-1} of DBC-MoS_2-PANI2 aerogel indicated a Volmer–Heyrovsky reaction path; *i.e.*, the desorption of H_2 was the rate-determining step. The better catalytic activity of hetero-nanostructured DBC-MoS_2-$PANI_2$ aerogel from that of MoS_2 QDs is for the following reasons: (i) the higher surface area of aerogels facilitated rapid electrolyte diffusion and the porosity in the network structure is helpful for the adsorption of H^+ on MoS_2 edges where the H atom gets rapidly reduced as the transfer of electrons to the MoS_2 surface is easier through the PANI network. (ii) The MoS_2 QDs and PANI possess synergistic coupling in the hybrid aerogels, facilitating the delocalization of electrons between MoS_2 QDs and PANI, reducing the hydrogen adsorption energy in the aerogels,[78] resulting in the desorption of product hydrogen to form molecular hydrogen improving HER activity.

Wu *et al.*[80] made a non-noble metal HER electro-catalyst using ultrafine Mo_2C NPs embedded into a 3D N-doped carbon foam with bacterial cellulose/$(NH_4)_6Mo_7O_{24}$ hybrid hydrogels. This HER electro-catalyst exhibited remarkable activity with a Tafel slope of 30.8 mV dec^{-1}, and worked well in the whole pH range (pH 0–14). The carbon-nanofiber network skeleton[81] derived from the bacterial cellulose hydrogel with nanosized MoS_2 showed HER electro-catalyst exhibiting a low onset over-potential value of 120 mV, with a Tafel slope of 44 mV dec^{-1}, and a high exchange current density of 0.09 mA cm^{-2}. In a recent review, polymeric aerogel nanomaterials including carbon nanotube and graphene acting as good electrocatalytic supports are briefly discussed for their durability, and active electrocatalysis particularly in low-temperature fuel cell applications.[82]

In summary, hybrid polymer gels are much used in making efficient and stable fuel cell membranes suitable for the conductance of ions and are also used as the catalyst for the electrode processes such as HER, OER, and ORR processes. The sol–gel process was efficiently used to dope SiO_2, and TiO_2 NPs into the Nafion membranes exhibiting increased fuel cell performance from pure Nafion by increasing the number of water storage sites facilitating continuous proton conductive pathways through the mesoporous structure. Further, the inorganic NPs confer stability to the polymer membrane, permitting the operation at high temperatures and reduced RH. Gel membranes of PBI and sulphonated PBI exhibit better proton conductivity and cell performance also exhibiting excellent durability. Using supramolecular hydrogels and copper atoms attached to, interconnected carbon fibers showed high atom utilization (96%) of Cu(I)–N_2 sites for ORR. The Tafel slope of DBC-MoS_2-PANI2 aerogel was very encouraging for HER and that of 3D N-doped carbon foam using bacterial cellulose/$(NH4)_6Mo_7O_{24}$ hybrid hydrogels exhibited remarkable HER electro-catalyst activity with a Tafel slope of 30.8 mV dec^{-1} promising their application to replace Pt electro-catalyst. Thus, hybrid polymer gels show good promise for making efficient fuel cells.

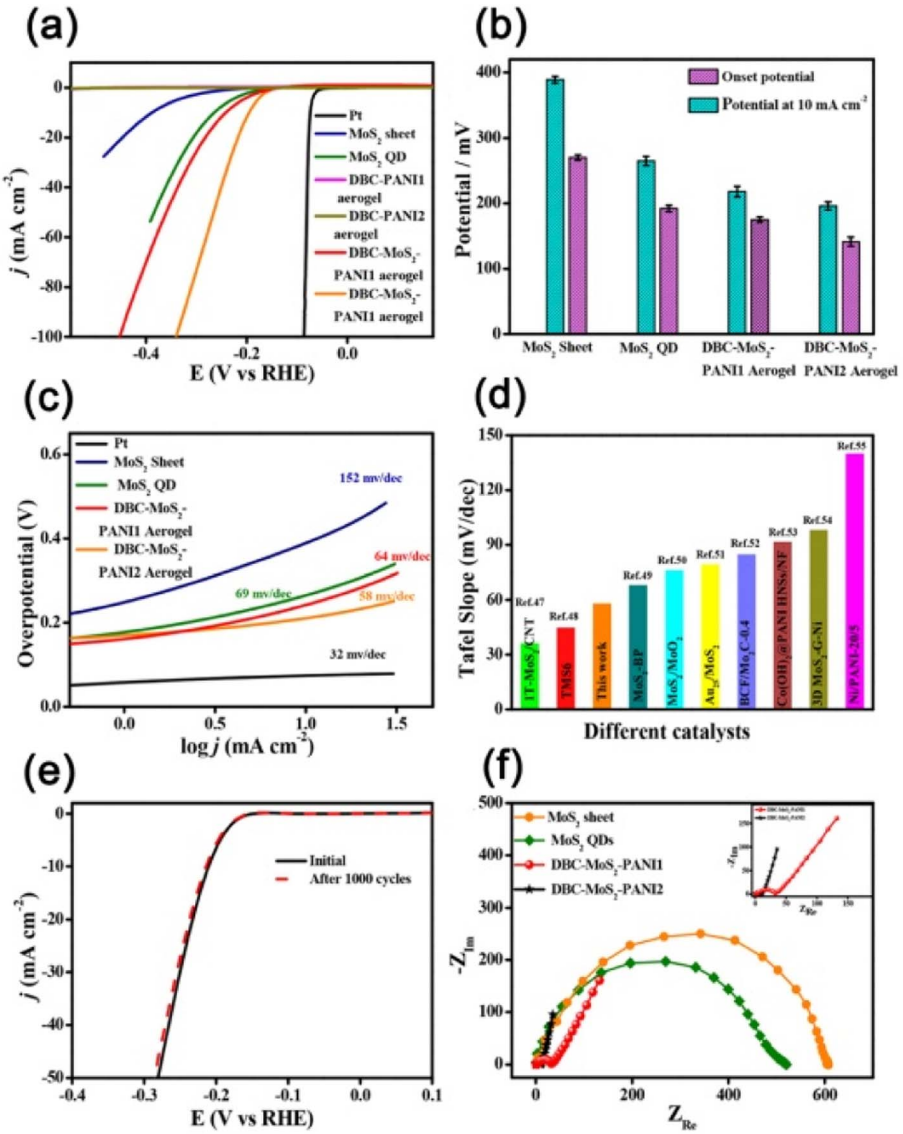

Fig. 11 (a) Polarization curves of MoS_2 sheet, MoS_2 QDs, DBC-PANI1, DBC-PANI2, DBC-MoS_2-PANI1, DBC-MoS_2-PANI2 aerogel, and high-quality commercial Pt catalyst. (b) Onset potential and potential at 10 mA cm^{-2} of MoS_2 sheet, MoS_2 QDs, DBC-MoS_2-PANI1, DBC-MoS_2-PANI2, and aerogel. (c) Corresponding Tafel plots of MoS_2 sheet, MoS_2 QDs, DBC-MoS_2-PANI1, DBC-MoS_2-PANI2 aerogel, and Pt catalyst. (d) Comparison of HER performance between DBC-MoS_2-PANI2 and other electrocatalysts in the literature. (e) Stability after 1000 times of CV cycles. (f) Nyquist plots of all components (inset: enlarged Nyquist plots of DBC-MoS_2-PANI1 and DBC-MoS_2-PANI2). Reproduced from ref. 76 with permission from American Chemical Society.

The merits of hybrid fuel cell membranes formed by the sol–gel process are that they exhibit good swelling, high acid doping level, high proton conductivity, higher power density, and excellent performance with very good durability compared to those made by the solution casting method. Also, these systems exhibit good mechanical properties, brilliant physicochemical properties, and healthy fuel cell performance. In the electrocatalysis phenomena, the hybrid gels due to their porous structure provide high catalyst performance, showing good ORR, also the HER catalyst activity increases when the NPs are attached to the gel fibres. Due to the presence of a large surface area catalytic activity is very high and the pores of the network facilitate the evaluation of oxygen/hydrogen gases. One shortcoming may appear in the chemical stability of the membrane because the porous nature of the gel network is easily vulnerable to chemical attack from toxic gases; however, nanoparticles incorporated into it can resist chemical degradation.

3 Hybrid polymer gels in battery applications

3.1 Introduction

In modern lifestyles, a steady supply of energy is very much necessary for our dynamicity, prosperity, and daily comfort. For this purpose, batteries are of supreme importance, especially

for mobile applications.[83] Batteries are high-energy-storage devices with a poor-energy-delivery capability (*e.g.*, low power density and rate capability) and the premier rechargeable solid-state lithium-ion batteries have much lightweight with high energy storage capacity compared to conventional rechargeable batteries.[84] It has three essential components, *e.g.*, Li^+ intercalation anode, cathode, and the electrolyte, through which Li^+ ions move from the cathode to the anode during charging and in a backward direction when discharging. The development of the high-performance battery involves optimization of every battery component, from the electrolyte, electrodes, and binder systems. The microstructure and nature of electrode materials are crucial for the energy densities, cycle lifetime, and safety of batteries.[84,85] There are different types of solid-state batteries *e.g.*, Li-ion batteries, sodium–sulfur batteries, vanadium batteries, sodium–metal halide batteries, *etc.*[83] among them Li-ion batteries (LIB) are very significant as they possess high energy density (theoretical value of 400 W h kg^{-1}).[86] Certainly, rechargeable LIBs are an attractive power source for applications in portable electronic devices and electric vehicles.[83,87,88] Efficient electrode materials involve long cycle life, high energy density, and excellent rate capability, with high reversible Li^+ storage capacity and rapid Li^+ transport. The use of nanomaterials can avoid the electrode kinetic issues of LIBs, reducing the lithium diffusion time[87] thus facilitating the Faradaic reactions of active particles for ion and electron transport processes. Still, it is a major challenge to develop electrode materials with rapid charge and discharge rates in LIBs, and to achieve it, intensive research is going on for new electrode and electrolyte materials with potential rate capability. In this part of the review, we delineate the efficacy of hybrid polymer gels in developing the battery components for improving the solid-state battery performance with special attention to LIBs. There is tremendous progress in this hot area of solid-state batteries using hybrid polymer gels as evident from the growing number of literature reviews[88–96] and to keep current updates in this field we include some new and important research work in this field.

3.2 Li-ion battery (LIB)

3.2.1 Hybrid polymer gel electrolyte (HPGE) membranes. Li *et al.*[97] prepared hybrid PVDF/PEO nanofibrous membranes by electro-spinning of PVDF/PEO solution in DMF at different weight ratios 2 : 1, 5 : 1, and 10 : 1 referred to as F/O-2, F/O-5, and F/O-10, respectively. The membranes of the hybrid gel polymer electrolytes (HPGEs) were activated by keeping them in a glove box, dipping into the liquid electrolyte (1 M $LiPF_6$ in propylene carbonate (PC)/ethylene carbonate (EC)/dimethyl carbonate (DMC) (1 : 1 : 1, v/v/v)) for 1 h and dried by wiping with filter paper. Fig. 12a shows the SEM micrograph exhibiting a 3D fibrillar network of a hybrid nanofibrous polymer membrane. XRD results indicate the formation of β-polymorph with all-trans conformation of PVDF but the β-polymorph decreases with increasing PEO concentration in the hybrid. DSC results indicated decreased crystallinities of the two polymers due to the interaction between $–CH_2CH_2O–$ and $–CH_2CF_2–$ units of the tangled polymer chains of the hybrid destroying the ordered array of polymer chains. The stress–strain curve of the membranes exhibits acceptable mechanical properties, making them suitable for cell membrane applications. The porosity and electrolyte uptake of the membranes gradually increased with the PEO content of PVDF/PEO nanofibrous membrane, helpful to high ionic conductivity. Pure PVDF-based PGE exhibits an ionic conductivity value of 2.517×10^{-3} S cm^{-1}, which increases with the PEO content for PVDF/PEO membrane-based HPGE showing the highest for the H–F/O-5 membrane.

Fig. 12b shows the variation of ionic conductivity with temperature (T) and the linear plots of HPGEs indicate that conductivity follows the Arrhenius equation: $\sigma = \sigma_0 \exp(-E_a/RT)$. In the figure, an increased slope of the curves from 50 to 65 °C for all HPGEs indicates higher conductivity as the PEO polymer chains tend to melt at ~60 °C, and the presence of more amorphous regions at higher temperatures in the HPGE systems contributed to the higher movement of the conductive ions. The electrochemical stability window of HPGE increased from 4.5 V of pure PVDF to 4.8 V for the H–F/O-2 and H–F/O-5 blends. The compatibility between nanofibrous membranes and liquid electrolyte (LE) and lower leakage of LE afforded better electrochemical stability, suggesting the suitability of HPGE membrane for high-voltage lithium-ion batteries. The electrochemical performance of the prepared HPGE membranes was studied from the charge/discharge tests of Li/HPGE/$LiCoO_2$ cells with the F/O-5 membrane. From Fig. 12c and d, it is clear that the cell at room temperature showed an initial discharge capacity of 171.8 mA h g^{-1} at 0.1C between 2.5 and 4.25 V and it preserved 86% discharge capacity after 60 cycles, indicating good cyclic stability. The PVDF/PEO HPGE assembled into the polymer lithium-ion battery exhibited good cyclic stability.

Vélez *et al.*[98] synthesized a homogeneous inorganic–organic hybrid solid electrolyte based on silica, ethylene oxide network with LiTFSI by sol–gel polycondensation and polymerization of the epoxide. The hybrid membranes of ethylene glycol diglycidyl ether (EGDE) and (3-glycidoxypropyl) trimethoxysilane (GPTMS) exhibited good thermal stability and mechanical properties supporting the practical utility of hybrid electrolyte in LIB. With increasing EGDE content in the hybrid ionic conductivity increases to 2.6×10^{-5} S cm^{-1} at room temperature and it also increases with $[Li^+]/[O]$ ratio, improving up to 0.10 and the best combination of mechanical properties and ionic conductivity was noticed for 50GPTMS-50EGDE $[Li^+]/[O] = 0.10$. The charge–discharge test and good electrochemical stability suggested that these hybrid materials are auspicious materials as solid electrolytes for LIB. SiO_2/polyacrylonitrile (PAcN) nanofiber membranes were prepared using the sol–gel and electrospinning methods and were tested for use in Li-ion batteries.[99] These electro-spun SiO_2/PAcN hybrid nanofiber membranes showed lower interfacial resistance, higher ionic conductivity, and better thermal stability than those of microporous PP membranes. Moreover, by increasing the SiO_2 content, the ionic conductivities and electrolyte uptake capacities were enhanced in SiO_2/PAcN hybrid membrane separators, showing outstanding cycling and C-rate performance. The

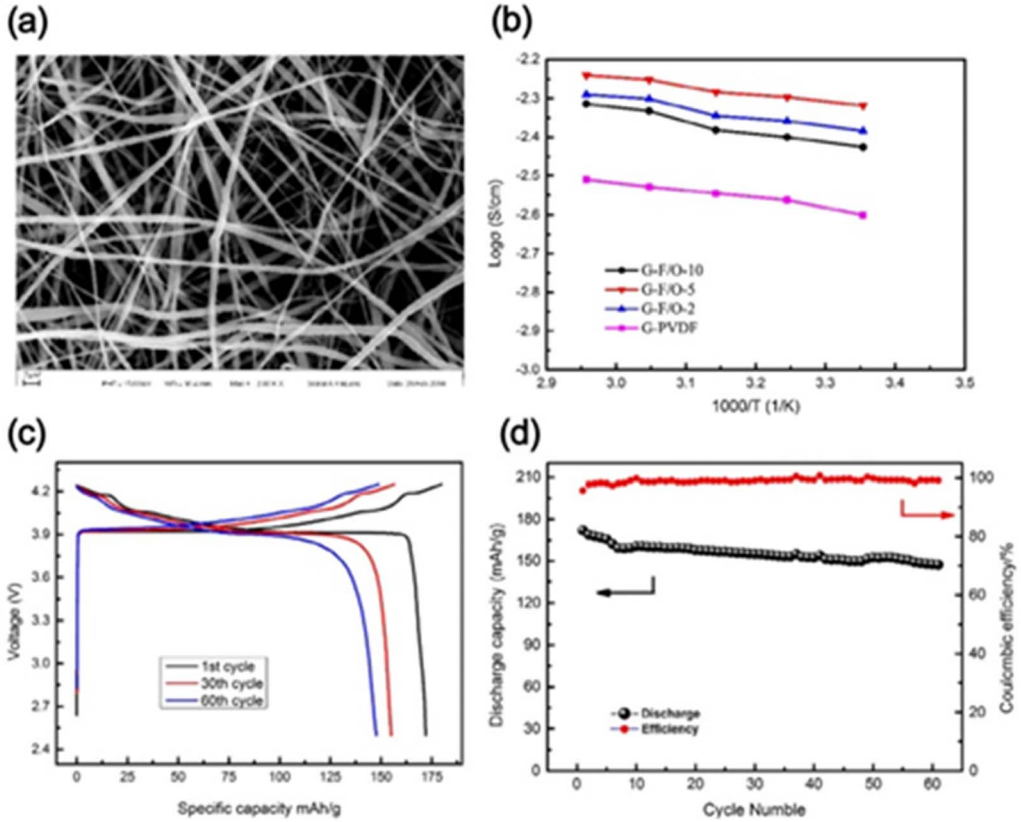

Fig. 12 (a) SEM images of nanofibrous membrane (F/O-5) (b) dependence of ionic conductivity on the reciprocal of temperature for different kinds of HGPEs (c) charge and discharge properties of the Li/HGPE/$LiCOO_2$ cell with H–F/O-5 (d) charge/discharge cycle performance the Li/HGPE/$LiCOO_2$ cell with H–F/O-5. Reproduced from ref. 97 with permission from Elsevier.

results demonstrated that SiO_2/PAcN hybrid nanofiber membranes are very good separators for high-performance LIBs. PVDF dissolved in the DMF/acetone mixture and mixed with TiO_2NPs were electro-spun producing 3D PVDF/TiO_2 nanofibers network.[100] The hybrid polymer electrolyte membrane, prepared by soaking 1 M $LiPF_6$ in EC:DEC (diethyl carbonate), by the composite nanofibers, exhibited high porosity, high electrolyte uptake, and high ionic conductivity from pure PVDF. The PVDF/TiO_2 hybrid electrolyte exhibited higher electrochemical stability as evidenced by linear sweep voltammetry. The PVDF/TiO_2 composite nanofiber polymer electrolyte was found to be very much suitable as the polymer electrolyte for LIBs.

Hybrid gel electrolytes have attracted great attention for their high mechanical strength and superior ionic conductivity. However, the poor interfacial stability between gel electrolytes and Li metal deters their practical applications. To eliminate this issue, Wu *et al.*[101] made a double polymer network gel electrolyte (DPNGE) *via* photopolymerization of the branched acrylate on the P(VDF-*co*-HFP) matrix. This DPNGE exhibited an increased ionic conductivity value of 9.5×10^{-4} S cm^{-1} at 25 °C and a wide range of electrochemical stability till 5.0 V. The systematic analysis indicated the formation of a stable solid electrolyte interphase layer deposition. The rate performances of the Li/DPNGE/$LiFePO_4$ battery showed that at rates of 0.2, 0.5, 1, 2, 3, and 5C (1C = 170 mA g^{-1}), the discharge capacities were 160.1, 153.2, 140.0, 120.2, 97.3, and 57.6 mA h g^{-1}, respectively (Fig. 13a and b).

It is to be noted that the specific capacity of the battery returned to the initial values after returning to 0.2C, indicating that the battery possesses good cyclic stability. The high capacity values at 3 and 5C rates of the battery indicate that DPNGE has the potential for fast-charging batteries. The long-term C under room temperature is shown in Fig. 13c and the first discharge capacity was very high 153.7 mA h g^{-1}, whereas the coulombic efficiency was 98%. The discharge capacity of the battery after 500 cycles was 142.5 mA h g^{-1} and capacity retention was 92.7%. After a long cyclic period, the battery retained a high capacity and coulombic efficiency close to 100%, indicating good compatibility between DPNGE and the electrodes. Thus, a stable solid electrolyte interphase (SEI) layer was formed regulating lithium plating improving the cycle performances.[102] In the previous cycles, the capacity of the battery gradually increased, indicating the gradual formation of a stable SEI layer. The charge–discharge cycles (Fig. 13d) exhibits overpotential between the first charge and discharge platform of 0.21 V, and the voltage difference after 200 and 500 cycles did not change, suggesting that during long-term cycling, DPNGE showed excellent stability. A certain size of DPNGE, lithium belt, and $LiFePO_4$ when assembled into a pouch battery

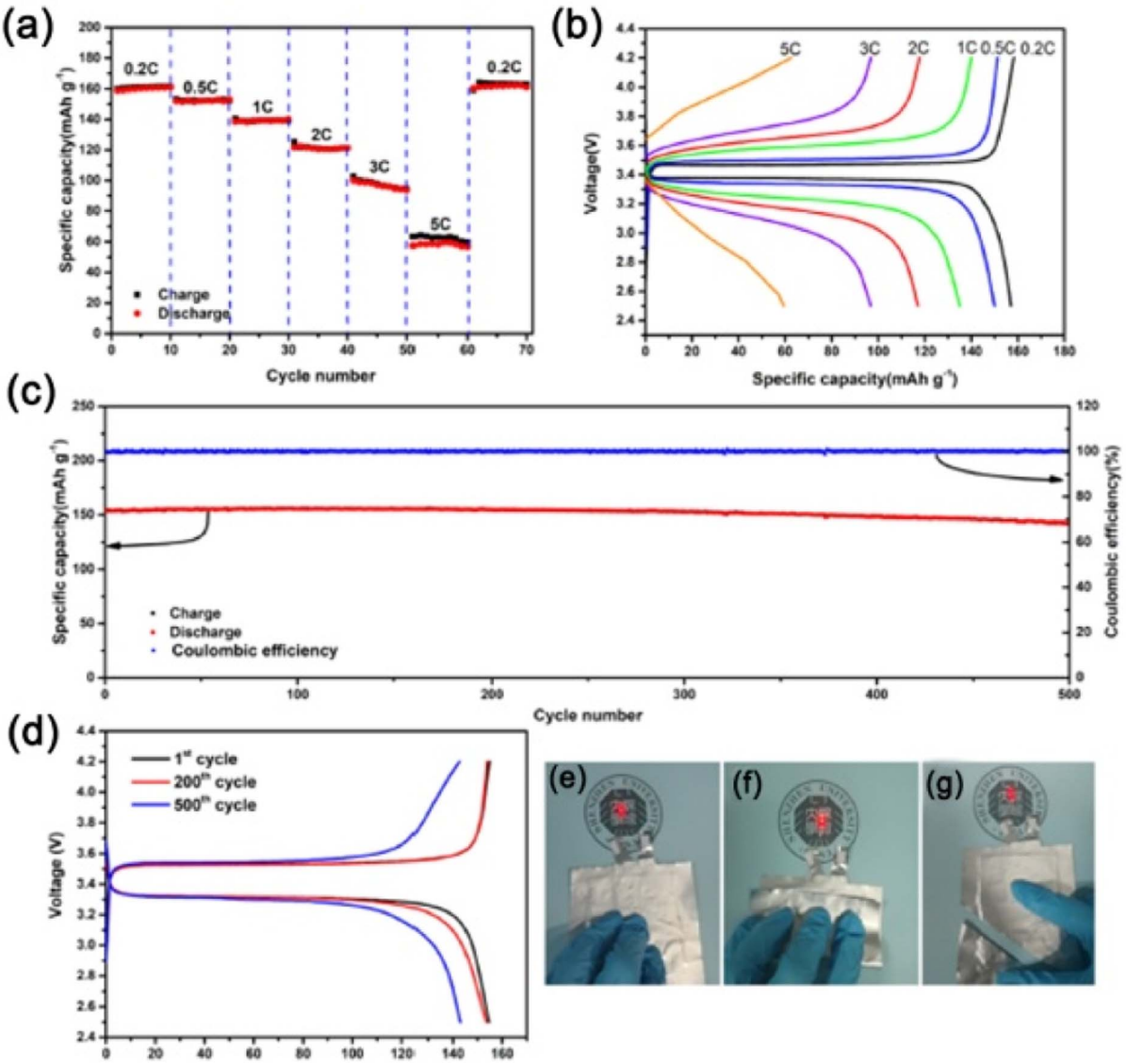

Fig. 13 (a) Rate performance of the Li/DPNGE/LiFePO4 battery (25 °C); (b) charge and discharge curves at different rates; (c) cycling performance at 0.5C rate (25 °C); (d) charge and discharge curves for different cycles; (e–g) performance tests of the Li/DPNGE/Li pouch battery at different states. The flat state (e) of the pouch battery after being folded (f) and being sheared (g). Reproduced from ref. 101 with permission from the American Chemical Society.

(Fig. 13e) showed that the pouch battery could help construct the light-emitting diode (LED), indicating that DPNGE can be used in pouch batteries. Fig. 13f and g show that the battery can make the LED light work normally at the folded and sheared state, respectively. Therefore, DPNGE has a great prospect of application in flexible and wearable solid-state lithium metal batteries.

Lee *et al.*[103] prepared an inorganic–organic hybrid crosslinker by synthesizing a ladder-like poly(methacryl oxypropyl) silsesquioxane (LPMASQ) from a base-catalysed system. Fully condensed LPMASQ revealed good electrochemical (~5.0 V) and thermal (~380 °C) stabilities. LPMASQ also exhibited good solubility in organic solvents and at a very low concentration (2 wt%) it gelled 1 M $LiPF_6$ in ethyl carbonate–diethyl carbonate (EC–DEC, 3/7, v/v) electrolyte through rapid thermal and photo-curing processes. The gelation occurred in the presence of polymeric LPMASQ containing greater than one hundred methacryl units on the rigid double-stranded siloxane backbone. This resulted in high ionic conductivity (~6.0 mS cm^{-1}), brilliant coulombic efficiency, and battery cell efficiency comparable with those of liquid electrolytes. The easy synthetic route of LPMASQ and hybrid PGEs with 2 wt% concentration, showed fast curing kinetics and good Li battery cell performance providing an opportunity towards industrial battery applications. The same group[104] investigated hybrid ionogels of 1 M LiTFSI in *N*-butyl-*N*-methylpyrrolidinium bis(trifluoromethylsulfonyl) imide (BMPTFSI) crosslinked with poly(-methacryloxy propyl) silsesquioxane (LPMASQ) as the ionogel electrolyte at high temperature for use in LIBs. The ionic liquid becomes gel at a low crosslinker concentration (~2 wt%),

showing high ionic conductivities analogous to liquid state ionic liquid. Fabrication of LIBs in these hybrid ionogels showed brilliant cell efficiency at different C-rates and at various temperatures analogous to liquid electrolytes. These hybrid ionogels exhibited exceptional cycling performance measured for 50 cycles at 90 °C, showing 98% coulombic efficiency. These hybrid ionogels, showing high ionic conductivity, thermal stability, non-flammability, excellent C-rate performance, and cyclability provide an opening for applications as high-temperature electrolytes.

Recently, Elizalde *et al.*[105] reported a dynamic, self-healable poly(urea-urethane) gel electrolyte for lithium-ion batteries by synthesizing dynamic cross-linking points based on polyurea thermosets from hindered urea bonds (HUBs), creating a self-healable cross-linked poly(urea-urethane) network by the addition of polyethylene glycol 2000 (PEG2000) referred to as HUB-PU network. This material exhibits self-healable properties and exhibited larger ionic conductivity from the commercial liquid electrolyte implanted in a porous Celgard® 2500 separator. Here, polyurethane gel electrolyte exhibits homogeneous Li stripping and plating in Li symmetrical cells. The polymer gel electrolyte exhibits excellent recovery of the electrochemical properties, after severe mechanical damage of the gel membrane by cutting more than 100 charge/discharge cycles. The specific capacity remained constant and comparable to the initial ones and before the cut, it was 161 mA h g^{-1} and became 159 mA h g^{-1} after the cut. Overall, the results contribute to optimizing and enhancing the execution of covalent adaptable linkages (HUBs) in the solid-state self-repairing materials for LIBs.

Li *et al.*[106] produced a PEO-based polymer electrolyte for solid-state LIBs using chitosan-silica (CS) hybrids as biomaterial-based fillers, which interacted with a polymer matrix to appreciably improve electrochemical performance. The CS hybrid nanoparticles were prepared by a sol–gel method by dissolving chitosan in 0.5% acetic acid to produce 5 wt% CS solution and 0.5 g tetraethyl orthosilicate (TEOS) was added into the chitosan solution and stirred forming homogeneous viscous sols and aged for 2 days, forming the composite gels. The composite gels were purified by immersing them in deionized water and were dried by freeze-drying. The PGE exhibits the highest ion conductivity 1.91×10^{-4} S cm^{-1} at 30 °C at the best mass ratio of CS and PEO 1 : 4 (PCS4). The all-solid-state $LiFePO_4$|PCS4|Li cells showed high coulombic efficiency and very stable cyclic stability, retaining capacity greater than 96.2% at 150 cycles. The broad electrochemical window (5.4 V) and steady interfacial stability promise the above cell for high-voltage battery applications. Here, the interaction between the large number of functional groups of CS and PEO enabled the electrolyte to show excellent electrochemical stability and high ionic conductivity. Also, the introduction of CS reduced the crystallinity of PEO, promoting good lithium-ion migration at the interface of PEO and fillers resulting in excellent cycling performance.

For uncontrollable lithium dendrite growth, lowering of coulombic efficiency and severe safety issue has largely decreased the practical application of LIBs with lithium metal as the anode. Zeng *et al.*[107] successfully prepared a novel single-ion copolymer electrolytes by UV-initiated radical polymerization of lithium bis(macid acid) borate (LiBMAB) and poly(-ethylene glycol) diacrylate(PEGDA) in the presence of PVDF-HFP producing [P(PEGDA-*co*-LiBMAB)@PVDF-HFP (PPLB)]. The homogeneous and transparent PPLB membranes display a low T_g (−50 °C) and high thermal stability. As a result, the copolymer GPE exhibits a large number of Li-migrations (0.65) with a broad electrochemical window (5.05 V *vs.* Li^+/Li at 1 mV s^{-1}) and high ionic conductivity of 1.03×10^{-3} S cm^{-1}. The symmetrical Li/PPLB-GPEs/Li battery runs for 700 h without any short circuit, indicating successful suppression of dendrite formation, and showing good interfacial compatibility between metallic lithium and PPLB-GPEs. The battery also exhibited good cycling performance, with 82% capacity retention, and showed stable coulombic efficiency (∼100%) at 0.5C at room temperature. The results display the broad use of GPEs as electrolytes in LiBs. In another work to avoid the dendrite formation in the Li anode of LIB, Wang *et al.*[108] synthesized GPE (*in situ*) with polyethylene glycol dimethacrylate (PEGDMA) and pentaerythritol tetraacrylate (PETEA). The GPE exhibits high conductivity (7.6 mS cm^{-1}) and high stability and interestingly, the GPE constructs a stable SEI on the Li anode surface showing long cycle life and 90% capacity retention in LiFePO4|GPE|Li battery after more than 500 cycles. Robust SEI formed by cross-linked species in GPE provides a physical barrier to reduce the lithium dendrite formation. The *in situ* polymerization of GPE with a hybrid polymer skeleton would certainly boost the mass production of solid-state Li metal batteries.

3.2.2 Hybrid polymer gels as electrodes in LIBs. The modulation of composite electrode architecture in LIBs is a major concern to improve both ionic and electronic conduction into the electrode to achieve the best energy delivery.

The conventional binder systems in electrodes contain nonconductive polymer binder and carbon additives that suffer from particle aggregation showing decreased electronic and ionic conductivities. To alleviate the problem Shi *et al.*[109] fabricated a 3D nano-structured hybrid inorganic-gel electrode using copper(II) phthalocyanine tetrasulfonate (CuPcTs) with cross-linked polypyrrole (C-PPy) and lithium iron phosphate (C-LFP) particles as a cathode showing high electronic conductivity and good mechanical strength. In Fig. 14a, a schematic presentation on the synthesis of C-LFP supported C-PPy is shown using pyrrole monomers, C-LFP particles, CuPcTs cross-linkers, and ammonium persulfate initiator, where gelation occurs within 1 min. The CuPcT-doped PPy showed a greater conductivity of 7.8 S cm^{-1}. Here the C-LFP particles became uniformly coated by PPy and embedded in the gel framework, forming a 3D nanostructured electrode. The characterization results indicated that the PPy gel framework produced for cross-linking *via* CuPcTs and active particles (C-LFP) are interconnected by the gel network. The rate characteristics of C-LFP/C-PPy hybrid gel measured by charging/discharging at the range 0.2C–30C are presented in Fig. 14b and c. The C-LFP/C-PPy hybrid gel showed greater capacity from the control sample at each current density showing that at a high charge/discharge rate of 30C, the hybrid gel can preserve a capacity of

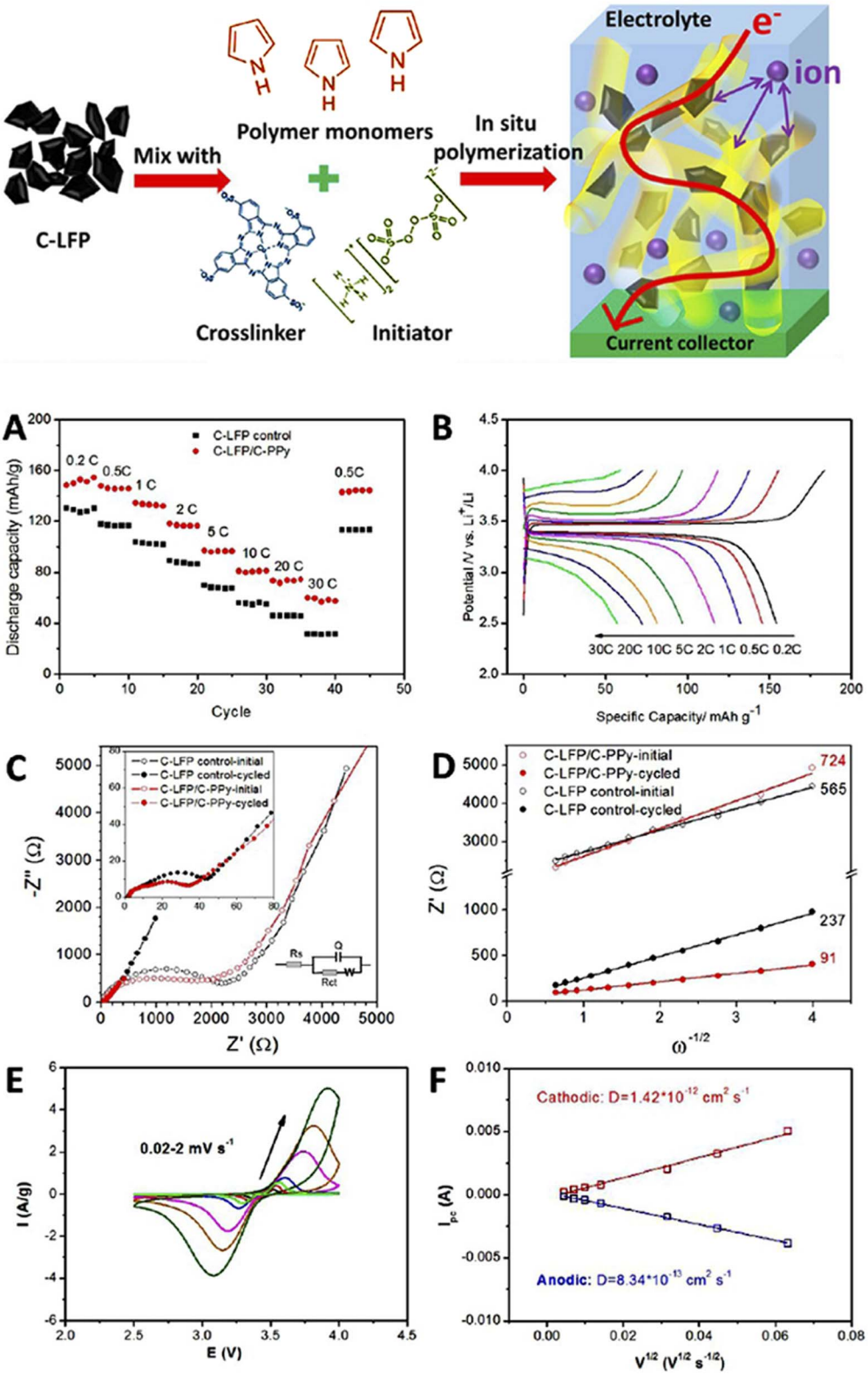

Fig. 14 (a) Schematic of synthetic and structural features of C-LFP/C-PPy hybrid gel framework (b) rate properties of different electrodes (c) voltage profiles of C-LFP/C-PPy hybrid gel framework at different charge/discharge rates (d and e) Nyquist curves and the Warburg plots of different electrodes before and after first cycle (f) cyclic voltammetry profiles of C-LFP/C-PPy, (g) average cathodic and anodic diffusion coefficients of C-LFP/C-PPy hybrid gel framework were calculated from the linear relationship between peak current and the square root of scanning rate. Reproduced from ref. 109 with permission from the American Chemical Society.

~60 mA h g^{-1} while the control C-LFP sample exhibited a capacity lower than 30 mA h g^{-1}. At a back current density of 0.5C, the gel framework recovered a capacity value of ~150 mA h g^{-1} demonstrating better rate capability of the C-LFP/C-PPy hybrid gel network. Impedance spectra were studied to understand the source of the largely improved rate capability of the C-LFP/C-PPy hybrid gel (Fig. 14d). Semicircles in the EIS curves at high-frequency charge transfer resistances of 35.4 and 44.8 Ω were observed for the hybrid gel framework and the control sample indicating that the electrons flow well within the conductive network and met the Li ions at the active sites permitting the charge transfer. The control C-LFP sample and the C-LFP/C-PPy gel framework showed Warburg coefficients 237 and 91 Ω $s^{-1/2}$, respectively, showing better ionic conductivity within the hybrid gel framework (Fig. 14e). The CV curves at various scanning rates of the C-LFP/C-PPy hybrid gel (Fig. 14f) exhibited that peak current was linear to the square root of the perusing rates (Fig. 14g). The average anodic and cathodic diffusion coefficients of the hybrid gel were determined to be 8.34×10^{-13} and 1.42×10^{-12} cm^2 s^{-1}, respectively, about four times higher than those for the control sample. Thus, the EIS and CV results showed that the diffusion of Li-ions in the hybrid PGE is easier in the whole electrode, facilitating improved rate performance in the hybrid gel. Thus, the *in situ* formed smooth polymer coating on the hybrid polymer gel surfaces assisted to retard the inorganic LFP particles from aggregating, thus promoting easier ion and electron transport. The mechanical robustness and chemical stability of the conductive hybrid gel was attributed to the improved cyclic performance of the battery electrode.

Nanocellulose plays an important role to produce flexible electrodes for LIBs, demonstrating superior electrical conductivity, good electrolyte wettability, high specific surface area, and chemical stability.[110] There are mainly four categories of nanocellulose-based materials *e.g.* nanocellulose/polymer composites, nanocellulose/nanocarbon composites, nanocellulose/metal compound composites, nanocellulose/conducting polymer composites. During the course of the preparation of the hybrid from the solution or gels by freeze drying or by electro-spinning methods the three-dimensional hybrid fibrillar net-work structures, characteristic of gels, were produced. To achieve superior electrical conductivity for flexible electrode materials good electrolyte wettability, large specific surface area, and chemical stability are required.[111] Nanocellulose possesses a high Young's modulus value of 130 GPa and high thermal stability making it attractive for electrode fabrication showing good flexibility and mechanical strength. The common active materials for cathodes are $LiCoO_2$, $LiMn_2O_4$, and $LiFePO_4$ in LIBs, but the rate capability and cycling life of these electrodes decrease for structural degradation through repetitive charge/discharge process and for sluggish kinetics for Li^+ and electron transport.[112,113] So, the flexible matrices of nanocellulose is good for producing cathode by making composites with conductive materials to augment the electronic and ionic conductivity of the electrode and to improve the stress/strain for keeping electrode integrity. Wang *et al.*[114] produced an MXene@CNF film by mixing MXene with cellulose nanofibers (CNF) as Li host *via* a spin steaming method. The film showed improved mechanical strength and flexibility. The LIB assembled with flexible (MXene@CNF–Li film) anode with a flexible cellulose nanofiber/$LiFePO_4$ showed high specific capacity and excellent stability. Cao *et al.*[115] made a free-standing lithium titanate (LTO)/carbon nanotube (CNT)/cellulose nanofibre (CNF) network composite film by pressure-controlled aqueous extrusion method. The CNF/CNT combination produced a strong conductive fibrous network and its combination with LTO produced good electronic conductive paths to the low conductive LTO. The flexible anode of LIBs exhibited high-rate cycling performance (142 mA h g^{-1} at 10C). Kuang *et al.*[116] reported a flexible conductive nanofiber network for high-loading thick electrodes, where neutral carbon black nanoparticles were anchored with negatively charged CNFs. Lithium iron phosphate (LFP) integrated with a conductive nanofiber network produced a compact electrode shortening the ion transmission path. This conductive network has interconnected nanopores, which are facilitated to act as a nanoscale electrolyte reservoir, and also provide ion-transport channels surrounding the electrode. The flexible Li-LFP battery exhibited a superior volumetric energy density of 538 W h m^{-3} due to its compact electrode structure and fast charge transfer kinetics. Thus, nanocellulose has great potential in fabricating flexible LIBs for its network entanglement structures, high mechanical strength, and high aspect ratio. Actually, the interface structure and interactions between nanocellulose and active materials play an important role to obtain an electrode with robust mechanical strength, good electrochemical performance, and high flexibility.

Shi *et al.*[117] synthesized a gel electrode by *in situ* polymerization of pyrrole dispersed in water containing Fe_3O_4 NPs (≈20 nm) as active materials and two different kinds of crosslinkers, *e.g.*, (i) phytic acid (named as P-PPy/Fe_3O_4) and (ii) copper(II) phthalocyanine tetrasulfonate salts (CuPcTs) (C-PPy/Fe_3O_4) with ammonium persulfate. The crosslinkers contain multiple functional groups, which interacted with conducting polymer chains, making a 3D network. Due to the protonated nature of the crosslinkers they act as dopants also, affording electrical conductivity in the polymer framework. The Fe_3O_4 NPs active materials were coated and connected in the conductive hybrid gel framework. The rate capability of the control, P-PPy/Fe_3O_4, and C-PPy/Fe_3O_4 samples charged and discharged from 0.1C to 2C (1C = 926 mA g^{-1}) are presented in Fig. 15a.

The capacity of the hybrid gel electrode was 1260, 1002, and 845 mA h g^{-1}, at increasing current rates from 0.1 to 1C, and 2C, respectively. For each current density, hybrid gel samples exhibited improved capacity than the control electrode prepared using a traditional binder system containing acetylene black, Fe_3O_4 NPs, and PVDF with a weight ratio of 15 : 75 : 10. The hybrid gels could retain capacity above 900 mA h g^{-1} while the control could maintain only 500 mA h g^{-1} at 1C as presented in Fig. 15b. At high discharge rates, the plateau appeared around 0.7 V for the hybrid gel electrodes, particularly C-PPy/Fe_3O_4. The enhanced rate capability of C-PPy/Fe_3O_4 could be attributed to the higher conductivity of the network of PPy by CuPcTs doping. Thus, the electrical conductivity of the gel

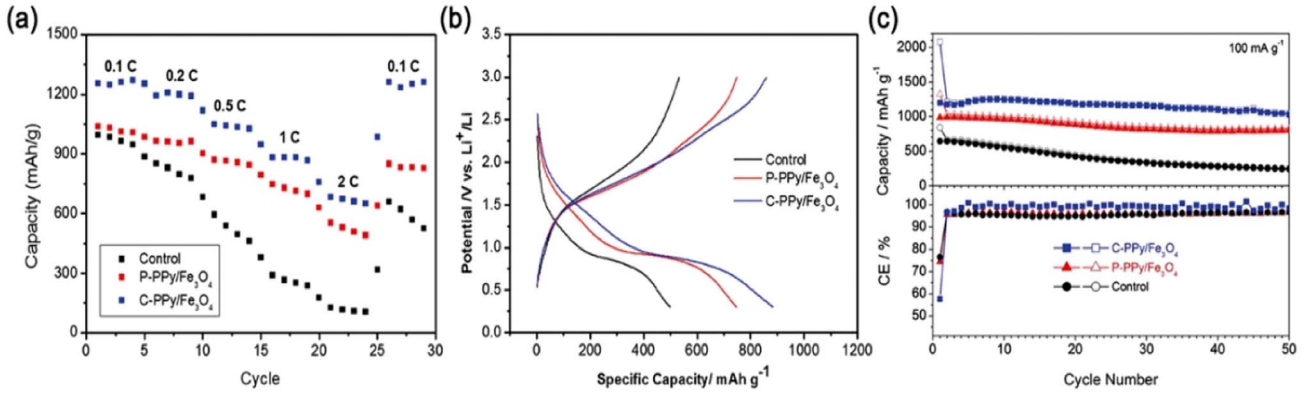

Fig. 15 (a) Rate characteristics of P-PPy/Fe_3O_4, C-PPy/Fe_3O_4, and control samples. (b) Charge/discharge profiles of P-PPy/Fe_3O_4, C-PPy/Fe_3O_4, and control samples at 1C rate. (c) Cyclic characteristics and corresponding coulombic efficiency of P-PPy/Fe_3O_4, C-PPy/Fe_3O_4, and control samples at a current density of 100 mA g^{-1} reproduced from ref. 117 with permission from Wiley-VCH.

framework can be tuned by changing the doping agents. The cycling stability of the gel framework-based electrodes (Fig. 15c), showed that the controlled electrode delivered an initial discharging specific capacity of 850 mA h g^{-1} at 100 mA g^{-1} current density, but after 50 cycles, a capacity of only ~300 mA h g^{-1} was retained, indicating fast decay. But using a 3D conductive polymer gel network, the hybrid electrode P-PPy/Fe_3O_4 showed higher specific capacity and much better cyclic stability with a stable capacity of ≈1000 mA h g^{-1}. It is very important to note that the C-PPy/Fe_3O_4 electrode showed an initial capacity value of ~2100 mA h g^{-1}, much higher than that for the P-PPy/Fe_3O_4 sample. The reason may be the excellent dispersion of Fe_3O_4 NPs in the gel framework resulting in a large interface between the active materials and the electrolyte forming the solid electrolyte interphase (SEI) layers. The CuPcTs showed catalytic functionality promoting the decomposition of electrolytes producing stable SEI layers, and showing higher coulombic efficiency from the second cycle. Thus, C-PPy/Fe_3O_4 hybrid gel electrode retains a good capacity value of 1100 mA h g^{-1} within 50 cycles, showing very good stability. In summary, the distribution of the active particles, the electrode microstructure, and the conductivity play important roles in determining the resulting electrochemical performance. As such, it may be argued that the conductive gel framework can be applied as a talented electrode material for the next-generation LIBs.

3.2.3 Hybrid polymer gels as binders in LIBs. Although different novel electrode materials with good rate capability and capacity are developed,[118,119] the cell efficiency of LIBs decreases with conventional binder systems.[120,121] The mixture of conductive phases does not have the required mechanical binding force for regular distribution, causing poor contact and hindering effective access to parts of the battery (Fig. 16a).[120,121] In an ideal electrode, each active particle is required to be coherently sized, shaped, dispersed, and wired to the collector and to the liquid or solid electrolyte with low-resistance and internal continuous pathways (Fig. 16b).[120,122] Hence the development of novel binder systems providing flexibility, mechanical adhesion, and surface compatibility can improve the dispersity of active particles facilitating both electron and ion transport, which is very much necessary for high-energy, high-power LIBs.[123] In conventional binders, a large volume change occurs during the electrochemical processes experiencing severe problems in ultrahigh-capacity electrodes. These electrode materials produce a large amount of stress, causing electrode fracture, and delamination.[122]

To increase the flexibility and stretchability of the binders, interfacial methods can be used to produce gels since they show improved elasticity for the presence of interconnected microstructure. In this regard, the conductive polymer gels provide multiple functions when applied as the binder materials for LIBs:[123] (i) the hierarchical pores in the gels facilitate ion and electrolyte diffusion, (ii) the conducting pathways connect the active particles continuously facilitative for electron transport, (iii) gel binders provide a uniform coating on active particles preventing particle aggregation and (iv) the robust gel network further provides mechanical strength, chemical stability, and improved long-term stability. Wu *et al.*[124] used the gel binders for the first time in SiNP-based electrodes. A polyaniline (PANI) gel network was prepared by *in situ* polymerization using phytic acid as both, the dopant and cross-linker, encapsulating Si NPs, forming a continuous conductive coating on the Si NPs surface. The electrostatic and hydrogen bonding interaction between PANI and the Si NP surface causes good compatibility between the conductive Si NPs and polymer gels. The PANI gel 3D network acted as continuous pathways facilitating electronic conduction and ion diffusion to occur through its hierarchical pores, resulting in superior rate performance of the electrodes. It showed outstanding stability as the 3D porous framework and a conformal coating layer on SiNPs could lodge the large volume expansion of SiNPs. These types of cross-linked 3D doped conductive polymer gels are potential multifunctional binders for battery electrode materials that are experiencing unstable SEI formation and large volume expansion.

Bao and his coworkers[125] incorporated chemical moieties within the conducting polymers to endorse dynamic

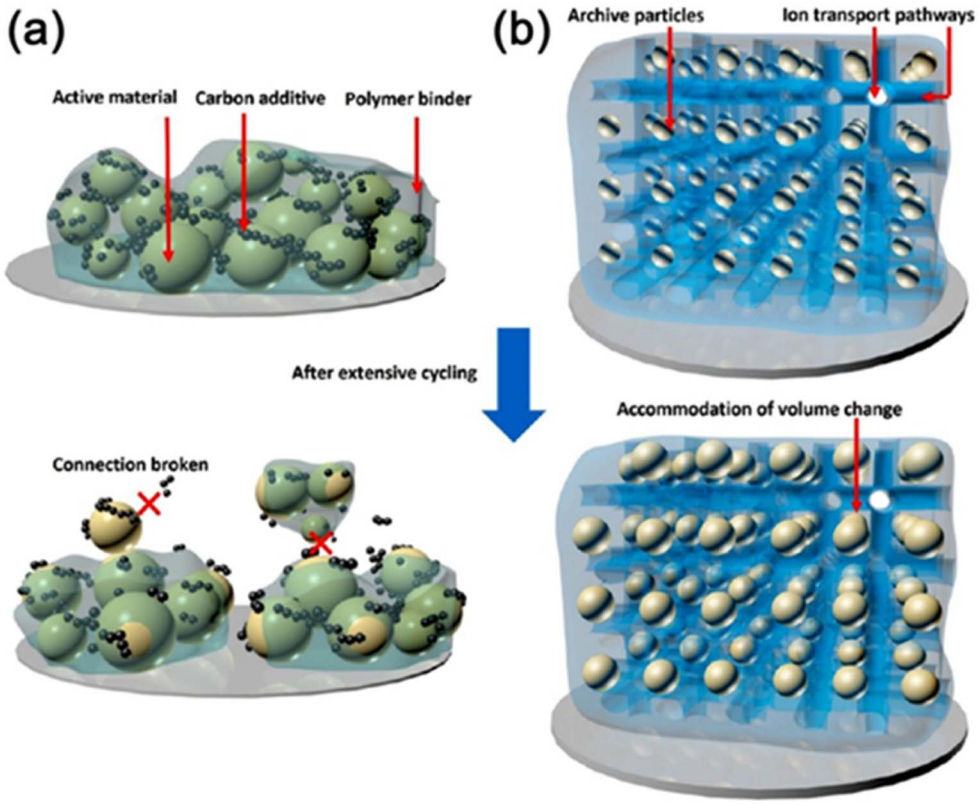

Fig. 16 Schematic illustration of conventional (a) and future battery electrodes (b) for high-energy lithium-ion batteries. Reproduced from ref. 120 with permission from the American Chemical Society.

noncovalent cross-linking, which experiences energy dissipation through bond breaking on the applied strain. The polymer gel showed improved intrinsic stretchability, preserving high charge transport abilities. Hybrid gels based on PPy and poly(*N*-isopropylacrylamide) (PNIPAM) were also produced with a combination of high thermo-responsive sensitivity, high electrical conductivity, and good mechanical properties.[126] These hybrid gels could play an important role in the appropriate modification and device design in the environmentally responsive binder systems, thus producing smart LIBs. The surface properties and conductivity of the binder could be optimized by chemical modification on polymer binders for surface passivation. The structure of PPy, PANI, and PTh conductive polymers could be modified by inserting side chains or functional groups on their backbones, thus modulating electronic structures such as band gap and HOMO/LUMO levels. Also, the surfactants or functional ligands could be incorporated into the active particle surfaces to enhance their chemical and electrical contact with polymer binders.

The unique structural features of the nano-structured hybrid conducting gels are also compatible with industry manufacturing for fabricating scalable solution-based electrodes with gel-based binders. Lithography and 3D printing techniques can be used in the future for developing binders with more ordered microscopic structures to further tune the electron/ion transport pathways and also improve the mechanical properties.

3.3 Hybrid polymer gels in Na-ion battery

The use of Na-ion instead of Li-ion solid-state rechargeable batteries could alleviate the shortage of lithium for the unlimited sources of sodium in nature, its lower price, and the simplicity of its recovery. In addition, for positive electrodes, the intercalation of sodium is very similar to that of Li. Moreover, the growth of a sodium-ion battery with good cell performance might have the benefit of using electrolytes with lower decomposition potential for a higher half-reaction potential of sodium than that of lithium. Thus, the operating voltage is low, making Na-ion cells cheaper, instead of organic electrolytes as water-based electrolytes could be used.[90]

3.3.1 Hybrid gel polymer electrolytes for Na ion batteries. Different kinds of gel electrolytes comprising with a plasticizer of high dielectric constant or its solution with various salts confined with polymer hosts, *e.g.*, poly(vinyl alcohol) (PVA), (polyethylene oxide) (PEO), *etc.* have been reported. The resultant polymeric gel electrolyte facilitates the ionic conduction process, and polymer blending improves the amorphous content by reducing the crystalline content. Thus, Kumar *et al.*[127] obtained a hybrid polymer gel electrolyte containing a polymer blend of PEO and poly(vinyl pyrrolidone) (PVP) complexed with NaF salt with great ionic diffusivity and ionic mobility. The properties of hybrid polymer gel electrolytes (HPGE) could deteriorate with time for the loss of liquid, hence high viscous solvents with ethylene carbonate (EC) or propylene

carbonate (PC) or ionic liquids were used. A sodium ion conducting HPGE was made using the solution of sodium triflate ($NaCF_3SO_3$) in ionic liquid EMI-triflate immobilized with the PVDF-HFP host by Kumar and Hashmi[128] showing high ionic conductivity with a wide electrochemical potential window and excellent thermal stability. The same group also reported nanocomposites of the polymer gel electrolyte of PMMA and silica nanoparticles in a mixture of EC and PC.[129] This filler improved the sodium ion transport and preserved a porous structure facilitating the adsorption of the liquid electrolyte, thus reducing the risk of leakage. The improvement of ionic conductivity depends on the filler concentration along with the amorphous phase content in the polymer host matrix. Wu and his coworkers,[130] reported a porous HPGE from P(VDF-HFP) membrane reinforced by nonwoven polypropylene (PP) and $NaClO_4$ (1 mol L^{-1}) solution in EC/dimethyl carbonate (DMC)/ethyl methyl carbonate (EMC) (1 : 1 : 1 by wt) mixture. The Na^+ conductivity of the HPGE-absorbed $NaClO_4$ solution (0.82 mS cm^{-1}) at room temperature was four times higher than the commercial separator adsorbed with the same electrolyte (0.16 mS cm^{-1}). The tensile strength of the P(VDF-HFP)-PP nonwoven composite significantly improved to nearly that of the commercial Celgard 2730 separator at both wet and dry states. The cyclic voltammetry experiments confirmed that the electrochemical reversibility for $Na_4Mn_9O_8$ cathode based on the as-prepared polymer electrolyte showed great promise for the application of the HPGE for SIBs with high energy density. The same research group[131] also prepared a highly porous polymer membrane of P(VDF-HFP) using a simple phase separation process for Na^+ conducting PGE. They dissolved P(VDF-HFP) in a DMF–water mixture; films were then cast on a glass plate, immersed in a water bath at 80 °C, producing a white porous membrane, and finally dried under vacuum at 100 °C. The dried film pieces were soaked in an organic electrolyte (1 M $NaClO_4$ in EC/DMC) to obtain PGE for SIB. The electrochemical reversibility of the Na/Na^+ couple between the sodium electrode and the polymer electrolyte was confirmed by cyclic voltammetric studies, suggesting that this P(VDF-HFP) based HPGE would be a suitable electrolyte for application in SIBs.

3.3.2 Hybrid polymer gels as the electrode of SIBs. Antimony is widely studied as an anode material for SIBs for its appropriate sodium insertion potentials, high sodium storage capacity, and flat charge–discharge plateau. However, due to the enormous volume change during cycling, it suffers from poor cycling stability. Lin *et al.*[132] prepared hollow NiSb spheres entrapped by the interconnected 3D carbon matrix (NiSb@3DCM) by cross-linking Ni^{2+} and alginate with a galvanic replacement reaction using Ni-polymer gels as the source of 3DCM and Ni. The Ni-polymer gels were made from the biosorption of Ni^{2+} with alginate, which performed the cross-linking reaction with Ni^{2+}-producing gels. Ni NPs remained tightly confined in 3DCM for specific interactions between the polymers and Ni^{2+}, yielding architecturally cross-linked gels on freeze-drying and carbonization in Ar/H_2 atmosphere. The galvanic replacement of Ni with Sb^{3+} produced hollow NiSb alloy, which remained confined within the 3DCM producing Ni@3DCM, with high porosity. These cause NiSb@3DCM to easily lodge the dynamic volume changes, preserving robust morphology and exhibiting outstanding performance, *e.g.* long-term life cycle and exceptional rate capability making an innovative SIB anode material. The storage performance of Na-ion in NiSb@3DCM was monitored by CV and the charge/discharge cycling test. Fig. 17a shows the CV curves at a scanning rate of 0.1 mV s^{-1}, where the first curve exhibits huge differences with the subsequent curves, due to the development of solid electrolyte interphase (SEI). From the second cycle, all the sodiation peaks remained stable at 0.83, 0.56, and 0.38 V.

On the other hand, the anodic peak continuously occurred at 0.76 V, with a small peak at 1.67 V arising from the deintercalation of sodium ions with the Sb layer. The overlapping of all the peaks indicated good reversibility of the process confirmed also by the cycling test at 0.1 A g^{-1} (Fig. 17b). The initial capacity of NiSb@3DCM at 0.1 A g^{-1} current density was 405 mA h g^{-1} and after 100 cycles, the composite exhibited no noticeable deterioration. Integrated with its robust and porous structure together with good carbon coating of hollow NiSb@3DCM, exhibited an excellent rate performance of 248 mA h g^{-1} at 5 A g^{-1}, and a high-capacity retention rate of 94.3% at 1 A g^{-1} after 400 cycles with excellent coulombic efficiency in the half cell of SIBs (Fig. 17c–e). Thus, using the hybrid polymer gel, the as-prepared hollow NiSb alloy entrapped in a porous carbon matrix (NiSb@3DCM) acted as a good anode material suitable for application in energy storage.

Zhang *et al.*[133] used NVP@CNTs to act as the cathode of the SIB synthesized by the sol–gel method using NH_4VO_3, $NH_4H_2PO_4$, Na_2CO_3, and oxalic acid (mol ratio 1 : 3 : 1.5 : 8) in a water–alcohol solution and adding CNTs dispersed in alcohol, and the sol to gel conversion occurred at 80 °C. The gel was made xerogel at 110 °C and annealed at 350 °C in an inert atmosphere to obtain carbon-coated NVP material. Then, by making a hybrid of NVP@CNTs with PVDF and super phosphorus (SP) (NVP@CNTs:PVDF:SP = 8 : 1 : 1 by wt) in NMP, then kept on the Al foil and dried at 110 °C to obtain the NVP cathode. They also prepared an innovative solid-state electrolyte of the PEG/PMA composite with 5% nano-α-Al_2O_3. The above cathode and the new CPE exhibited a good performance showing an ionic conductivity value of 1.46×10^{-4} S cm^{-1} at 70 °C, a high capacity of 85 mA h g^{-1} at 0.5C with retention of 94.1% after 350 cycles facilitating the development of all-solid-state SIBs.

3.3.3 Hybrid polymer gel as the binder of SIBs. Polymer binder in an electrode plays a vital role in the cell's electrochemical performance, cycle life, and irreversible capacity losses. Phosphorus (P) acts as an anode in SIBs but it shows a large volume change above 300% during the charging and discharging process, making it hard to keep the electrode structure. To incorporate the active P-CNT hybrids into electrodes, a polymer binder having a cross-linked gel network structure was exploited by Song *et al.*[134] using an aqueous NaCMC polymer and citric acid (CA) as a cross-linker. The network was made by drying electrodes composed of the P-CNT hybrid, carbon black, NaCMC, and CA at 150 °C and chemical bonding occurred between the –OH group of NaCMC with carboxyl groups of

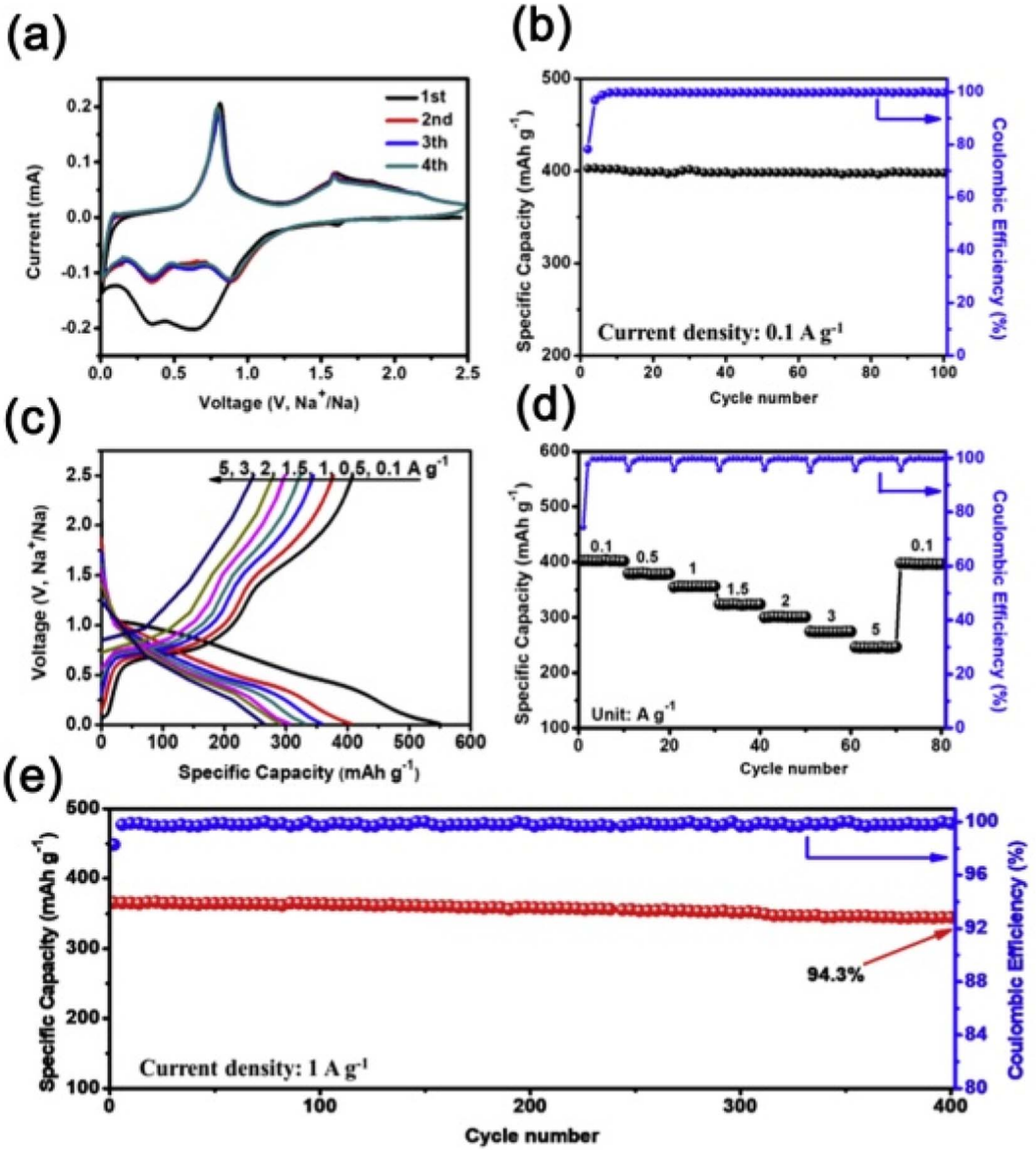

Fig. 17 (a) CV curves of NiSb@3DCM anode at a scan rate of 0.1 mV^{-1} for the first four cycles. (b) Cycling performance of NiSb@3DCM anode at 0.1 A g^{-1}. (c) Discharge/charge profiles of NiSb@3DCM anode at different current densities from 0.1 to 5 A g^{-1} and (d) the corresponding rate performance. (e) Cycle stability of NiSb@3DCM at 1.0 A g^{-1}. Reproduced from ref. 132 with permission from Elsevier.

CNTs. Electrodes composed of P-CNT hybrid, carbon black, and the chemically crosslinked (c-NaCMC)-CA binder (70 : 15 : 15, weight ratio) were used as the working electrodes, electrolyte (1 mol L^{-1} $NaClO_4$ in EC:DEC; fluoroethylene carbonate (FEC), 10 vol%) and sodium was used as the counter electrode for the SIB. This anode exhibited a stable capacity value of 1586.2 mA hg^{-1} after 100 cycles, good initial coulombic efficiency of 84.7%, and a succeeding cycling efficiency of ~99%. The effect of multiple chemical bonding among electrode components can be understood from the schematic diagram (Fig. 18). The P–O–C bond in the P-CNT hybrid allowed close electrical contact between phosphorus and CNT, thus tolerating successive volume changes of the phosphorus upon cycling, facilitating fast electron transfer and improved cycling stability.

3.4 Hybrid polymer gels in other batteries

An ideal membrane in a vanadium redox flow battery (VRFB), should have good chemical stability, low electrical resistance, resistance to a highly oxidizing environment, high permeability to the hydrogen ions, low permeability to polyhalide and vanadium ions, and good mechanical properties. The hybrid polymer gels are good to fulfill this purpose and there is a recent review in this regard.[94] There are many advantages of these sol–gel methods, *e.g.*, they are eco-friendly, have good porosity, excellent chemical stability, and purity, lower processing temperature, easy to form hybrid polymers, and films can be deposited in consecutive layers. The use of the sol–gel technique, the organic part control electrochemical performances, and the inorganic domains improved the mechanical property

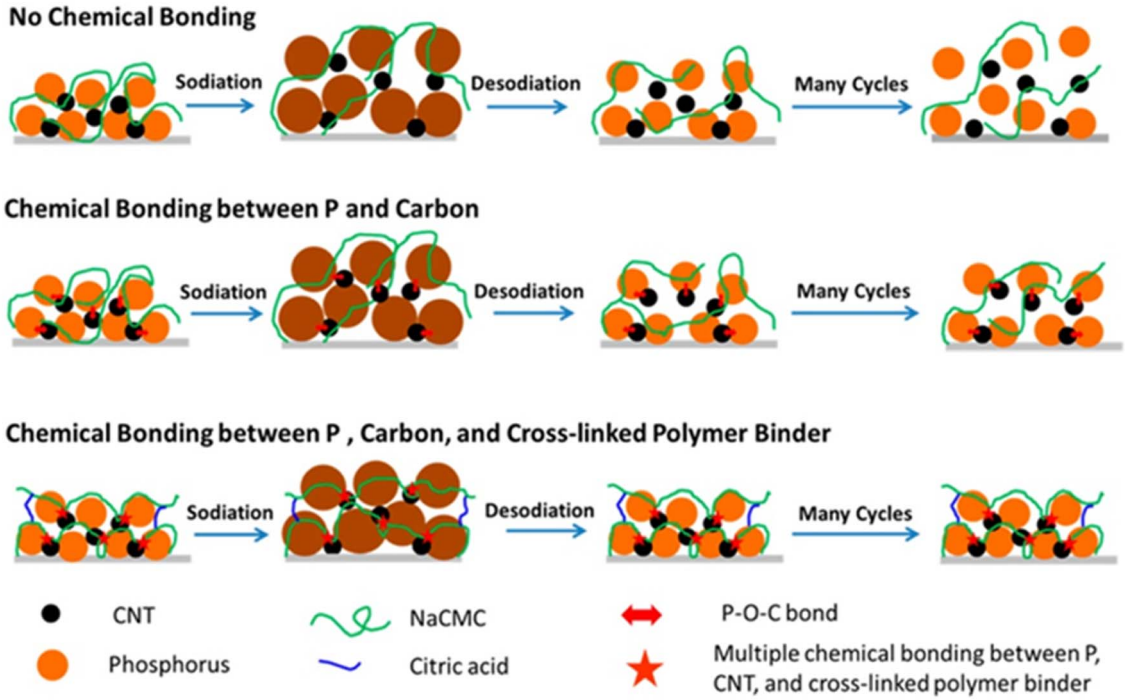

Fig. 18 Schematic illustration of structure evolution of phosphorus-base anode during cycling reproduced form ref. 134 with the permission from American Chemical Society.

of the membrane. Zhang *et al.*[135] developed a cross-linked graphene oxide/Nafion 212 (CLGO/Nafion 212) hybrid membrane where the surface of Nafion 212 was decorated with a large number of amino groups from 3-aminopropyltriethoxysilane using an *in situ* sol–gel chemistry approach, followed by the deposition of a thin layer of *m*-xylene diamino-crosslinked GO by the spin-coating method. From the pure Nafion 212, the modified CLGO/Nafion 212 hybrid membrane exhibited improved potential performance in the VRFB system. Ling *et al.*[136] have reported the charge–discharge performance of Nafion-115 and PVDF/SiO_2–SO_3H membrane prepared using the sol–gel technique at a current density of 50 mA cm^{-2}. The VRFB charge–discharge cycling showed that the hybrid membrane exhibited higher coulombic efficiency (CE, 90.3%), voltage efficiency (VE, 83.5%), and energy efficiency (EE, 75.6%) values compared to those of Nafion 115, which is attributed to the low permeation of vanadium ions through the membrane.

Huang *et al.*[137] recently reported a dual-cross-linked gel solid electrolyte (SE), Zn-reinforced SA–PAM SE (Zn-reinforced sodium alginate–polyacrylamide SE), where Zn^{2+} and Na^{+} coexisted. The tensile and compressive strength of Zn-reinforced SA–PAM SE were considerably improved to 674.28 kPa and 16.29 MPa, respectively, compared to those of the pure PAM gel. The hybrid SE exhibited a high dc-conductivity value of 19.74 mS cm^{-1}. Using the robust electrolyte, they developed a novel hybrid cell with $Na_{0.5}FeFe(CN)_6$–CNT (PB@CNT) as the Na^{+} intercalation-type cathode and metallic Zn as the anode. The hybrid cell exhibited very good stability for 10 000 cycles with a very small loss of capacity 0.0027% per cycle, arising from the prohibition of free water molecules from making low-spinning metallic sites (Fe–C) in $Na_{0.5}FeFe(CN)_6$ by the Zn-reinforced SA–PAM SE. They noticed that the corrosion and dendrites at the Zn^{2+}/Zn plating anode were greatly impeded by the presence of a hybrid robust gel electrolyte. In the zinc ion battery, the water-tempted issues, such as the corrosion reaction and hydrogen evolution, certainly occur on the Zn anode during cycling, which causes poor electrochemical performance. The GPE can reduce the above reactions with water and a biodegradable gum arabic was used by Wu *et al.*[138] to prepare the polymer gel electrolyte for aqueous zinc-ion batteries. The hydrogen-bond between gum arabic and water reduces HER and corrosion. Also in the PGE, the uniform distribution of zinc ions mitigates Zn dendrite growth, and the Zn||Zn symmetric cell with PGE showed a long life of >1300 h, longer than that in the aqueous electrolyte.

The Li–Mg hybrid battery (LMIBs) exhibited high capacity and increased safety but their development was constrained for using toxic and corrosive liquid electrolytes. To eliminate this roadblock, Herzog-Arbeitman *et al.*[139] produced an HPGE with the P(VDF-*co*-HFP) polymer matrix, swelled in 1-ethyl-2-methyl imidazolium bis(trifluoromethyl sulfonyl) imide (EMITFSI) ionic liquid (IL) solution having both lithium bis(trifluoromethyl sulfonyl)-imide (LiTFSI) and $Mg(TFSI)_2$ salts, producing a flexible conductive film. They fabricated a quasi-solid-state Li–Mg battery, using a $LiFePO_4$ (LFP) cathode, Mg anode, and HPGE electrolyte. Ion dynamics within HPGE differed from the bulk IL solutions. The incorporation of the IL into the polymer matrix favors aggregation at the pore center, giving a passage for high mobility at the pore edge. The quasi-solid-state LMIB exhibited a high initial capacity of

141.5 mA h g^{-1} and coulombic efficiencies higher than 90%. The coulombic efficiency of each cycle was almost constant for 100 cycles, indicating that the electrolyte was stable and retained high performance during the extended cycling. A novel PNIPAM hydrogel-based Al^{3+}/H^{+} conductive quasi-solid-state electrolyte was used by Wang *et al.*[140] to produce rechargeable Al^{3+}/H^{+} hybrid-ions battery (HIB) composed of the $Al_XVOPO_4\cdot 2H_2O$ cathode and MoO_3 anode. The above PNIPAM gel electrolyte showed high ionic conductivity and could inhibit the dissolution and volume expansion of the electrode materials, providing an outstanding cycling environment for batteries. Consequently, the HIB delivered a specific capacity of 125 mA h g^{-1} at 0.1 Ag^{-1} and exhibited long-term cyclic stability with almost no capacity decay over 10 000 cycles at 2 Ag^{-1}. The thermo-reversibility of the gel electrolyte, averted the safety problems of the HIB effectively, such as overheating and shorting, and interestingly, the electrochemical performance resumed after cooling down. The exceptional long-term cycling stability and high intrinsic safety of HIB give a future promise for low-cost rechargeable aqueous HIBs. Apart from the Li-ion battery, polymer gel electrolytes are also used in Li–O_2 batteries. Chamaani *et al.*[141] used HPGE using a UV-curable polymer, glass microfillers, tetraglyme solvent, and lithium salt for Li–O_2 batteries. HPGEs with 1 wt% microfillers showed increased ionic conductivity than pure PGEs at various concentrations of lithium salt. Li–O_2 batteries with HPGE exhibited better charge/discharge cycle for 500 mA h g^{-1} cycle capacity with a 400% increase for HPGE at 0.1 mol kg^{-1} over pure PGE. This stabilization during the period of cycling helped increase the cycling life of the batteries. There are some other examples of Li–O_2 batteries using hybrid polymer gels that are provided in a review article.[142]

Thus, the use of hybrid polymer gel electrolyte not only increases the mechanical stability but also induced cyclic stability improving the cell performance. The hybrid polymer gels are useful for all types of batteries such as Li^{+}, Na^{+}, vanadium, hybrid ion, Li–O_2, and Li salt batteries. Furthermore, they are useful as electrolytes, electrodes, and binders in all solid-state rechargeable batteries to improve the cell performance, cyclic stability, and intrinsic safety of the batteries. The use of different polymer gels (physical, chemical) is thus highly increasing to meet the overwhelming demand for green energy for different sectors from different miniature electronics to heavy vehicles.

There are many advantages of the sol–gel method of making HPGE for batteries, *e.g.*, they have good porosity, lower processing temperature excellent chemical stability and purity, layer-by-layer deposition of the films, and are eco-friendly. The organic part of sol–gel material control electrochemical performances, and the inorganic part reinforces the mechanical property of the membrane. This is because the high porosity of the membrane can easily cause dynamic volume changes as it afforded great ionic diffusivity and ionic mobility, preserving robust morphology. This results in outstanding electrochemical cell performance, *e.g.*, long-term life cycle and exceptional rate capability. Lithography and 3D printing techniques can be applied for developing more ordered microscopic structures to tune the membrane, electrode, and binder properties. The polymer gel showed improved intrinsic stretchability, flexibility, and bending ability preserving high charge transport abilities. Due to the presence of a three-dimensional network, hybrid conducting polymer gels exhibited high electrical conductivity and good mechanical properties and could accommodate large volume expansion making it an ideal architecture for the ion movement occurring during the electrochemical process. In the battery electrode materials, a large amount of stress is produced, causing electrode fracture and delamination for the conventional binder systems in electrodes. Nonconductive polymer binders and carbon additives suffer from particle aggregation showing decreased electronic and ionic conductivities. In this respect, conductive polymer gels as binder materials provide multiple functions, *e.g.*, (i) hierarchical pores of gels help the electrolyte and ion diffusion, (ii) provide a uniform coating on active particles preventing particle delamination (iii) the conducting pathways connect the active particles continuously making easy electron transport, and (iv) the robust gel network further provides mechanical strength, chemical stability and improve long-term stability. The interconnected nanopores in the gels act as a nanoscale electrolyte reservoir, and also give ion-transport channels surrounding the electrode. An important drawback of the polymer gel electrolyte is the poor interfacial stability between the gel electrolytes and Li metal hindering their practical application. The porosity and electrolyte uptake of the membranes gradually increased the interfacial stability, yielding high ionic conductivity. The self-healing polymer gel electrolyte exhibits excellent recovery of the electrochemical properties, after severe mechanical damage of the gel membrane by cutting and it can work in the folded and sheared states. Thus, hybrid gel electrolytes have attracted great attention in energy storage devices for their high mechanical strength and superior ionic conductivity.

4 Supercapacitors

The supercapacitor is an alternative mode for electrochemical energy storage (EES) other than batteries. Here, energy storage occurs *via* the ion storage on the electrode surface followed by instantaneous polarization either through electrostatic interactions (EDLC) or redox electron transfers between the electrode surface and electrolyte ions at their interfaces (pseudocapacitance).[143] Thus, supercapacitors allow rapid charging–discharging leading to high power density and long cycle life as the ion storage is a surface or near-surface phenomenon; appreciable stress is not induced on the electrode material during charging or discharging processes.[144] Despite offering manifold greater power density than batteries, the exposed surface area of the supercapacitors is usually not very high during applications and they suffer from the problem of lower energy density. This remains a big challenge in the way of widespread applications of supercapacitors in the future replacing batteries (particularly during applications requiring high power supply) as the latter modules suffer from poor power density despite having attractive energy density parameters.[145] Thus, the worldwide energy research community is currently

devoting its central attention to designing energy storage devices, which should have battery-like energy density with supercapacitor-like power density sensing the complementarity in the deliverables of these two EES modules.[146] This has paved the way for the generation of hybrid supercapacitors having one battery-like electrode (operating through the diffusion-controlled redox processes offering bulk charge storage) and the other supercapacitor-like EDLC-based electrode most commonly made up of carbon materials.[147] Further development in this regard is the double hybridization strategy as has been pointed out by Dubal *et al.* where the battery-like electrode is also a composite of the battery electrode material and highly conducting electrochemical double-layer capacitor material so as to match the rate of ion accumulation–deaccumulation in both electrodes and also to improve the conductivity of the composite electrode material (Fig. 19).[147]

Nanostructuring of the electrode has remarkably improved the deliverable electrochemical performances of the supercapacitor or the battery electrodes.[148,149] However, further development in technological as well as material chemistry parts is required to reflect the development of the intrinsic material properties at the commercial device scale (usually requiring much greater mass loading of the electrode material).[150] This can be obtained *via* the prudent design of the electrode material particularly when flexible energy storage device generation is in focus. In this regard, solid state supercapacitors having flexible electrode material and gel electrolyte or 'all-in-gel' model where both the electrodes and electrolytes are gel materials gaining increased attention.[151] Application of the 'all-in-gel' strategy helps to alleviate the contact problem at the electrode/electrolyte interface along with better adhesion with the current collectors eliminating the use of typically non-conductive/less conductive adhesive materials. This strategy is definitely very much beneficial in respect of improved conductivity, lightweight, and improved electrochemical properties of the assembled cell, particularly when conductive gel materials are used. Furthermore, the use of gel electrode materials can better withstand the volume change during the charging/discharging cycles of battery electrode materials (Fig. 20).[152] The following sections give a rather concise account of exciting research efforts recently made in this direction.

4.1 Hybrid polymer gel electrodes for supercapacitors

Alshareef and coworkers[153] reported a solid-state asymmetric supercapacitor by electrochemically depositing PANI and PEDOT over Au-coated polyethylene naphthalate (PEN) substrates acting as negative and positive electrodes, respectively, while using PVA/H_2SO_4 gel electrolyte. The device exhibited the highest power density of 2.8 W cm^{-3} at the energy density value of 9 mW h cm^{-3} and the fabricated tandem asymmetric supercapacitors were found to be suitable for powering a red-light emitting diode for 1 minute after 10 seconds of charging. An all-solid-state supercapacitor using electrodes of CNF/RGO/CNT hybrid aerogels and PVA/H_2SO_4 gel electrolyte was reported by Zheng *et al.*[154] The flexible supercapacitors were made without a binder, electroactive additives, and current collectors. The outstanding electrolyte absorption behavior of the CNFs and porous structure present in the CNF/RGO/CNT aerogel electrodes resulted in a high capacitance (252 F g^{-1} at discharge current density of 0.5 A g^{-1}) with amazing cyclic stability (>99.5% capacitance retention after 1000 cycles at a current density of 1 A g^{-1}). Vlad *et al.*[155] reported carbon redox-polymer-gel hybrid supercapacitors by compositing pseudocapacitive poly(2,2,6,6-tetramethyl-1-piperinidyloxy-4-yl methacrylate) (PTMA) with high surface active carbon (~2,000 m^2 g^{-1}) and carbon nanotubes. In this work, the surface-active carbon-CNT mat was flooded into a PTMA gel to produce a hybrid composite electrode. The hybrid gel electrode exhibited nearly ideal properties such as high ionic and electrical conductivity, fast surface and redox charge storage, and amazing cyclic stability. The fabricated carbon hybrid redox-polymer-gel electrodes displayed an extraordinary discharge rate of 1000C with 50% of capacity delivered in <2 seconds. In order to maintain good contact with the electrode and gel electrolyte at their interfaces Wang and coworkers.[151] prepared a new "all-in-gel" supercapacitor using two IL-based Bucky gel electrodes separated by an ionogel composite electrolyte (utilizing the same IL). The so-called Bucky gel, a gelatinous electrode material was prepared by grinding either short single-wall carbon nanotubes (SWCNT-s) or multi-wall carbon nanotubes (MWCNT), or long single-wall carbon nanotubes (SWCNT-l), acetylene black (AB) 1-ethyl-3-methylimidazolium tetrafluoroborate ($EMIMBF_4$), and PVDF-HFP. It has been further argued that the ionic liquid interacts well with SWCNTs with interactions like π–π and/or cation–π of imidazolium ion component of ionic liquid. The fabricated supercapacitor device showed improved electrochemical properties (49 mF cm^{-2} capacitance at 0.1 mA cm^{-2}), better self-healing property as well as mechanical robustness. Conducting polymers have drawn significant interest in the last 2 to 3 decades as electrode materials in energy storage devices owing to their fast and reversible electron transfer processes along with appreciably high conductivity. Easier synthesis of conducting polymers allowed their preparation in different morphologies and hence exploited their microstructure-dependent properties. Conducting polymer films of various morphologies have already received significant attention for being used as the electrodes of flexible supercapacitor/battery devices owing to their high flexibility. However, despite high flexibility and pseudocapacitance, conducting polymer-based electrodes suffer from the problem of rapid decay in capacitance and poor cyclic stability because of a high volume change during the electrochemical processes. In this regard, conducting polymer gels having a 3D network structure is very much beneficial as interconnected conducting polymer chains provide pathways for electron transfer, small ion diffusion pathways, and a high surface area for redox reactions. Furthermore, the gel structure can better accommodate the volume changes during electrochemical reactions. Recently, conducting polymer gels are being prepared by following two strategies, either (i) integrating with traditional gel materials to exploit the best of their mechanical, electrochemical, and self-healing properties or (ii) pristine conducting polymer-based gels prepared using cross-linkers, which are at

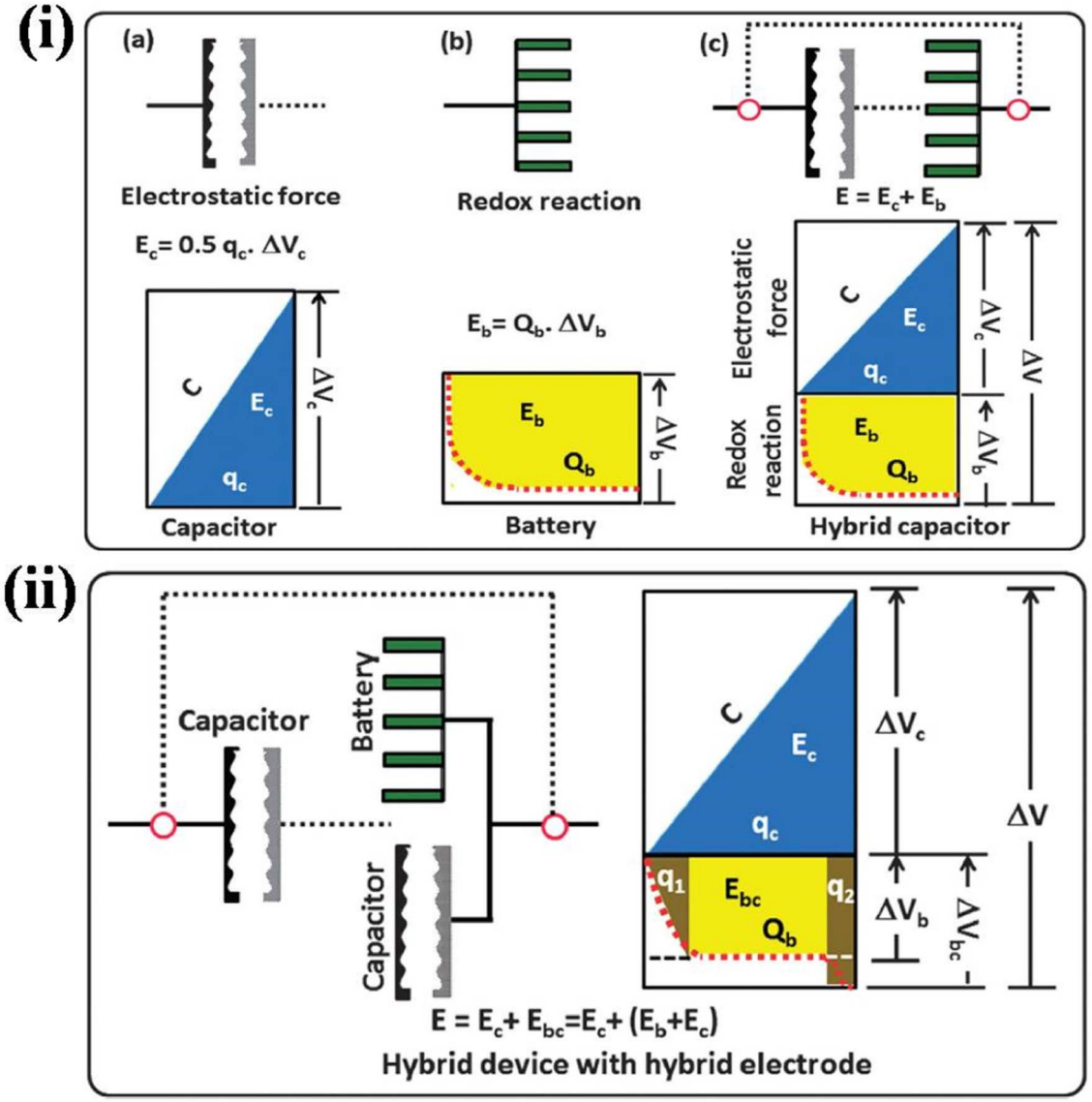

Fig. 19 Schematic representations of (i) a single electrode system (a), capacitor (b) battery and (c) an asymmetric capacitor system with an aqueous electrolyte according to the charge–potential profile with corresponding equations for energy storage; (ii) hybrid combination of a hybrid electrode (hybridized battery and capacitor components) and a capacitor electrode according to the charge–potential profile with corresponding equations for energy storage. Reprinted with permission from ref. 147, with permission from Royal Soc. of Chemistry.

the same time dopants helping to have improved conductivity. Another approach is the preparation of the conducting polymer-based hybrid hydrogels where the active electrode materials remain embedded within the gel. Such hybrid gels can act both as the electrode and binder replacing nonconductive binder materials. The active electrode materials remain interconnected in the 3D conducting polymer gel network structure, furthermore, the conducting polymer chains and ion channels help to maintain improved contact and electronic/ionic conduction with the current collector materials. A large number of research efforts have already been documented in this field, and the following gives a brief account of some exciting research.

The journey of conducting polymer gel-based electrodes for supercapacitors began in 1999 when Ghosh and Inganäs[156] reported the synthesis of highly swelled conducting polymer gels consisting of crosslinked PEDOT-PSS colloidal particles offering nano-dimensional conductive networks having large surface area. Indeed, this has been an important milestone in the context of the development of flexible supercapacitor devices. This was followed by several reports on the preparation of CP hydrogels, including PPy, PANI, and PEDOT hydrogels, for supercapacitors. Preparation of PANI hydrogels[157] was carried out using different multiple hydroxyl groups containing cross-linker cum dopants as phytic acid or amino trimethylene phosphonic acid (ATMP)[157,158] (Fig. 21a–c).

In every case, the improved electrochemical properties were reported for the presence of large surface area, hierarchical 3D porous structure, and high electrical conductivity. The spray-

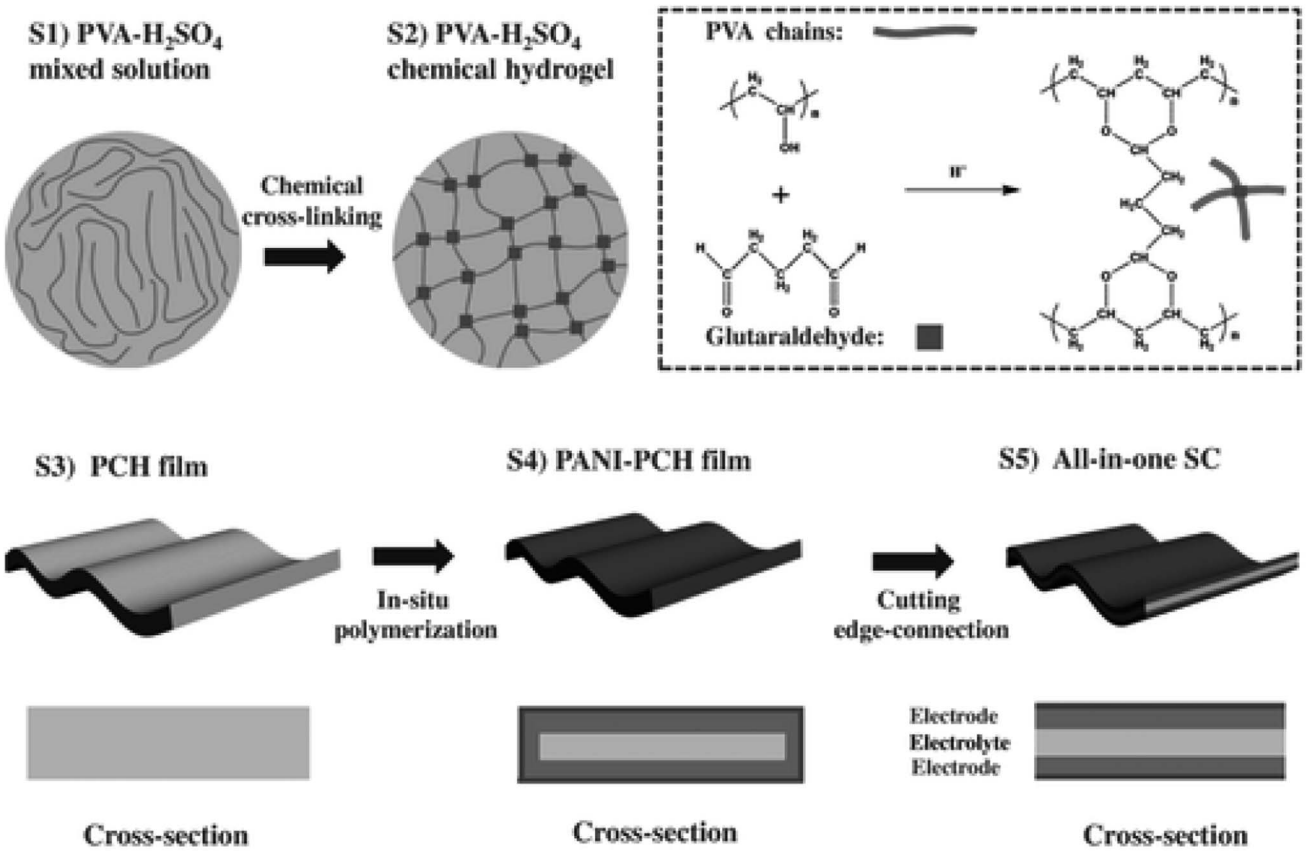

Fig. 20 (S1) The PVA-H_2SO_4 blended solution. The blue solid lines represent PVA polymer chains with a random alignment. (S2) The PVA-H_2SO_4 chemical hydrogel (PCH) produced by adding glutaraldehyde (GA), which acts as a crosslinking reagent, to form 3D network connections with multiple junction zones. (S3) The free-standing PCH film was cast by a mould-casting or blade-coating process. (S4) PANI was grown *in situ* on the PCH film. (S5) The edge-connections of the PANI layers on a PANI-PCH film were cut to obtain an all-in-one supercapacitor (SC). Adapted from ref. 152 with permission from Wiley.

coated or ink-jet printed phytic acid-doped gel material exhibited a high conductivity value of 0.11 S cm^{-1}. Furthermore, the supercapacitor electrodes from PANI hydrogel exhibited a high specific capacitance value of 480 F g^{-1}. In another independent study, a hierarchically 3D nanostructured elastic PPy hydrogel was also prepared using the same cross-linker and dopant (phytic acid or ATMP) *via* the oxidative polymerization of pyrrole at the interface of water/isopropanol. The prepared PPy hydrogel showed an appreciably high conductivity of 0.5 S cm^{-1} in the xerogel state with a high elasticity and mechanical strength striking for flexible supercapacitors. The flexible symmetric PPy hydrogel supercapacitors prepared with high mass loading of 20 mg cm^{-2} exhibited a high areal capacitance value of 6.4 F cm^{-2} along with a good cycling stability[159] (lower than 7% capacitance degradation after 2000 cycles). However, incorporating non-conducting cross-linkers could diminish the electrical conductivity of the PANI gel therefore, self-cross-linked PANI hydrogels were likewise made by a sol–gel method using the aniline monomer and APS oxidant.[160] This led to the formation of 3D porous PANI hydrogel having a coral-like morphology of ramous nanofibers. The microstructure of the PANI hydrogel is very much favorable for the electrochemical performance enhancement and with no surprise, the PANI hydrogel electrode showed the highest specific capacitance of 750 F g^{-1} at 1 A g^{-1} current density. Zhou *et al.* prepared a hydrogel of PANI nanofibers using $V_2O_5 \cdot nH_2O$ as both a hard template and oxidizing agent by *in situ* polymerization.[161] The oxidant template-assisted preparation of PANI nanofibers endorsed the cross-linked 3D assembly of PANI hydrogel with high conductivity (0.12 S cm^{-1}) and capacitance values of 636 and 626 F g^{-1} at current densities of 2.0 and 25 A g^{-1}, respectively, with remarkably large capacitance retention of 83.3% after 10 000 cycles. This oxidant-templating methodology is useful for the preparation of PEDOT or PPy hydrogels having porous conductive tracks. In order to improve the flexibility and mechanical properties of the pristine conducting polymer hydrogels, various hybrid CP hydrogels have been developed as electrode materials for flexible supercapacitors. The most commonly used flexible substrate in this regard has been the PVA-based hydrogels[162–164] while poly(acrylamide)(PAAM),[165,166] graphene oxide/graphene,[167,168] sodium alginate[169] and G-Zn-*t*Py[170] have also been used for the same purpose. The stretchability, foldability, compressibility, and self-healing properties are promising for applications in portable/wearable electronics. In a very much interesting report, a supramolecular strategy was introduced to crosslink PVA and PANI through dynamic

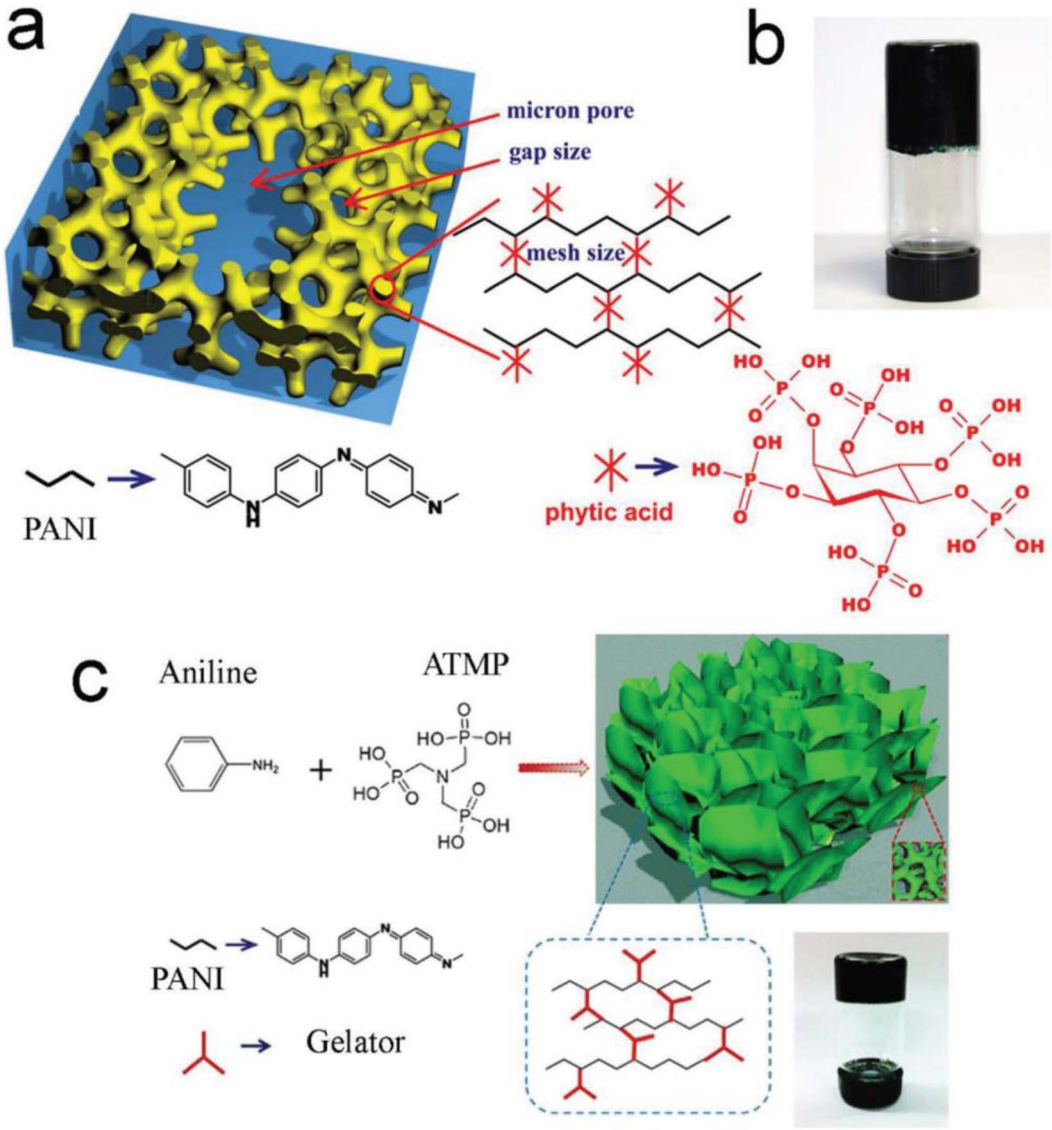

Fig. 21 (a) Schematic illustrations of the 3D hierarchical microstructure of the gelated PANI hydrogel where phytic acid plays the role as a dopant and a crosslinker. Three levels of hierarchical porosity from angstrom, nanometer to micron size pores have been highlighted by red arrows. (b) A photograph of the PANI hydrogel inside a glass vial. Reproduced from ref. 157 with permission from National Academy of Sciences, USA. (c) Schematic illustration of the formation of the 3D hierarchical nanostructured PANI hydrogel and a photograph of the PANI hydrogel inside a glass vial. Reproduced from ref. 158 with permission from Springer.

bonding,[162] where 3-aminophenylboric acid (ABA), having both boronic acid and amino groups was copolymerized. The synthesized PANI containing functional monomer repeating units were crosslinked with PVA by the condensation reaction of –OH. The resultant hydrogel exhibited a conductivity (0.1 S cm^{-1}), along with high mechanical properties such as tensile strength (5.3 MPa), elongation at break (250%), and high compress stress (30 MPa), analogous to other hydrogels.[171–176] The flexible supercapacitors constructed using PANI/PVA composite hydrogel electrodes exhibited high electrochemical properties such as capacitance 306 mF cm^{-2} (153 F g^{-1}), high energy density 13.6 W h kg^{-1} along with 100% and 90% capacitance retentions after mechanical folding and charge–discharge cycles of 1000 times, respectively. The conductive hybrid hydrogel containing cross-linked rigid and soft polymer chains with a mesoporous structure was attributed to the remarkable observed properties. In a different approach, using vapor phase polymerization Zang *et al.* produced PPy/PVA hybrid hydrogels of PPy in the 3D crosslinked network of PVA.[164] The interpenetrating network structure of PPy chains within the PVA gel framework resulted in high mechanical strength and good electrochemical performance in flexible supercapacitors fabricated with this electrode material. Further improvements in electrical and mechanical properties were reported in PANI/graphene hybrid hydrogels made by hydrothermally treating a PANI dispersion.[167] An appreciably large areal capacitance value of 484 mF cm^{-2} with an energy density of 42.96 mW h cm^{-2} was reported in a flexible solid-state

supercapacitor based on this hybrid hydrogel electrode.[168] It is highly desirable to develop "all-in-one" flexible high-performance supercapacitors for wearable electronics maintaining a crease-free electrode–electrolyte assembly even when a large number of stretching or bending motions are applied to them. In this context, Wang *et al.*[152] reported a very interesting strategy where an integrated supercapacitor device was fabricated by embedding two PANI layers (acting as electrodes) in a 3D porous PVA-H_2SO_4 hydrogel film acting as the solid-state electrolyte. In this, 'all-in-one' strategy, the surface and sub-surface of the PVA-H_2SO_4 hydrogel film coated with 40 μm thick PANI film was made by *in situ* polymerization. Thus, the entire material served as both the electrolyte and electrode for flexible supercapacitors, exhibiting a remarkably high areal capacitance value of 488 mF cm^{-2}, along with outstanding cyclic stability and flexibility. In another approach, Xu, Dai, and coworkers suggested a simple and universal strategy for manufacturing flexible supercapacitors with a three-dimensional hybrid structure.[177] They designed a universal loader type having a three-dimensional hybrid structure where acetylene black and active material (as per the demand) were enriched in the PVA matrix. The basic loader itself is an electrode with good electrochemical as well as mechanical performance and offers further possibilities for the development of more powerful, flexible electrodes in an easy and accurate way following the same steps. Loading the active polyaniline/carbon nanotube composite material in this basic electrode delivered non-negligible surface capacity (*e.g.* 1.1 F cm^{-2} in surface capacitance) with good response, rate performance, excellent durability (10 000 times of charge–discharge), and good foldability (1000 times of folding).

There are some interesting reports where conductive polymer gel-embedded active nanostructured electrode materials have been used as scaffolds and binders for the construction of flexible supercapacitors or batteries. Nandi *et al.*[178] reported the synthesis of folic acid-PANI 3D network hydrogel (FP) material having acceptably high mechanical properties as well as a good electrical conductivity of 0.04 S cm^{-1}. The obtained gel material exhibited a good specific capacitance of 295 F g^{-1} (at 1 A g^{-1}), which has been attributed to the relatively high surface area (238 m^2 g^{-1}) and interconnected 3D porous network of the gel electrode material. In the next step silver nanoparticles (AgNPs) were elegantly grown inside the gel matrix, which resulted in remarkable improvements in electrical conductivity (reached 0.21 S cm^{-1}), specific capacitance (as high as 646 F g^{-1} at 1 A g^{-1}), brilliant rate capability (62% capacitance retention at 20 A g^{-1}) and high cycling stability. Not being limited to the improved energy storage performance, Ag NP-embedded 3D FP hydrogel also resulted in significant improvement in photocurrent (increased from ~2 mA in FP gel to 56 mA in Ag NP-embedded FP gel). The observed improvements were attributed to the possible interactions between the plasmons of AgNPs and the polaronic band of the doped PANI. In another interesting work, the same group reported MoS_2 quantum dot (QD)/PANI (DMP) hydrogel where MoS_2 QDs were embedded into a 3D fibrillar network. An all-solid-state symmetric supercapacitor was fabricated by directly loading the hybrid gel electrode material over flexible graphite paper with PVA/H_3PO_4 gel material resulting in high electrochemical properties as a specific capacitance of 331 F g^{-1} (at 1 A g^{-1}), energy density 29.4 W h kg^{-1}, and a power density 398 W kg^{-1} along with 84.2% capacitance retention after 10 000 charge–discharge cycles (Fig. 22).[179] A similar strategy has been applied in nanoparticle-based lithium-ion batteries where polypyrrole-embedded high-capacity Fe_3O_4 nanoparticles were used as the electrode. These 3D hybrid polymer electrodes exhibited higher capacity at higher charge/discharge rates than 2D electrodes.[117] The high electrical conductivity of the PPy conductive framework, uniform dispersity of nanoparticles, and robustness of the polymeric scaffold to withstand the mechanical stress during cycling have been attributed to the observed improvement. Furthermore, there are several other reports and reviews where the application of the 3D conductive polymer framework as scaffolds for anode or cathode has resulted in significant improvement in the deliverables of lithium-ion batteries.[109,124,180–182]

4.2 Hybrid polymer gel electrolytes (HPGE) in supercapacitors

In energy storage devices, liquid electrolytes (LE) play an essential role by the virtue of their high conductivity (10^{-3}–10^{-2} S cm^{-1}) and fruitful contact with electrodes. However, safety issues such as leakage or combustion in the case of organic electrolytes or the inevitable growth of lithium dendrites in the case of lithium batteries put major concern over the use of LEs. This has triggered significant research efforts to develop solid-state or gel electrolytes. Nevertheless, these electrolytes also suffer from major issues such as poor ionic conductivity (10^{-8}–10^{-5} S cm^{-1}) and meager interfaces with electrodes causing worsened cyclic performance.[183–186] Polymer gel electrolytes (PGEs) have the advantages of both liquid electrolytes as well as solid electrolytes having improved mechanical properties. Furthermore, the flexibility and elasticity of PGEs can accommodate the volume change of electrode materials and dendrites of lithium metal through the electrochemical charging processes.[187–190] This has generated global attention over PGEs as electrolytes for various electrochemical energy storage devices such as lithium-ion batteries (LIB), supercapacitors (SC), lithium–oxygen (Li–O_2) batteries, sodium-ion batteries, zinc–air batteries, and lithium–sulphur batteries.[191–193] To meet the necessity of the general devices for flexibility and deformability, more special PGEs with tough,[194] stretchable[195] and compressible[196] functionalities have also been developed. The existing types of gel electrolytes may be categorized as follows: (i) aqueous polymer gel electrolyte, (ii) non-aqueous polymer gel electrolyte, (iii) ionic liquid polymer gel electrolyte (iv) redox gel electrolyte (redox additives in gel electrolyte). The preparation of the polymer gel network may involve network formation either by physical cross-linking such as electrostatic interactions, hydrogen bonding, and entanglement of chains, or *via* chemical cross-linking to form three-dimensional network gels that are through covalent bond formation involving different strategies.[197,198]

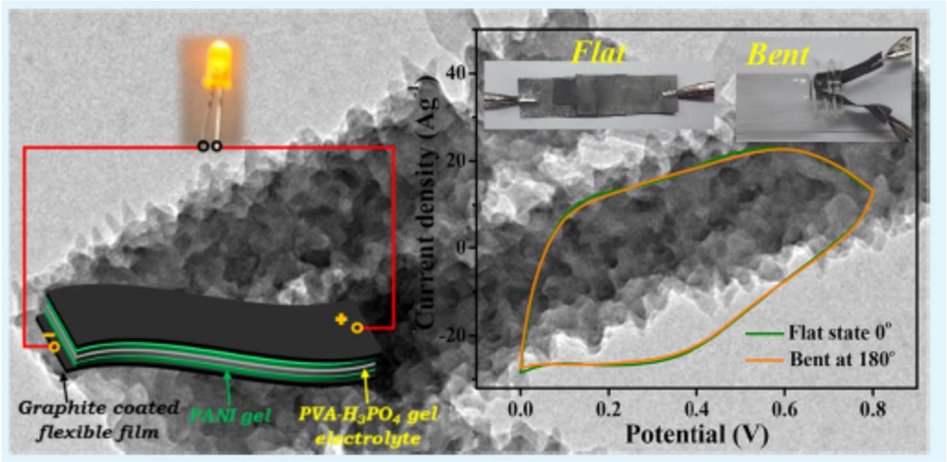

Fig. 22 Flexible supercapacitor assembled with MoS_2 quantum dot (QD)/PANI hydrogel electrodes and PVA/H_2SO_4 gel electrolyte, reproduced with permission from ref. 179 with permission from the American Chemical Society.

4.2.1 Polymer gel electrolytes. Different organic polymers, *e.g.*, PVDF, PAN, PMMA, PEO, PVA, *etc.* based on gel electrolytes have been used during the construction of PGEs.[199] Among them, PVA-based PGEs have drawn significant attention due to the improved solubility, biodegradability, and biocompatibility of this hydrophilic polymer. In addition, with easy processing, easy film formation, and low price, PVA-based gels have excellent bending properties. Ever since the development of highly conducting PVA/H_3PO_4 proton conductive polymer electrolyte by Petty-Weeks *et al.* in the 1980s,[200] researchers have developed gel electrolytes of different types: (1) acidic gel electrolytes such as PVA/H_3PO_4,[201] PVA/H_2SO_4,[53,202–208] (2) alkaline gel electrolytes such as PVA/KOH,[209–214] PVA/LiOH (ref. 215) and (3) neutral salt based gel electrolytes such as PVA/Na_2SO_4,[216–218] PVA/KNO_3,[219] PVA/KCl,[220] and PVA/LiCl (ref. 221–223) for extensive application under different conditions. A significant research effort has been devoted to ensuring the full contact of the gel electrolyte with the internal pores of the electrode, which is highly desirable during the construction of flexible supercapacitors to form a charge–discharge interface. Shao *et al.*[224] obtained a low charge transfer resistance of 2.31 Ω using PVA as a host polymer, PVA/H_3PO_4 as the electrolyte, and 3D graphene film as the electrode material. The resulting flexible supercapacitors exhibited a 0.9 mF cm^{-2} areal capacitance at a scan rate of 1000 mV s^{-1} while having capacitance retention of 89.4% after the 1000th cycle bending in the 0°–120° range. The use of a 3D honeycomb graphene film is beneficial for different gel electrolytes as it offered decreased ion diffusion resistance even under the prevailing highly viscous medium. The mechanical properties of the PVA/H_3PO_4 gel electrolyte were further improved by crosslinking with polyacrylamide (PAM, 16 wt%).[225] The resulting gel electrolyte offered a very high tensile strain (>17.42 mm mm^{-1}) along with an improved ionic conductivity value of 138 mS cm^{-2}. The flexible supercapacitor built up with this electrolyte produced a specific capacitance value of 169.7 F g^{-1} for bending 230° with 80.9% capacitance retention after 5000 cycles. Furthermore, the device obtained a remarkable capacitance retention of 80.5% at 100% tensile strain condition, which is indeed very encouraging from the perspective of wearable device fabrication. In another report, Guo *et al.*[53] prepared a self-healing composite hydrogel electrolyte using the physical cross-linking method and placed the nanocomposite electrode material to the surface of the hydrogel electrolyte by *in situ* polymerization and deposition methods to develop a flexible all-in-one self-healing supercapacitor of high electrochemical performance. The analysis of mechanical properties of the physically crosslinked PVA/H_2SO_4 hydrogel showed tensile stress of 4.7×10^5 Pa after stretching up to 7.6 cm. In addition, compared with any other chemically crosslinked hydrogel, the physically crosslinked PVA/H_2SO_4 hydrogel film had the unique advantage of repairing itself without any stimulus. The self-healing efficiency was well retained at ~80% after the fifth self-healing cycle. The flexible supercapacitor device exhibited an areal capacitance of 15.8 mF cm^{-2} at 0.044 mA cm^{-2} current density. In an interesting report, Yang *et al.*[226] photopolymerized a PVA/poly(*N*-hydroxyethyl acrylamide)/H_2SO_4 (PVA/PHEA/H_2SO_4) gel electrolyte showing high toughness, high strength, rapid self-recovery, self-healing, and fatigue-resistant capabilities. The resulting gel electrolyte exhibited high stretchability (about 5 times at different test states), an outstanding ionic conductivity value of 85 mS cm^{-1} and a broad operating window (0–3 V). The flexible supercapacitor showed similar CV profiles at various bending angles (0–180°). In addition, an improved self-healing property of the fabricated flexible supercapacitor exhibited ~84% capacitance retention from the initial 98 mF cm^{-2} after the 7th self-healing cycle. In a very recent and interesting report, Um and coworkers exploited the amorphous and intrinsically highly electrostatic nature of DNA for the fabrication of gel electrolytes for application in next-generation green wearable and flexible energy storage devices. The gel material displayed superior mechanical properties, and conductivity, and also improved electrochemical properties when assembled as a supercapacitor device using a pair of activated carbon electrodes.[227]

Besides acidic gel electrolytes, the fabrication of flexible supercapacitors is also gaining increased interest with alkaline gel electrolytes.[215,228–230] Among various electrolyte salts, KOH has received maximum attention for conductive OH^- ion in aqueous gel electrolytes for its better compatibility and low price.[231] In this regard, Zhao *et al.*[232] reported some excellent works where they used PVA/KOH gel electrolyte for the fabrication of an asymmetric flexible supercapacitor device having a Ni–Co hydroxyl carbonate monolayer (1.07 nm) as the electrode. The device has shown a working voltage window of 1.6 V, (Fig. 23a and b) along with excellent reversibility within 5 mV s^{-1} to 2 V s^{-1} producing a large volumetric capacity of 566 mF cm^{-2} at 100 mA g^{-1} of current density. Furthermore, even at a high applied current density of 2 A g^{-1}, the flexible device achieved 100% capacity retention even after 19 000 cycles (Fig. 23c).

They attributed the great electrochemical performance to the characteristic structure having a short ion diffusion channel and a large number of bare atoms in the electrochemical reactions, as presented in Fig. 23d. In another work, they fabricated a symmetric flexible supercapacitor device with two similar N–P–O co-doped 3D graphene electrodes and PVA/KOH as the gel electrolytes.[233] The working potential window of the device could be extended to 1.4 V. Thus, the extension of the working potential window in both of the above works indicated outstanding stability of the gel electrolyte. The fabricated symmetric electrode device exhibited a high capacitance value of 426 F g^{-1} and an appreciable energy density value of 25.3 W h kg^{-1} at a power density of 93.1 W kg^{-1} along with brilliant cycling stability of 96.2% after 10 000 cycles.

Interestingly the use of graphene oxide (GO) in the PVA-based electrolyte has become very effective both to increase the ionic conductivity of the gel as well as to enhance mechanical properties. Huang *et al.*[234] incorporated GO into boron cross-linked PVA gel electrolyte (GO-B-PVA/KOH), significantly increasing the conductivity (till ~20 mS cm^{-1} for 20 wt% GO doping) along with good mechanical properties. The device fabricated with the above gel electrolyte resulted in a remarkable hike in the capacitance of about 129% compared to the device using a KOH aqueous electrolyte. In another work, Hou *et al.*[235] incorporated hyperbranched poly(amine ester) nano-silica ($HBPAESiO_2$) into PVA/KOH gel electrolyte, increasing ionic conductivity, also producing an excellent electrode–electrolyte interface. The application of this electrolyte resulted in a significant increase in conductivity (7.09 mS cm^{-1}) compared to that in PVA/KOH electrolyte (1.32 mS cm^{-1}), which was for the hydrolysis of the ester groups by KOH to generate carboxylate salt moieties. The fabricated device exhibited 88% capacity retention after 10 000 cycles. In very recent work, Xu and coworkers fabricated a flexible supercapacitor having excellent electrochemical performance using an alkaline PEGMA hydrogel electrolyte sandwiched between Zn foil and graphite paper.[236] They prepared the ionically conducting hydrogel by copolymerizing ethylene glycol methyl ether acrylate (MEA), acrylamide (AM), and poly(ethylene glycol) methyl ether acrylate (PEGMA), and KOH to produce conductive hydrogel electrolyte. The assembled supercapacitor (PEGMA-ZHS) showed superior electrochemical performances, such as a high energy density value of 356.6 W h kg^{-1} (at a power density of 2647.4 W kg^{-1}) in a wide operating voltage range of 1.8 V

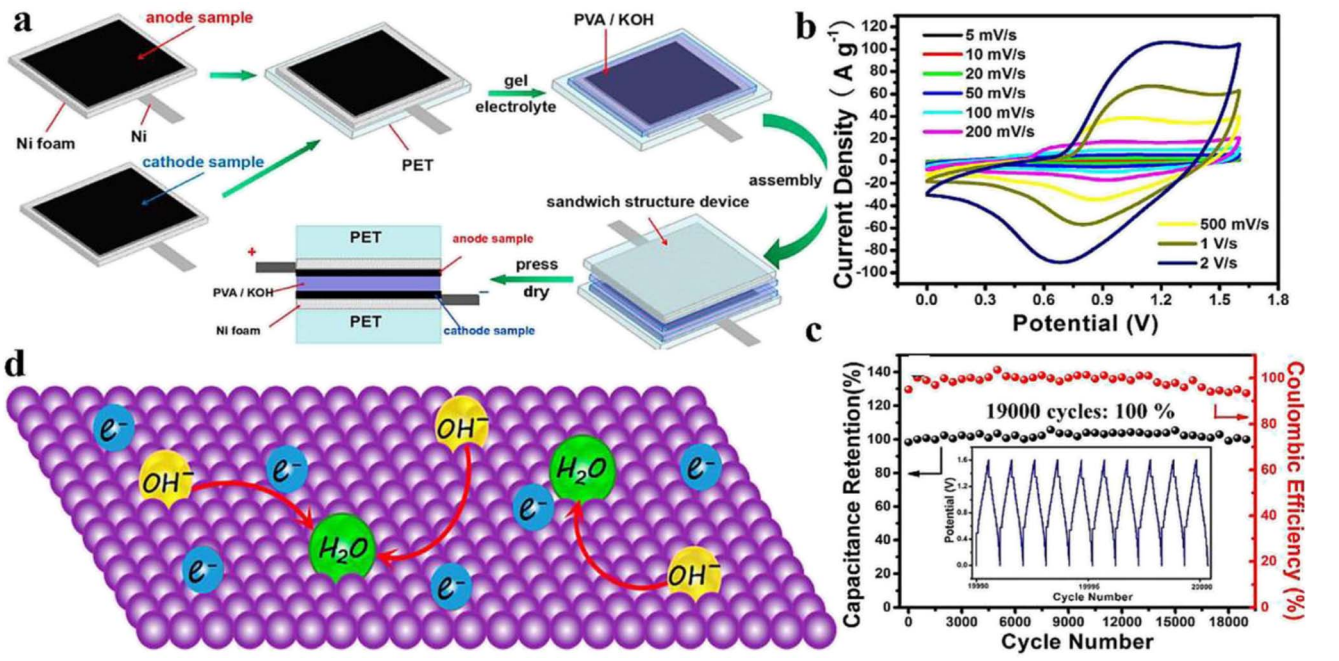

Fig. 23 The flexible supercapacitor device performance. (a) The preparation progress of the device. (b) CV curves at various scan rates in PVA/KOH gel electrolyte system. (c) Cycling performance and coulombic efficiency of the all-solid ASC at current density of 2 A g^{-1}; (d) schematic illustration of the energy storage mechanism on monolayer Ni, Co-HC. Reproduced from ref. 232 with permission from the American Chemical Society.

along with high cyclic stability of ~100% capacity retention after 10 000 charging/discharging cycles at a current density of 10 A g^{-1}.

Agarose-based hydrogels are very much useful as the gel matrix due to the high mechanical stability of the 3D gel network and the presence of submicron range pores. In this regard, Moon *et al.*[237] have fabricated a flexible supercapacitor using NaCl-agarose gel electrolyte and obtained excellent capacity of 286.9 F g^{-1} and ~80% capacity retention even above 1200 cycles. In another interesting work, an integrated flexible supercapacitor (FSC) device was fabricated by Lu *et al.*[216] using PVA/Na_2SO_4 neutral gel electrolyte and nanostructured cobalt hexacyanoferrate–molybdenum oxide thin films grown on the flexible carbon fiber cloth as the electrode, which exhibited a maximal energy density of 67.8 W h kg^{-1} at a power density of 1003 W kg^{-1} and 74% capacitance retention after 10 000 cycles. Sun *et al.*[220] integrated a polypyrrole electrode with an electrolyte of boron cross-linked PVA/KCl hydrogel showing energy density of 20 μW h cm^{-2} at 600 μW cm^{-2} power density and capacitance retention until 97% after 500 bending cycles. The outstanding electrochemical properties are due to high ionic conductivity (38 mS cm^{-1}) and improved mechanical properties of the PVA/KCl hydrogel electrolyte. Similarly, Peng *et al.*[238] made a self-healing hydrogel electrolyte by fixing GO into the PVA network and achieved an ionic conductivity value of 47.5 mS cm^{-1}.

Dehydration of hydrogel electrolytes poses a major concern in the performance of flexible supercapacitors while operating under a different range of temperatures due to decreased ion migration. Thus, the increased water retention ability of the hydrogels at relatively higher temperatures is highly desirable to have further improvement in the performance of the hydrogel electrolyte-based energy storage devices.[225,239] In this respect, the use of super-concentrated aqueous electrolyte, named the "water-in-salt" (WIS) strategy is beneficial where water molecules interact more actively with metal ions (reducing the dehydration extent) as well as broaden the electrochemical window. Liu *et al.*[221] demonstrated excellent water retention ability under 100 °C and broadening of working potential up to 1.8 V using 21 m LiTFSI/PVA gel. A robust cation–anion interaction improvement in the water retention ability of the hydrogel electrolyte was demonstrated by these authors using density functional theory molecular dynamics (DFTMD) and simulation studies. They also demonstrated the improved electrochemical performance by a flexible supercapacitor fabricated using 21 m LiTFSI/PVA gel electrolyte to exhibit an areal capacitance of 936.4 mF cm^{-2} at 4 mA cm^{-2} current density and a capacitance retention of 80.8% after 500 cycles at 80 °C. A comparison of alkaline/acidic gel electrolytes with polymer-salt-based gel electrolytes showed a relatively broader and stable operational voltage window due to much lower H^+ and OH^- concentrations in neutral salts, which resulted in the reduced level of hydrogen/oxygen evolution. Despite the relatively poor voltage window, and the problem of dehydration, the aqueous gel electrolyte has the benefits of being nontoxicity, environment-friendly, high conductivity, and cheap, compared to the organic solvent electrolytes. Therefore, the majority of researchers still prefer aqueous gel electrolytes for academic research. However, this should be further mentioned that the low voltage window of the aqueous gel electrolyte causes the power density and energy density of the flexible supercapacitors to fail to meet the market demands.

4.2.2 Non-aqueous polymer gel electrolyte. The principal advantage of organic solvents as the medium for gelation in gel-polymer electrolytes lies in offering a higher operating potential window of the fabricated devices. Hence, researchers are seriously engaged in developing non-aqueous gel polymer electrolytes (NAGEs).[143,240,241] However, lower interfacial conductance, lower conductivity, poor electrochemical performance, and desired high purity of the organic solvents raise significant restrictions during practical applications of non-aqueous polymeric gel electrolytes. Among organic solvents, propylene carbonate (PC) has been the most elegantly used so far, as PC-based electrolytes have good conductivity, are environment-friendly, and offer a wide voltage window.[242] There is a good number of reports where PC-based gel electrolytes have been used for the fabrication of high-performance flexible supercapacitors.[243,244] Na *et al.*[245] suggested a PGE (alcohol ethoxylate/acrylamide/$LiClO_4$) having improved conductivity 31.1 mS cm^{-1} by virtue of a large number of ion-conductive amine and ethylene oxide functional groups. The fabricated supercapacitor device exhibited excellent electrochemical performance with a capacitance value of 130.3 F g^{-1} at 0.5 A g^{-1} and a maximum energy density value of 8.99 W h kg^{-1} at 67.84 W kg^{-1} power density along with 90.1% capacitance retention above 5000 cycles. Wang and his coworkers[246] have synthesized high-performance flame retardant non-aqueous PGE by cross-linking brominated epoxy resins with novel flame retardants. They utilized poly(ethylene glycol) copolymers along with an epoxy ring-opening polymerization technique. They used tetrabromobisphenol A as a matrix and an organic electrolyte (a lithium salt in PC) for swelling. The PGE exhibited an appreciably high ionic conductivity of 1.09 mS cm^{-1} coming from the poly(ethylene glycol) portion of the flame-retardant PGE. The device fabricated has a high capacitance of 166.69 F g^{-1} at 0.5 A g^{-1}, and superior flexibility under bending conditions in the context of other flexible supercapacitors containing liquid organic electrolytes. The device also exhibited excellent energy density as well as power density.

4.2.3 Ionic liquid-mixture electrolyte. Ionic liquids (ILs) are safer and improved candidates for the construction of supercapacitor electrolytes compared to organic electrolytes (as discussed above) for their inflammability, higher ionic conductivity, and broadened potential windows. The present literature shows the existence of various IL cation and anion combinations, however, imidazolium cation-based-ILs are the most important for their high conductivity as a result of the planer cationic core of the imidazolium ring. The advantages of ILs as EDLC electrolytes include a wide open potential window (up to 6 V)[247] and large intrinsic capacitance, which are extremely desirable for the fabrication of high-energy electrochemical devices.[248,249] In addition, their incombustibility and lower vapor pressure made them less vulnerable under elevated temperatures. Nevertheless, as ILs are still liquids in nature,

they are associated with the typical problems related to liquid electrolytes (as stated previously). These problems may however be avoided by immobilizing ILs into solid media such as polymers and silica gels, solid-state ILs, namely ionogels.

PVA-based IL gel electrolytes have received significant interest so far for their physical and chemical properties such as high thermal and electrochemical stability, good flexibility, non-flammability, non-toxicity, and environmentally benign nature.[250,251] Jeong *et al.*[251] fabricated a flexible supercapacitor device with PVA-based IL ($BMIMBF_4$) gel electrolyte, single-wall carbon nanotubes (SWCNTs and reduced graphene oxide (rGO)) as electrodes. The flexible supercapacitor device presented rectangular CV curves with a large current owing to the high ionic conductivity of the PVA/H_3PO_4/$BMIMBF_4$ gel electrolyte. High stability and flexibility of the supercapacitors composed of the PVA/H_3PO_4/$BMIMBF_4$ electrolyte is apparent from 64.6% capacitance retention after 300 bending with 4000 charge/discharge cycles. In a later work, Zhang *et al.*[252] incorporated Li_2SO_4 and IL BMIMCl into the PVA-based IL gel electrolyte, which proved beneficial, both, for enhancing ionic conductivity and relatively higher working potential window of the flexible supercapacitor device (1.5 V) Fig. 24a). The electrolyte showed the highest ionic conductivity value of 37 mS cm^{-1} (Fig. 24b) with no change in ionic conductivity even at the bending angle of 180°. The high flexibility of the fabricated flexible supercapacitor device was apparent in Fig. 24c where unchanged electrochemical properties were noticed in the bending tests ranging from 0° to 135° with capacitance retention of 82% after 1000 cycles. In another work, Tang *et al.*[253] reported PVA/BMIMCl-based IL gel electrolyte and cellulose paper electrodes to make a flexible supercapacitor device. In this work, acidic PVA/BMIMCl/lactic acid/LiBr and neutral PVA/BMIMCl/sodium acetate/LiBr hydrogel polymer electrolytes were utilized as catholyte and anolyte, respectively. The CV curves of the device with two PVA/IL-based gel electrolytes (as shown in Fig. 24d and e made it apparent that there were no obvious changes under different bending angles. Furthermore, the device delivered 93.4% capacitance retention after 10 000 cycles at a current density of 1 A g^{-1} (Fig. 24f). Further improvement with respect to the stability of the electrolytes was reported by Wang *et al.*[254] where a Na^+ conducting PVA-based IL PGE was fabricated using 1-ethyl-3 methylimidazolium trifluoromethanesulfonate (EMITf) as the plasticizer. The gel electrolyte exhibited excellent thermal stability (up to 150 °C) and a wide operating potential window of 4.7 V. An appreciably high conductivity of up to 3.8 mS cm^{-1} was reported in the PVA/NaTf/EMITf gel and the fabricated device showed capacitance values of 103.7 and 127.8 F g^{-1} at cut-off voltages of 1.6 and 2.0 V, respectively.

PVDF is another interesting candidate, which has drawn significant attention in the construction of the gel skeleton of ion gels. The principal advantages of these polymer systems include high mechanical and electrochemical stability, good compatibility with other materials as well as increased dielectric constant.[255–258] Literature shows a good number of reports where methylimidazolium-based ionic liquids with PVDF-based polymer matrix are used as electrolytes with carbon-based electrodes for the construction of flexible supercapacitors.[245,259–262] In a very interesting work, Liu *et al.*[259] designed a 3.5 V flexible supercapacitor using (EMIMBF4/PVDF-

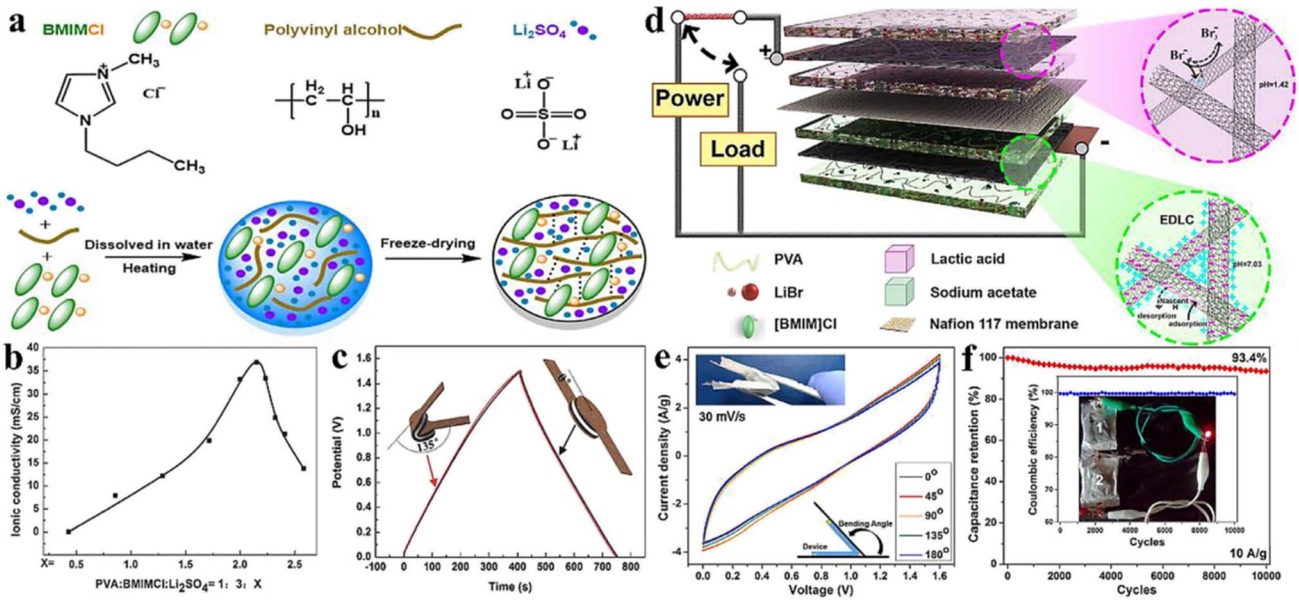

Fig. 24 The performance and preparation progress of flexible supercapacitor devices with IL-based gel electrolyte. (a) Schematic illustration of PVA/BMIMCl/Li_2SO_4 gel electrolyte. (b) Ionic conductivity of PVA/BMIMCl/Li_2SO_4 gel electrolyte with different counts of Li_2SO_4. (c) The electrochemical performance of the FSC device at a current density of 0.15 A g^{-1} under the different bending angles conditions. Reproduced from ref. 252 with permission from WILEY-VCH. (d) Schematic illustration of the supercapacitor. (e) CV profiles of the device at different bending angles. (f) The electrochemical performance of the FSC device at the current density of 10 A g^{-1}, and the coulombic efficiency and the digital photo of the light-emitting diode were displayed in the inset. Reproduced from ref. 253, with permission from the American Chemical Society.

HFP) ion-gel electrolyte with hierarchical carbon as the electrode having excellent electrochemical performance with a specific capacitance value of 201 F g^{-1} at a current density of 0.5 A g^{-1} along with 90.1% capacitance retention after 1000 bending cycles (0° to 180°). In another work, Deng *et al.*[261] reported asymmetric flexible supercapacitor devices by using a similar ion gel electrolyte (EMIMBF4/PVDF-HEP). The CV analysis demonstrated excellent repeatability under various bending extents, in addition, the device has shown remarkable cycle stability of 71% retention after 10 000 cycles. The fabricated device has been demonstrated as a successful energy supplier for power electronics where a relatively smaller dimension of the device (2×2 cm^2) was used for lightening up a pattern "TJU" (manufactured by 19 red LEDs) for 1 min. Furthermore, Yang *et al.*[262] exploited the membrane-forming capability of PVDF to fabricate a highly porous structure *via* a chemical cross-linking and immersion approach. They used tetraethylammonium tetrafluoroborate (Et_4NBF_4) as the electrolyte in an acetonitrile medium. The gel electrolyte exhibited excellent properties such as non-flammability, a high ionic conductivity of 14.4 mS cm^{-1} and a broad potential window of 2.9 V. The flexible supercapacitor constructed with this electrolyte showed a high energy density of 5.16 mW h cm^{-3}, a volumetric capacitance value of 5.2 F cm^{-3} and about 100% capacitance retention even at a bending angle of 145°. Zhu, Gomez-Romero, and coworkers reported a GPE-based supercapacitor concept with improved pathways for ion transport, by the creation of a coherent continuous distribution of the electrolyte throughout the electrode.[263] In this work, PVDF-HFP was chosen as the polymer framework for organic electrolytes. A permeating distribution of the gel polymer electrolyte into the electrodes played a multifarious role as an integrated electrolyte and binder, as well as a thin separator. This model is conducive to ion diffusion and at the same time increases the active electrode–electrolyte interface, which leads to improvements both in capacitance and rate capability. The said gel electrolyte arrangement showed improved capacitive performance with a novel hybrid nanocomposite material, formed by the tetraethylammonium salt of the 1 nm-sized phosphomolybdate cluster and activated carbon (AC/TEAPMo12). A significant improvement in the volumetric capacitance (~40%) along with three times more energy density at higher power densities and equivalent cycle stability of a symmetric supercapacitor made with the hybrid electrodes compared to a cell with parent AC symmetric capacitors electrodes was attributed to the synergy between permeating gel polymer electrolyte and the hybrid electrodes.

Despite the advantages of PVDF-based gelators, crystallization of this polymer leads to various difficulties such as poor flexibility and poor ionic conductivity. In this regard, synthetic amorphous polymers, which may be either physically or chemically cross-linked are gaining significant importance. However, it is not at all surprising that physically cross-linked gels are more attractive as chemical cross-linking requires further steps after the introduction of potential cross-linkable moieties on the polymer chains. Generally, tri-block copolymers used in the construction of such ion gels should have selective solubility for a particular block in the ionic liquid used. In the gel, IL soluble block domains provide pathways for ionic conduction as well as the flexibility to the gel and IL insoluble, self-assembled block domains provide strength and stability to the gel material. However, it should be further remembered here that judicious selection of the block copolymer types (in respect of a segmental motion, T_m or T_g of the polymer), as well as their lengths in the copolymer, would provide optimized ionic conductivity and strength to the gel material.[264] Apart from these, the molecular design of the block copolymers has been found to have a profound effect on the conductivity as well as mechanical strength of the prepared gel material. Triblock copolymers as polystyrene-*b*-poly(methyl methacrylate)-*b*-polystyrene (SMS) or polystyrene-*b*-poly-(ethylene oxide)-*b*-polystyrene (SOS) have been used as gelators with typical ILs as ethyl-3-methylimidazolium bis-(trifluoromethyl sulfonyl)imide ([EMI][TFSI]) and 1-butyl-3-methylimidazolium bis(trifluoromethyl sulfonyl)imide ([BMI]-[TFSI])[265–269] for a long time. In the recent past, a very interesting comparison between the SMS triblock copolymer and six arm star shaped block copolymer (poly(methyl methacrylate)-*b*-polystyrene)$_6$ ((MS)$_6$) based gel has been presented. The (MS)$_6$ has been suggested as a gelator equivalent to three SMS chains tied to the core. Thus, a much greater number of physical cross-linking points with the insoluble high T_g PS blocks are expected to impart increased mechanical robustness of the gel. A significant increase in the sol–gel transition temperature for the six-arm star block copolymer (up to ~180 °C) based gel compared to the linear triblock (SMS) copolymer-based gel (~83 °C) has been reported.[270]

Other molecular architectures, such as graft copolymers have also been used as gelators. For instance, a gel electrolyte composed of a mixture of a graft copolymer poly(ethylene glycol) behenyl ether methacrylate-*g*-poly((2-acetoacetoxy)ethyl methacrylate) (PEGBEM-*g*-PAEMA) and IL $EMIMBF_4$ resulted in appreciably high ionic conductivity of 1.23 mS cm^{-1}, which was attributed to the faster ionic mobility arising from the polarity of the polymer matrix. The fabricated flexible supercapacitor with this gel electrolyte allowed an electrochemical window of 3 V with high electrochemical performance and without any leakage problem even when very high loading of IL was done.[271] Despite several advantages, the difference in polarities between the organic polymers and ionic liquids gives rise to issues such as non-compatibility leading to reduced conductivity of the prepared gel. This issue has been well addressed through the preparation of polymeric ionic liquids (PILs)[272–278] in cases where a similarity in structure is found between the polymer and ILs. PILs offer many advantages, *e.g.*, easier processability, high mechanical stability, durability, and of course improved compatibility with the polymer matrix. In a very interesting work, Yang *et al.* reported a novel highly flexible bromide-based polycationic conducting copolymer poly(vinyl acetate-*co*-1-ethyl-3-vinylimidazolium bromide) poly(VAC-*co*-EVImBr) thin film electrolyte, which shows the broad electrochemical window of 6.0 V and appreciably high conductivity of 2.04×10^{-6} S cm^{-1}. They fabricated a 4.2 V flexible all-solid-state flexible supercapacitor, which showed

superior charge–discharge capabilities at both 25 °C and 60 °C.[276] Nevertheless, it must be admitted that the use of ILs as additives in gel electrolytes for the fabrication of flexible supercapacitors is yet to get the desired level of attention, which may be attributed to their tedious purification, stringent assembly procedures under moisture-free conditions, their high viscosity and of course high cost.

4.3 Redox gel electrolyte for flexible supercapacitors

The addition of redox-active materials in the gel electrolytes provides further room for increasing the capacitance of the device, where, apart from the capacitance of the electrode, electrolytes also contributed to pseudocapacitance. Thus, the total capacitance of the device along with energy density increases.[279–283] The redox additives may be both inorganic/organic in nature and iodide/iodine-based redox couple has received maximum attention in this regard[284–290] possibly due to lower toxicity, relatively low molecular weight, and high solubility of iodide salts. In a very interesting work, Zhou *et al.*[284] demonstrated the introductions of NaI and I_2 into the PEO-based polymer gel electrolyte (PEO/$LiClO_4$), resulting in significantly high conductivity (20.2 mS cm^{-1}) and improved electrochemical properties along with 90% capacitance retention after 3000 charge/discharge cycles. In another work, Kim *et al.*[286] used KI in an alkaline PVA electrolyte gel (PVA/KOH/KI) and assembled a supercapacitor with $MgCo_2O_4$ nanoneedles as the electrodes. The flexible supercapacitor device exhibited excellent electrochemical performance showing a maximum energy density of 41.3W h kg^{-1} at a power density of 464.7 W kg^{-1}. Similarly, Park *et al.*[290] introduced KI into the acidic PVA/H_3PO_4 to prepare PVA/H_3PO_4/KI gel electrolyte. The addition of KI into the gel electrolyte resulted in significant improvement in the electrochemical properties. Furthermore, the authors constructed a flexible supercapacitor device of 47 cm in length and obtained a charge storage ability of 75.7 mF.

4.3.1 Redox gel electrolyte with organic compound additives. Besides inorganic compounds, organic redox additive molecules are also introduced within the gel electrolytes resulting in significant performance improvement.[279,291–294] The redox activity of *p*-nitroaniline is presented in Scheme 2,[295] which shows each nitroaniline molecule reversibly producing a couple of electrons and protons thus, it can significantly improve the overall device capacitance by generating additional pseudocapacitance.

Hydroquinone (HQ) additives have been used as redox additive molecules under neutral, acidic as well as basic conditions. Jinisha *et al.* successfully introduced HQ into the alkaline PVA/KOH gel. The flexible supercapacitor device fabricated with PVA/KOH/HQ gel showed a specific capacitance of 326.53 F g^{-1} with capacitance retention of ~84.2% after the 1000th cycle.[296] The redox gel electrolytes so prepared have also been used successfully to fabricate high-performance flexible supercapacitors.[297,298] Xu *et al.*[298] introduced HQ in the acidic PVA/H_2SO_4 gel and the PVA/H_2SO_4/HQ gel electrolyte exhibited a significantly improved conductivity of 23.2 mS cm^{-1}. The device fabricated using this gel electrolyte with CNT/PPy electrode reportedly produced an aerial capacitance of 1168 mF cm^{-2} due to the redox reaction of HQ and benzoquinone. Besides HQ, sodium salts of 1,3-napthaquinone sulfonic acid or anthraquinone-2-sulfonic acid are also successfully used as redox additives in the PVA/H_2SO_4 gel electrolyte. Apart from quinone derivatives, *p*-nitroaniline, polydopamine, phloroglucinol *etc.*, other molecules have also been successfully used for the preparation of redox gel electrolytes which have resulted in high-performance flexible supercapacitor devices.

4.3.2 Redox gel electrolyte with IL additives. Despite the disadvantages of IL additives in the gel electrolytes, they can be of the potential application when used with organic gel polymer electrolytes in view of their plasticizing effect (when used in sufficient concentration) by helping the softening of the matrix polymer and thereby increasing the ionic conductivity. In this regard, Tu *et al.*[299] used iodide or chloride salts of 1-butyl-3-methylimidazolium ions with PVA/Li_2SO_4 gel electrolyte, where a significant improvement has been reported in the tensile property (1200% and tensile strength of about 2.0 MPa) as well as electrochemical properties (energy density of 29.3 W h kg^{-1}) due to the pseudocapacitance contribution from the ILs in the fabricated flexible supercapacitor device. A comparison of different PGEs in their capacitance values, cyclic stability, *etc.* is presented in Table 1.

In summary, hybrid polymer gels are highly used for producing electrodes and gel electrolytes with different additives to fabricate high-performance supercapacitors with high stability. Here, the most important benefits are high flexibility, stretchability, foldability, compressibility, and self-healing properties, maintaining crease-free electrode–electrolyte assembly, which can find promising applications in portable/wearable electronics. PGEs have the advantages of both liquid electrolytes as well as solid electrolytes having improved mechanical properties. Furthermore, the flexibility and elasticity of PGEs can accommodate the volume change of electrode materials, generating global attention over PGEs as electrolytes for various electrochemical energy storage devices. However,

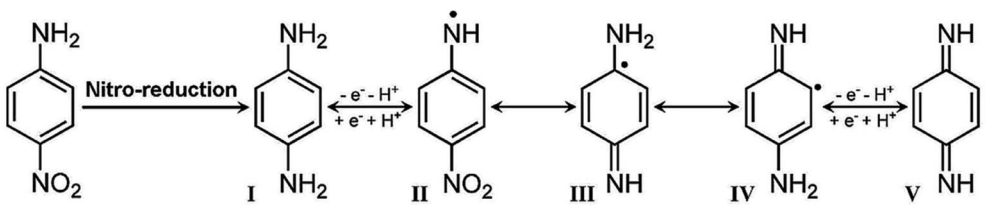

Scheme 2 The schematic process of PNA in the PVA/H_2SO_4 gel electrolyte system. Reproduced with permission ref. 295 with permission from Elsevier.

Table 1 Comparison of different PGEs in the supercapacitor performances from different works

Entry no.	Soft electrolyte/electrode	Capacitance/capacity	Cyclic stability (retention/cycles)	Flexibility (bending angle/radius)	Reference
1	PVA/H_3PO_4[a]	2662 mF cm^2	95%/5000	5.7 mm	300
2	PVA/H_2SO_4[a]	267 F g^{-1}	99.5%/6000	—	202
3	PVA/KOH[a]	1590 F g^{-1}	95%/5000	180	210
4	PVA/KOH[a]	288 mF cm^{-2}	100%/10 000	—	301
5	PVA/Na_2SO_4[a]	689 F g^{-1}	74%/10 000	—	216
6	PVA/KNO_3[a]	4.17 mF cm^{-2}	78%/2000		219
7	PVA/KCl[a]	224 mF cm^{-2}	92%/2000	180	302
8	PVA/LiTFSI[a]	541.9 mF cm^{-2}	80.8%/500 (80 °C)	180	303
9	PVA/LiCl[a]	152.1 mF cm^{-2}	92%/2000	135	304
10	PC/$LiClO_4$[a]	111 F g^{-1}	80%/11 000	—	244
11	PC/$LiClO_4$/PEG-TBBPA[a]	166.69 F g^{-1}	78%/3000	90	305
12	PVDF-HFP/$EMIMBF_4$[a]	201 F g^{-1}	80.1%/10 000	180	306
13	PVDF-HFP/[EMIM][NTf_2][a]	153 F g^{-1}	97%/10 000	—	307
14	PVA/BMIMCl/Li_2SO_4[a]	136 F g^{-1}	82%/1000	135	252
15	PVA/KOH/$K_3[Fe(CN)_6]$[a]	430.95 F g^{-1}	89.3%/1000	—	308
16	PVA/KOH/KI[a]	185.88 C g^{-1}	89.3%/5000	—	309
17	PVA/H_2SO_4/HQ[a]	644.4 F g^{-1}	73%/2000		310
18	PANI hydrogel[b]	480 F g^{-1} at 0.5 A g^{-1}	—	Can be inkjet printed	157
19	PANI hydrogel[b]	480 F g^{-1} at 5 mV S^{-1}	—	Bendable	311
20	PANI-αCD hydrogel[b]	322 F g^{-1} at 2 A g^{-1}	—	Stretchable and foldable	165
21	PANI/PVA all in one hydrogel[b]	15.8 mF cm^{-2} at 0.044 mA cm^{-2}	—	Stretchable and healable	53
22	PPy/porous cellulose fabric[b]	4117 mF cm^{-2} at 2 mA cm^{-2}	—	Bendable and twistable	312

[a] Soft electrolyte. [b] Soft electrode.

the use of PGE also has some disadvantages originating from their typically higher viscosity such as (i) lower ionic conductivity and large charge transfer resistance for bulky cations and anions, leading to relatively poor capacitance as well as poor rate performance compared to that with organic or aqueous based electrolytes, particularly during low temperature applications,[313–316] increased viscosity of PGEs would likely to decrease the ionic conductivity but the pseudo-capacitive redox process rather becomes easier and increases the potential window, which is conducive to attaining high energy density value despite the relatively lower capacity/capacitance of the electrode.[317] PGEs exhibit high toughness, high strength, rapid self-recovery, self-healing and fatigue-resistant capabilities. Thus, the PGEs usually possess a broad operating window (0–3 V), thus overcoming the low voltage window of the aqueous gel electrolyte resulting in higher power and energy densities of the flexible supercapacitors suitable to meet the market demands. Recently works are dealing with integrated energy conversion and storage devices by interfacing solar cells with supercapacitors and batteries, *i.e.*, between energy harvesting and storage and it can simplify the final scaling up of this important and demanding technological field.[318]

5 Outlook and perspectives

"Green Energy" is the most important requirement to advance our civilization protecting our beloved world from natural disasters arising mainly from the burning of fossil fuels. The world economy and power are still mostly governed by the storage of fossil fuels, which are not evenly distributed throughout the world, as a result, outbreaks of war, famine, and diseases are increasingly questioning the survival of human beings and civilization. Consequently, research on green energy generation and its storage for fruitful utilization is enormously increasing with preliminary successes as it is yet too far to substitute fossil fuels. The only source of green energy is the sun and water, (as here no fossil fuel is burnt to generate carbonaceous gases) so to generate energy mostly photovoltaics and fuel cells are of great interest with a minimal contribution from wind, tidal, hydro, *etc.* Apart from energy generation, for its fruitful use, energy storage through batteries and supercapacitors exploiting chemical processes are so far important breakthroughs. Energy is required not only for running heavy vehicles but also is required for computers, mobile phones, and also most importantly in biology/biotechnology. As such, energy generation and storage devices should be of different shapes, sizes, flexibility, self-healing, elasticity, biocompatibility, *etc.* To tune the above factors, polymer gels are the most important, hence in this review, we concentrated our discussion on the use of polymer gels as energy materials.

Among polymer gels, conducting polymer gels are the most important in this regard, because energy generation and storage processes require electronic/ionic conductivity and the conjugated backbone of conducting polymers and their π-stacked self-assembly are conducive to the flow of above charges through the device and also in the outer circuit. Also, the porous morphology of the gel can accommodate the volume changes, which occur during the electrochemical process in the energy generation and storage in the gels. However, the important drawback of the use of only conducting polymer gels is their low

mechanical properties along with their brittleness in the xerogel state causing difficulty in device fabrication. To overcome these drawbacks, scientists have adopted the concept of hybrid polymer gels where the conducting polymer network is mixed with other polymers, nano-particles, cross-linkers, *etc.*, which form either the double network, reinforcement by nanoparticles and/or by cross-linking (chemical or supramolecular), to enhance their mechanical strength and also to impart elasticity requiring to produce flexible but stable devices. This review has delineated the different aspects of hybrid gels in the processes of photovoltaics, fuel cells, battery, and supercapacitor devices considering the most important and recent works in these fields from the literature.

It is evident from the review that in the energy generation using DSSCs with thieno-indole-based organic dyes and porphyrin sensitizer have achieved a high PCE of 11.6% using the I^-/I_3^- redox liquid electrolyte (LEs) but the use of $[Co(bpy)_3]^{2+/3+}$ redox LEs with the same dye a PCE has improved to 14.2% under 1 sun.[25] The LEs in these highly efficient DSSCs contain volatile organic liquids causing instability under outdoor conditions, hence the concept of PGEs came about. The overall PCE in the PGE-based QSS-DSSCs with $[Co(bpy)_3]^{2+/3+}$ redox system was reduced to 9.72% from that of 14.2% in LEs, however, using SGTPGE-based QSS-DSSC with indoor white LED light of 1000 lx showed the best PCE of 21.26% with very long-term device stability.[40] At an optimal concentration of ZnO nanofillers, the PCE of MPN-based QS-DSSC showed a PCE value of 20.11% at 200 lx illumination retaining 98% efficiency for 1044 h at 35 °C. The MPN-based DSSC containing a 90 nm PEDOT layer showed a very high PCE of 26.9% under 1000 lx illumination.[47] A new solar cell architecture with a double-layered gel electrolyte of the PEO/PVDF blend containing ZnO nanoparticles outperformed its liquid-state counterpart at indoor fluorescent-light conditions.[48] Also, the TiO_2 active layer of the photo-electrode was fruitfully replaced using trihybrid PANI gel containing GO and a gelator molecule.[20] As such, new research by introducing different nanoparticles in the PGEs to improve PCE and durability of DSSCs is required along with an intelligent choice of different hybrid polymeric gels as well as different device architectures. A direct borohydride fuel cell (DBFC) obtained from a PGE of Sago, a natural polymer, exhibits a maximum power density of 8.818 mW cm^{-2} at a discharge performance of 230 mA h at a nominal voltage of 0.806 V.[66] A tetrazole-based PEM fuel cell containing 5-(4-hydroxyphenyl)-1*H*-tetrazole inorganic–organic hybrid polymer membranes made by *in situ* sol–gel process in the presence of H_3PO_4 catalyst cum dopant, and the porous e-PTFE film reinforcing agent at low humid conditions showed good fuel cell performance with short-circuit current of 770 mA cm^{-2} and peak power density 120 mW cm^{-2} at 20 °C increasing to 190 mW cm^{-2} at 120 °C, which is adequate for many microelectronic devices.[71] The DBC-MoS_2-PANI2 hybrid gel exhibited good HER catalytic activity with a lower overpotential of 196 mV at 10 mA cm^{-2}, Tafel slope value of 58 mV per decade close to that of platinum due to synergistic coupling at the interface of MoS_2 QDs and PANI fibers of the aerogels.[77] The carbon-nanofiber skeleton network[83] derived from bacterial cellulose hydrogel, mixed with nanosized MoS_2 shows HER electrocatalyst exhibiting a low onset over-potential value of 120 mV, with a Tafel slope of 44 mV dec^{-1}. Thus, hybrid polymer gels are good for making efficient and stable fuel cell membranes suitable for the conductance of ions and are also an efficient catalyst for the electrode processes. Gradual progress in this field is going on by changing different gel networks and nanoparticles.

In energy storage devices, the development of high-performance batteries requires optimization of every battery component, from electrolyte, electrodes, and binder systems, and in this regard, hybrid polymer gels have a great opportunity. The Li-battery containing the Li/HPGE/$LiCoO_2$ cell with PVDF/PEO (F/O-5) gel membrane delivered an initial discharge capacity of 171.8 mA h g^{-1} at 0.1C retaining 86% discharge capacity after 60 cycles, indicating good cyclic stability.[97] A double polymer network gel electrolyte (DPNGE) of branched acrylate on the P(VDF-*co*-HFP) matrix showed a first discharge capacity of 153.7 mA h g^{-1}, whereas the coulombic efficiency was 98% and after 500 cycles, the discharge capacity showed a capacity retention of 92.7%. After a long cyclic period, the battery retained a high capacity and coulombic efficiency close to 100%, indicating good compatibility between DPNGE and the electrodes. The C-LFP/C-PPy hybrid gel electrode showed much higher capacity than the control sample at each current density showing a capacity of ~60 mA h g^{-1} at a high charge/discharge rate of 30C, while the control C-LFP sample exhibited a capacity less than 30 mA h g^{-1}. The P-PPy/Fe_3O_4, and C-PPy/Fe_3O_4 hybrid gel electrodes showed stable capacities of 1260, 1002, and 845 mA h g^{-1}, at increasing current rates from 0.1 to 1C, 2C, respectively. The hybrid gels exhibited much higher capacity than the control electrode prepared using a traditional binder system containing Fe_3O_4 NPs, acetylene black, and PVDF with a weight ratio of 75 : 15 : 10. The hybrid gels could maintain more than 900 mA h g^{-1} of capacity while the control sample could maintain only 500 mA h g^{-1} at 1C.[117] Thus, the hybrid polymer gels showed better battery performance from that using the control systems. The most interesting development in supercapacitors has been the construction of stretchable/flexible self-healing devices. For example, a self-healing flexible all-in-one self-healing supercapacitor based on PVA/H_2SO_4 gel offers high electrochemical performance (areal capacitance of 15.8 mF cm^{-2} at a current density of 0.044 mA cm^{-2}).[53] A DNA-based gel electrolyte for application in next-generation green wearable and flexible energy storage devices offers improved electrochemical properties with a pair of activated carbon electrodes.[227] An 'all-in-one' integrated supercapacitor device made by embedding two PANI layers (serving as electrodes) in a 3D porous PVA-H_2SO_4 PGE exhibited a remarkably high areal capacitance of 488 mF cm^{-2}, along with excellent cycling stability and flexibility.[152]

As such, it is very much evident from the above discussions that hybrid conducting polymer gels are very important in fabricating different energy devices such as solar cells, fuel cells, batteries, and supercapacitors. Of course, another important part that is not discussed here is the role of polymer gels in bio-energy, *i.e.*, the energy related to biological processes and there is a great scope for future work in this barren area as most of the

biological molecules such as proteins, nucleotides, and enzymes remain in the self-assembled states. In the present context, there is enough scope for molecular designing of polymer gelators, which includes copolymerization, *e.g.*, random, alternate, block, star, and graft copolymers to effectively prepare physical/chemical cross-linked gels. No doubt, the microstructure of the polymer would influence the device's performance. It is important to note that the use of PGE in the organic medium of the perovskite solar cell may improve the stability and also enhance PCE. Apart from electron-conducting polymer and polyelectrolyte, gels containing ions in conducting polymer chains are the most important because they can exhibit mixed ionic and electronic conductivity (MEIC) properties, which would enhance the device's performance. In the hybrid polymer gels, the MEIC property can be introduced easily by mixing them with ionic compounds, surfactants, and ionic liquids, thus there is enough scope for work in this important field. The introduction of different carbon, metal, metal oxides, sulfides, *etc.*, into the polymer gel network, is a growing area of research to fabricate different electrodes, electrolytes, binders, *etc.* showing higher device performances, including their stability. Redox materials in the hybrid gels are the most important as they govern the electrochemical device performances and the judicious choice of this redox couple is a good area for future work to improve the device efficiency. To understand the electrode and electrolyte processes theoretical calculation would be an important area of work for developing high-performance devices. Besides the choice of different stimuli-responsive polymers as a component in the hybrid gels may impart thermal, pH, and mechano-responsive properties in the device, in addition to its flexibility and self-healing for applications in different appliances. The polymeric devices would be light, flexible, and low cost, and energy generation and storage could be achieved with high efficiency in the presence or absence of sunlight. In the near future, we anticipate that the use of green energy would outperform the use of fossil fuels.

Conflicts of interest

There are no conflicts of interest in the work to declare.

Acknowledgements

We gratefully acknowledge CSIR New Delhi (ES grant (21(1055)/18-EMR-II)) for financial support. We also thank Dr U. Basak for helping in the organization of the manuscript.

References

1 S. Chu and A. Majumdar, *Nature*, 2012, **488**, 294.
2 A. Manthiram, Y. Fu, S. H. Chung, C. Zu and Y. S. Su, *Chem. Rev.*, 2014, **114**, 11751.
3 C. Liu, F. Li, L. P. Ma and H. M. Cheng, *Adv. Mater.*, 2010, **22**, 28.
4 N. K. Mahenderkar, Q. Chen, Y.-C. Liu, A. R. Duchild, S. Hofheins, E. Chason and J. A. Switzer, *Science*, 2017, **355**, 1203–1206.
5 K. S. Kim, Y. Zhao, H. Jang, S. Y. Lee, J. M. Kim, K. S. Kim, J. H. Ahn, P. Kim, J. Y. Choi and B. H. Hong, *Nature*, 2009, **457**, 706–710.
6 P. Chakraborty, S. Das and A. K. Nandi, *Prog. Polym. Sci.*, 2019, **88**, 189–219.
7 P. J. Flory, Introductory lecture, *Discuss. Faraday Soc.*, 1974, **57**, 7–18.
8 C. Daniel, C. Dammer and J. M. Guenet, *Polymer*, 1994, **35**, 4243–4246.
9 D. Dasgupta and A. K. Nandi, *Macromolecules*, 2007, **40**, 2008–2018.
10 D. Dasgupta and A. K. Nandi, *Macromolecules*, 2005, **38**, 6504–6512.
11 F. Zhao, Y. Shi, L. Pan and G. Yu, *Acc. Chem. Res.*, 2017, **50**, 1734–1743.
12 Y. Shi, J. Zhang, L. Pan, Y. Shi and G. Yu, *Nano Today*, 2016, **11**, 738–762.
13 Q. Zhang, E. Uchaker, S. L. Candelaria and G. Cao, *Chem. Soc. Rev.*, 2013, **42**, 3127–3171.
14 M. S. Su'ait, M. Y. A. Rahman and A. Ahmad, *Sol. Energy*, 2015, **115**, 452–470.
15 H. Jiang, P. Taranekar, J. R. Reynolds and K. S. Schanze, *Angew. Chem., Int. Ed.*, 2009, **48**, 4300–4316.
16 S. Thomas, T. G. Deepak, G. S. Anjusree, T. A. Arun, S. V. Nair and A. S. Nair, *J. Mater. Chem. A*, 2014, **2**, 4474.
17 M. Gratzel, *Acc. Chem. Res.*, 2009, **42**, 1788.
18 E. Singh and H. S. Nalwa, *Sci. Adv. Mater.*, 2015, **7**, 1863.
19 P. Bairi, P. Chakraborty, A. Shit, S. Mondal, B. Roy and A. K. Nandi, *Langmuir*, 2014, **30**, 7547–7555.
20 S. Das, P. Chakraborty, A. Shit, S. Mondal and A. K. Nandi, *J. Mater. Chem. A*, 2016, **4**, 4194.
21 A. K. Nandi, *Polymer Functionalized Graphene*, Royal Society of Chemistry, 2021, Polymer Chemistry series 35, ch. 9, pp. 277–279.
22 M. K. Nazeeruddin, P. Péchy, T. Renouard, S. M. Zakeeruddin, R. Humphry-Baker, P. Comte, P. Liska, L. Cevey, E. Costa, V. Shklover, L. Spiccia, G. B. Deacon, C. A. Bignozzi and M. Grätzel, *J. Am. Chem. Soc.*, 2001, **123**, 1613–1624.
23 P. Wang, S. M. Zakeeruddin, J. E. Moser, M. K. Nazeeruddin, T. Sekiguchi and M. Grätzel, *Nat. Mater.*, 2003, **2**, 402–407.
24 Q. Liu, J. Wu, Z. Lan, M. Zheng, G. Yue, J. Lin and M. Huang, *Polym. Eng. Sci.*, 2015, **55**, 322–326.
25 Q. Li, X. Chen, Q. Tang, H. Xu, B. He and Y. Qin, *J. Mater. Chem. A*, 2013, **1**, 8055–8060.
26 C. Wu, L. Jia, S. Guo, S. Han, B. Chi, J. Pu and L. Jian, *ACS Appl. Mater. Interfaces*, 2013, **5**, 7886–7892.
27 J. M. Ji, H. Zhou, Y. K. Eom, C. H. Kim and H. K. Kim, *Adv. Energy Mater.*, 2020, **10**, 2000124.
28 Q. Wang, S. Ito, M. Gratzel, F. Fabregat-Santiago, I. Mora-Sero, J. Bisquert, T. Bessho and H. Imai, *J. Phys. Chem. B*, 2006, **110**, 25210–25221.
29 A. Gunasekaran, A. Sorrentino, A. M. Asiri and S. Anandan, *Sol. Energy*, 2020, **208**, 160–165.
30 Q. Li, Q. Tang, N. Du, Y. Qin, J. Xiao, B. He, H. Chen and L. Chu, *J. Power Sources*, 2014, **248**, 816–821.

31 C.-L. Chen, H. Teng and Y.-L. Lee, *J. Mater. Chem.*, 2011, **21**, 628–632.
32 Z. Yu, D. Qin, Y. Zhang, H. Sun, Y. Luo, Q. Meng and D. Li, *Energy Environ. Sci.*, 2011, **4**, 1298–1305.
33 S. K. Ahn, T. Ban, P. Sakthivel, J. W. Lee, Y.-S. Gal, J.-K. Lee, M.-R. Kim and S.-H. Jin, *ACS Appl. Mater. Interfaces*, 2012, **4**, 2096–2100.
34 S.-Y. Shen, R.-X. Dong, P.-T. Shih, V. Ramamurthy, J.-J. Lin and K.-C. Ho, *ACS Appl. Mater. Interfaces*, 2014, **6**, 18489–18496.
35 C.-L. Chen, T.-W. Chang, H. Teng, C.-G. Wu, C.-Y. Chen, Y.-M. Yang and Y.-L. Lee, *Phys. Chem. Chem. Phys.*, 2013, **15**, 3640–3645.
36 C.-L. Chen, H. Teng and Y.-L. Lee, *Adv. Mater.*, 2011, **23**, 4199–4204.
37 V. M. Mohan, K. Murakami, A. Kono and M. Shimomura, *J. Mater. Chem. A*, 2013, **1**, 7399.
38 S. Venkatesan, S.-C. Su, S.-C. Kao, H. Teng and Y.-L. Lee, *J. Power Sources*, 2015, **274**, 506–511.
39 S. Venkatesan, S.-C. Su, W.-N. Hung, I.-P. Liu, H. Teng and Y.-L. Lee, *J. Power Sources*, 2015, **298**, 385–390.
40 Masud, K. M. Kim and H. K. Kim, *ACS Appl. Mater. Interfaces*, 2020, **12**, 42067–42080.
41 Y. Rong, X. Li, G. Liu, H. Wang, Z. Ku, M. Xu, L. Liu, M. Hu, Y. Yang, M. Zhang, T. Liu and H. Han, *J. Power Sources*, 2013, **235**, 243–250.
42 W. Xiang, W. Huang, U. Bach and L. Spiccia, *Chem. Commun.*, 2013, **49**, 8997–8999.
43 S. Venkatesan, I.-P. Liu, L.-T. Chen, Y.-C. Hou, C.-W. Li and Y.-L. Lee, *ACS Appl. Mater. Interfaces*, 2016, **8**, 24559–24566.
44 S. M. Lim, J. Moon, G. H. Choi, U. C. Baek, J. M. Lim, J. T. Park and J. H. Kim, *Nanomaterials*, 2019, **9**, 1418.
45 R.-X. Dong, S.-Y. Shen, H.-W. Chen, C.-C. Wang, P.-T. Shih, C.-T. Liu, R. Vittal, J.-J. Lin and K.-C. Ho, *J. Mater. Chem. A*, 2013, **1**, 8471.
46 N. M. Saidi, F. S. Omar, A. Numan, D. C. Apperley, M. M. Algaradah, R. Kasi, A.-J. Avestro and R. T. Subramaniam, *ACS Appl. Mater. Interfaces*, 2019, **11**, 30185–30196.
47 S. Venkatesan, W. H. Lin, T. H. Hsu, H. Teng and Y. L. Lee, *ACS Sustain. Chem. Eng.*, 2022, **7**, 2473–2483.
48 I. P. Liu, Y. Y. Chen, Y. S. Cho, L. W. Wang, C. Y. Chien and Y. L. Lee, *J. Power Sources*, 2021, **482**, 228962.
49 N. M. Saidi, N. K. Farhana, S. Ramesh and K. Ramesh, *Sol. Energy*, 2021, **216**, 111–119.
50 N. K. Farhana, F. S. Omar, N. M. Saidi, G. Z. Ling, S. Bashir, R. Subramaniam, R. Kasi, J. Iqbal, S. Wageh, H. Algarni and A. G. Al-Sehemi, *Polymers*, 2022, **14**, 3426.
51 P. Raut, V. Kishnani, K. Mondal, A. Gupta and S. C. Jana, *Micromachines*, 2022, **13**, 680.
52 M. C. Williams, Fuel Cells, in *Fuel Um: Technologies For Fuel Processing*, ed. D. Shekhawat, J. J. Spivey and D. A. Berry, Elsevier, 2011, ch. 2, pp. 11–27.
53 Y. Guo, K. Zheng and P. Wan, *Small*, 2018, **14**, 1704497.
54 D. J. Kim, M. J. Jo and S. Y. Nam, *J. Ind. Eng. Chem.*, 2015, **21**, 36–52.
55 K. D. Kreuer, *J. Membr. Sci.*, 2001, **185**, 29–39.
56 A. M. Samsudin, M. Bodner and V. Hacker, *Polymers*, 2022, **14**, 3565.
57 J. Joseph, C. Y. Tseng and B. J. Hwang, *J. Power Sources*, 2011, **196**, 7363–7371.
58 S. Bose, T. Kuila, T. X. H. Nguyen, N. H. Kim, K.-t. Laua and J. H. Lee, *Prog. Polym. Sci.*, 2011, **36**, 813–843.
59 R. Devanathan, *Energy Environ. Sci.*, 2008, **1**, 101–119.
60 C. Laberty-Robert, K. Valle, F. Pereira and C. Sanchez, *Chem. Soc. Rev.*, 2011, **40**, 961–1005.
61 N. Shaari and S. K. Kamarudin, *Int. J. Energy Res.*, 2019, **43**, 2756–2794.
62 B. P. Tripathi and V. K. Shahi, *Prog. Polym. Sci.*, 2011, **36**, 945–979.
63 E. I. Santiago, R. A. Isidoro, M. A. Dresch, B. R. Matos, M. Linardi and F. C. Fonseca, *Electrochim. Acta*, 2009, **54**, 4111–4117.
64 M. Amjadi, S. Rowshanzamir, S. J. Peighambardoust and S. Sedghi, *J. Power Sources*, 2012, **210**, 350–357.
65 A. Jamaludin, Z. Ahmad, Z. A. Ahmad and A. A. Mohamad, *Int. J. Hydrog. Energy*, 2010, **35**, 11229–11236.
66 L. Geng, Y. He, D. Liu, X. Dai and C. Lü, *Microporous Mesoporous Mater.*, 2012, **148**, 8–14.
67 A. Sannigrahi, S. Ghosh, S. Maity and T. Jana, *Polymer*, 2011, **52**, 4319–4330.
68 J. A. Mader and B. C. Benicewicz, *Macromolecules*, 2010, **43**, 6706–6715.
69 N. A. Choudhury, J. Ma and Y. Sahai, *J. Power Sources*, 2012, **210**, 358–365.
70 M.-K. Song, H. Li, J. Li, D. Zhao, J. Wang and M. Liu, *Adv. Mater.*, 2014, **26**, 1277–1282.
71 Z. W. Seh, J. Kibsgaard, C. F. Dickens, I. Chorkendorff, J. K. Nørskov and T. F. Jaramillo, *Science*, 2017, **355**, 4998.
72 Z. Fang, P. Li and G. Yu, *Adv. Mater.*, 2020, **32**, 2003191.
73 Y. Guo, Z. Fang and G. Yu, *Polym. Int.*, 2021, **70**, 1425–1432.
74 P. Li, Z. Jin, Y. Qian, Z. Fang, D. Xiao and G. Yu, *Mater. Today*, 2020, **35**, 78–86.
75 P. Li, Z. Jin, Y. Qian, Z. Fang, D. Xiao and G. Yu, *ACS Energy Lett.*, 2019, **4**, 1793–1802.
76 S. Das, R. Ghosh, P. Routh, A. Shit, S. Mondal, A. Panja and A. K. Nandi, *ACS Appl. Nano Mater.*, 2018, **1**, 2306–2316.
77 S. Xu, D. Li and P. Wu, *Adv. Funct. Mater.*, 2015, **25**, 1127–1136.
78 Q. Liu, Q. Fang, W. Chu, Y. Wan, X. Li, W. Xu, *et al.*, *Chem. Mater.*, 2017, **29**, 4738–4744.
79 H. Li, C. Tsai, A. L. Koh, L. Cai, A. W. Contryman, A. H. Fragapane, J. Zhao, H. S. Han, H. C. Manoharan, F. Abild-Pedersen, J. K. Nørskov and X. Zheng, *Nat. Mater.*, 2016, **15**, 48–53.
80 Z. Wu, B. Hu, P. Wu, H. Liang, Z. Yu, Y. Lin, Y. Zheng, Z. Li and S. Yu, *NPG Asia Mater.*, 2016, **8**, 288.
81 X. Guo, G. Cao, F. Ding, X. Li, S. Zhen, Y. Xue, Y. Yan, T. Liu and K. Sun, *J. Mater. Chem. A*, 2015, **3**, 5041.
82 S. H. Osman, S. K. Kamarudin, S. Basri and N. A. Karim, *Int. J. Energy Res.*, 2022, **46**, 16264–16280.
83 Z. Yang, J. Zhang, M. C. W. Kintner-Meyer, X. Lu, D. Choi, J. P. Lemmon and J. Liu, *Chem. Rev.*, 2011, **111**, 3577–3613.

84 R. J. Brodd, K. R. Bullock, R. A. Leising, R. L. Middaugh, J. R. Miller and E. J. Takeuchi, *J. Electrochem. Soc.*, 2004, **151**, K1–K11.
85 L. L. Zhang and X. S. Zhao, *Chem. Soc. Rev.*, 2009, **38**, 2520–2531.
86 M. Park, X. Zhang, M. Chung, G. B. Less and A. M. Sastry, *J. Power Sources*, 2010, **195**, 7904–7929.
87 M. Armand and J.-M. Tarascon, *Nature*, 2008, **451**, 652.
88 B. Dunn, H. Kamath and J.-M. Tarascon, *Science*, 2011, **334**, 928.
89 J. Y. Song, Y. Y. Wang and C. C. Wan, *J. Power Sources*, 1999, **77**, 183–197.
90 V. Palomares, P. Serras, I. Villaluenga, K. B. Hueso, J. Carretero-Gonzalez and T. Rojo, *Energy Environ. Sci.*, 2012, **5**, 5884–5901.
91 J. Kim, J. H. Kim and K. Ariga, *Joule*, 2017, **1**, 739–768.
92 Y. Shi, L. Peng and G. Yu, *Nanoscale*, 2015, **7**, 12796–12806.
93 J. Kim, J. Lee, J. You, M.-S. Park, S. A. Hossain, Y. Yamauchi and J. H. Kim, *Mater. Horiz.*, 2016, **3**, 517–535.
94 J. Balaji, M. G. Sethuraman, S.-H. Roh and H.-Y. Jung, *Polym. Test.*, 2020, **89**, 106567.
95 Y. Shi and G. Yu, *Chem. Mater.*, 2016, **28**, 2466–2477.
96 X. Cheng, J. Pan, Y. Zhao, M. Liao and H. Peng, *Adv. Energy Mater.*, 2018, **8**, 1702184.
97 W. Li, Y. Wu, J. Wang, D. Huang, L. Chen and G. Yang, *Eur. Polym. J.*, 2015, **67**, 365–372.
98 J. F. Vélez, M. Aparicio and J. Mosa, *Electrochim. Acta*, 2016, **213**, 831–841.
99 M. Yanilmaz, Y. Lu, J. Zhu and X. Zhang, *J. Power Sources*, 2016, **313**, 205–212.
100 M. V. Bhute, Y. P. Mahant and S. B. Kondawar, *J. Mater. NanoSci.*, 2017, **4**, 6–12.
101 Q. Wu, Y. Yang, Z. Chen, Q. Su, S. Huang, D. Song, C. Zhu, R. Ma and C. Li, *ACS Appl. Energy Mater.*, 2021, **4**, 9420–9430.
102 J.-Y. Hwang, S.-J. Park, C. S. Yoon and Y.-K. Sun, *Energy Environ. Sci.*, 2019, **12**, 2174–2184.
103 A. S. Lee, J. H. Lee, J.-C. Lee, S. M. Hong, S. S. Hwang and C. M. Koo, *J. Mater. Chem. A*, 2014, **2**, 1277–1283.
104 J. H. Lee, A. S. Lee, J.-C. Lee, S. M. Hong, S. S. Hwang and C. M. Koo, *J. Mater. Chem. A*, 2015, **3**, 2226–2233.
105 F. Elizalde, J. Amici, S. Trano, G. Vozzolo, R. Aguirresarobe, D. Versaci, S. Bodoardo, D. Mecerreyes, H. Sardon and F. Bella, *J. Mater. Chem. A*, 2022, **10**, 2588–12596.
106 C. Li, Y. Huang, C. Chen, X. Feng, Z. Zhang and P. Liu, *J. Colloid Interface Sci.*, 2022, **608**, 313–321.
107 X. Zeng, L. Dong, J. Fu, L. Chen, J. Zhou, P. Zong, G. Liu and L. Shi, *Chem. Eng. J.*, 2022, **428**, 131100.
108 Q. Wang, X. Xu, B. Hong, M. Bai, J. Li, Z. Zhang and Y. La, *Chem. Eng. J.*, 2022, **428**, 131331.
109 Y. Shi, X. Zhou, J. Zhang, A. M. Bruck, A. C. Bond, A. C. Marschilok, K. J. Takeuchi, E. S. Takeuchi and G. Yu, *Nano Lett.*, 2017, **17**, 1906–1914.
110 T. Xu, H. Du, H. Liu, W. Liu, X. Zhang, C. Si, P. Liu and K. Zhang, *Adv. Mater.*, 2021, **33**, 2101368.
111 L. Chen, Z. Huang, H. Liang, Q. Guan and S. Yu, *Adv. Mater.*, 2013, **25**, 4746.
112 P. J. Kim, K. Kim and V. G. Pol, *Energy Storage Mater.*, 2019, **19**, 179.
113 D. Cao, Y. Xing, K. Tantratian, X. Wang, Y. Ma, A. Mukhopadhyay, Z. Cheng, Q. Zhang, Y. Jiao, L. Chen and H. Zhu, *Adv. Mater.*, 2019, **31**, 1807313.
114 C.-Y. Wang, Z.-J. Zheng, Y.-Q. Feng, H. Ye, F.-F. Cao and Z.-P. Guo, *Nano Energy*, 2020, **74**, 104817.
115 S. Cao, X. Feng, Y. Song, X. Xue, H. Liu, M. Miao, J. Fang and L. Shi, *ACS Appl. Mater. Interfaces*, 2015, **7**, 10695.
116 Y. Kuang, C. Chen, G. Pastel, Y. Li, J. Song, R. Mi, W. Kong, B. Liu, Y. Jiang, K. Yang and L. Hu, *Adv. Energy Mater.*, 2018, **8**, 1802398.
117 Y. Shi, J. Zhang, A. M. Bruck, Y. Zhang, J. Li, E. A. Stach, K. J. Takeuchi, A. C. Marschilok, E. S. Takeuchi and G. Yu, *Adv. Mater.*, 2017, **29**, 1603922.
118 F. Bonaccorso, L. Colombo, G. Yu, M. Stoller, V. Tozzini, A. C. Ferrari, R. S. Ruoff and V. Pellegrini, *Science*, 2015, **347**, 1246501.
119 L. Peng, P. Xiong, L. Ma, Y. Yuan, Y. Zhu, D. Chen, X. Luo, J. Lu, K. Amine and G. Yu, *Nat. Commun.*, 2017, **8**, 15139.
120 Y. Shi, X. Zhou and G. Yu, *Acc. Chem. Res.*, 2017, **50**, 2642–2652.
121 N. J. Dudney and J. Li, *Science*, 2015, **347**, 131–132.
122 K. Kirshenbaum, D. C. Bock, C.-Y. Lee, Z. Zhong, K. J. Takeuchi, A. C. Marschilok and E. S. Takeuchi, *Science*, 2015, **347**, 149–154.
123 Y. Shi, L. Peng, Y. Ding, Y. Zhao and G. Yu, *Chem. Soc. Rev.*, 2015, **44**, 6684–6696.
124 H. Wu, G. Yu, L. Pan, N. Liu, M. T. McDowell, Z. Bao and Y. Cui, *Nat. Commun.*, 2013, **4**, 1943.
125 J. Y. Oh, S. Rondeau-Gagné, Y.-C. Chiu, A. Chortos, F. Lissel, G.-J. N. Wang, B. C. Schroeder, T. Kurosawa, J. Lopez, T. Katsumata, J. Xu, C. Zhu, X. Gu, W.-G. Bae, Y. Kim, L. Jin, J. W. Chung, J. B.-H. Tok and Z. Bao, *Nature*, 2016, **539**, 411–415.
126 Y. Shi, C. Ma, L. Peng and G. Yu, *Adv. Funct. Mater.*, 2015, **25**, 1219–1225.
127 K. K. Kumar, M. Ravi, Y. Pavani, S. Bhavani, A. K. Sharma and V. V. R. N. Rao, *Phys. B*, 2011, **406**, 1706–1712.
128 D. Kumar and S. A. Hashmi, *Solid State Ionics*, 2010, **181**, 416–423.
129 D. Kumar and S. A. Hashmi, *J. Power Sources*, 2010, **195**, 5101–5108.
130 Y. Zhu, Y. Yang, L. Fu and Y. Wu, *Electrochim. Acta*, 2017, **224**, 405–411.
131 Y. Q. Yang, Z. Chang, M. X. Li, X. W. Wang and Y. P. Wu, *Solid State Ionics*, 2015, **269**, 1–7.
132 Z. Lin, G. Wang, X. Xiong, J. Zheng, X. Ou and C. Yang, *Electrochim. Acta*, 2018, **269**, 225–231.
133 X. Zhang, X. Wang, S. Liu, Z. Tao and J. Chen, *Nano Res.*, 2018, **11**, 6244–6251.
134 J. Song, Z. Yu, M. L. Gordin, X. Li, H. Peng and D. Wang, *ACS Nano*, 2015, **9**, 11933–11941.
135 D. Zhang, Q. Wang, S. Peng, X. Yan, X. Wu and G. He, *J. Membr. Sci.*, 2019, **587**, 117189.
136 L. Ling, M. Xiao, D. Han, S. Ren, S. Wang and Y. Meng, *J. Membr. Sci.*, 2019, **585**, 230–237.

137 J. Huang, X. Chi, J. Yang and Y. Liu, *ACS Appl. Mater. Interfaces*, 2020, **12**, 17583–17591.
138 K. Wu, J. Cui, J. Yi, X. Liu, F. Ning, Y. Liu and J. Zhang, *ACS Appl. Mater. Interfaces*, 2022, **14**, 34612–34619.
139 A. Herzog-Arbeitman, S. Maletti, S. Oswald, T. Schmeida, L. Giebeler and D. Mikhailova, *ACS Appl. Energy Mater.*, 2021, **4**, 1906–1914.
140 H. Wang, P. Wang, Z. Ji, Z. Chen, J. Wang, W. Ling, J. Liu, M. Hu, C. Zhi and Y. Huang, *Nano Res.*, 2021, **14**, 4154–4162.
141 A. Chamaani, M. Safa, N. Chawla and B. El-Zahab, *ACS Appl. Mater. Interfaces*, 2017, **9**, 33819–33826.
142 B. Li, Y. Liu, X. Zhang, P. He and H. Zhou, *Green Energy Environ.*, 2019, **4**, 3–19.
143 P. Simon and Y. Gogotsi, *Nat. Mater.*, 2008, **7**, 845–854.
144 G. Wang, L. Zhang and J. Zhang, *Chem. Soc. Rev.*, 2012, **41**, 797–828.
145 M. R. Lukatskaya, B. Dunn and Y. Gogotsi, *Nat. Commun.*, 2016, **7**, 12647.
146 D. P. Chatterjee and A. K. Nandi, *J. Mater. Chem. A*, 2021, **9**, 15880–15918.
147 D. P. Dubal, O. Ayyad, V. Ruiz and P. Gomez-Romero, *Chem. Soc. Rev.*, 2015, **44**, 1777–1790.
148 J. R. Miller and P. Simon, *Science*, 2008, **321**, 651–652.
149 Z. Yu, L. Tetard, L. Zhai and J. Thomas, *Energy Environ. Sci.*, 2015, **8**, 702–730.
150 H. Sun, J. Zhu, D. Baumann, L. Peng, Y. Xu, I. Shakir, Y. Huang and X. Duan, *Nat. Rev. Mater.*, 2019, **4**, 45–60.
151 C. Yin, X. Liu, J. Wei, R. Tan, J. Zhou, M. Ouyang, H. Wang, S. J. Cooper, B. Wu, C. George and Q. Wang, *J. Mater. Chem. A*, 2019, **7**, 8826–8831.
152 K. Wang, X. Zhang, C. Li, X. Sun, Q. Meng, Y. Ma and Z. Wei, *Adv. Mater.*, 2015, **27**, 7451–7457.
153 N. Kurra, R. Wang and H. N. Alshareef, *J. Mater. Chem. A*, 2015, **3**, 7368–7374.
154 Q. Zheng, Z. Cai, Z. Ma and S. Gong, *ACS Appl. Mater. Interfaces*, 2015, **7**, 3263–3271.
155 A. Vlad, N. Singh, S. Melinte, J.-F. Gohy and P. M. Ajayan, *Sci. Rep.*, 2016, 22194.
156 S. Ghosh and O. Inganäs, *Adv. Mater.*, 1999, **11**, 1214.
157 L. J. Pan, G. H. Yu, D. Y. Zhai, H. R. Lee, W. T. Zhao, N. Liu, H. L. Wang, B. C. K. Tee, Y. Shi, Y. Cui and Z. N. Bao, *Proc. Natl. Acad. Sci. U. S. A.*, 2012, **109**, 9287.
158 P. Dou, Z. Liu, Z. Z. Cao, J. Zheng, C. Wang and X. H. Xu, *J. Mater. Sci.*, 2016, **51**, 4274.
159 Y. Shi, L. Pan, B. Liu, Y. Wang, Y. Cui, Z. Bao and G. Yu, *J. Mater. Chem. A*, 2014, **2**, 6086–6091.
160 H. T. Guo, W. N. He, Y. Lu and X. T. Zhang, *Carbon*, 2015, **92**, 133.
161 K. Zhou, Y. He, Q. C. Xu, Q. E. Zhang, A. A. Zhou, Z. H. Lu, L. K. Yang, Y. Jiang, D. T. Ge, X. Y. Liu and H. Bai, *ACS Nano*, 2018, **12**, 5888.
162 W. W. Li, F. X. Gao, X. Q. Wang, N. Zhang and M. M. Ma, *Angew. Chem., Int. Ed.*, 2016, **55**, 9196.
163 W. W. Li, H. Lu, N. Zhang and M. M. Ma, *ACS Appl. Mater. Interfaces*, 2017, **9**, 20142.
164 L. M. Zang, Q. F. Liu, J. H. Qiu, C. Yang, C. Wei, C. J. Liu and L. Lao, *ACS Appl. Mater. Interfaces*, 2017, **9**, 33941.
165 G. P. Hao, F. Hippauf, M. Oschatz, F. M. Wisser, A. Leifert, W. Nickel, N. Mohamed-Noriega, Z. K. Zheng and S. Kaskel, *ACS Nano*, 2014, **8**, 7138.
166 M. A. Smirnov, M. P. Sokolova, N. V. Bobrova, I. A. Kasatkin, E. Lahderanta and G. K. Elyashevich, *J. Power Sources*, 2016, **304**, 102.
167 M. Ates, M. El-Kady and R. B. Kaner, *Nanotechnology*, 2018, **29**, 175402.
168 Y. B. Zou, Z. C. Zhang, W. B. Zhong and W. T. Yang, *J. Mater. Chem. A*, 2018, **6**, 9245.
169 H. B. Huang, J. K. Yao, Y. L. Liu, X. Tuo, Y. M. Da, X. P. Zeng and L. Liu, *J. Macromol. Sci. Phys.*, 2017, **56**, 532.
170 Y. Shi, M. Wang, C. B. Ma, Y. Q. Wang, X. P. Li and G. H. Yu, *Nano Lett.*, 2015, **15**, 6276.
171 Y. Okumura and K. Ito, *Adv. Mater.*, 2001, **13**, 485.
172 K. Haraguchi and T. Takehisa, *Adv. Mater.*, 2002, **14**, 1120.
173 J. P. Gong, Y. Katsuyama, T. Kurokawa and Y. Osada, *Adv. Mater.*, 2003, **15**, 1155.
174 M. Malkoch, R. Vestberg, N. Gupta, L. Mespouille, P. Dubois, A. F. Mason, J. L. Hedrick, Q. Liao, C. W. Frank and K. Kingsbury, *Chem. Commun.*, 2006, **26**, 2774.
175 S. Sasaki and S. Koga, *J. Phys. Chem. B*, 2002, **106**, 11893.
176 T. Huang, H. Xu, K. Jiao, L. Zhu, H. R. Brown and H. Wang, *Adv. Mater.*, 2007, **19**, 1622.
177 Z. Wu, C. Guo, J. Dai, Z. Lu, C. Yuan, B. Zeng, Y. Xu and L. Dai, *J. Colloid Interface Sci.*, 2022, **616**, 268–278.
178 S. Das, P. Chakraborty, S. Mondal, A. Shit and A. K. Nandi, *ACS Appl. Mater. Interfaces*, 2016, **8**, 28055–28067.
179 S. Das, R. Ghosh, D. Mandal and A. K. Nandi, *ACS Appl. Energy Mater.*, 2019, **2**, 6642–6654.
180 B. Liu, P. Soares, C. Checkles, Y. Zhao and G. Yu, *Nano Lett.*, 2013, **13**, 3414–3419.
181 A. K. Das, B. Ramulu, E. G. Shankar and J. S. Yu, *Chem. Eng. J.*, 2022, **429**, 13248.
182 N. S. Shaikh, S. B. Ubale, V. J. Mane, J. S. Shaikh, V. C. Lokhande, S. Praserthdam, C. D. Lokhande and P. Kanjanaboos, *J. Alloys Compd.*, 2022, **893**, 161998.
183 I. Osada, H. de Vries, B. Scrosati and S. Passerini, *Angew. Chem., Int. Ed.*, 2016, **55**, 500.
184 M. J. Park, I. Choi, J. Hong and O. Kim, *J. Appl. Polym. Sci.*, 2013, **129**, 2363.
185 J. Kalhoff, G. G. Eshetu, D. Bresser and S. Passerini, *ChemSusChem*, 2015, **8**, 2154.
186 S. Tan, Y. J. Ji, Z. R. Zhang and Y. Yang, *ChemPhysChem*, 2014, **15**, 1956.
187 Y. Takeda, O. Yamamoto and N. Imanishi, *Electrochemistry*, 2016, **84**, 210.
188 L. Porcarelli, C. Gerbaldi, F. Bella and J. R. Nair, *Sci. Rep.*, 2016, **6**, 19892.
189 Q. Lu, Y.-B. He, Q. Yu, B. Li, Y. V. Kaneti, Y. Yao, F. Kang and Q.-H. Yang, *Adv. Mater.*, 2017, **29**, 1604460.
190 J. Hu, J. Tian and C. Li, *ACS Appl. Mater. Interfaces*, 2017, **9**, 11615.

191 H. Gao, B. Guo, J. Song, K. Park and J. B. Goodenough, *Adv. Energy Mater.*, 2015, **5**, 1402235.
192 J. Jin, Z. Wen, X. Liang, Y. Cui and X. Wu, *Solid State Ionics*, 2012, **225**, 604.
193 S.-Y. Lee, A. Ogawa, M. Kanno, H. Nakamoto, T. Yasuda and M. Watanabe, *J. Am. Chem. Soc.*, 2010, **132**, 9764.
194 J. Chen, M. Asano, T. Yamaki and M. Yoshida, *J. Membr. Sci.*, 2006, **269**, 194.
195 C. Zhao, C. Wang, Z. Yue, K. Shu and G. G. Wallace, *ACS Appl. Mater. Interfaces*, 2013, **5**, 9008.
196 Y. Huang, M. Zhong, F. Shi, X. Liu, Z. Tang, Y. Wang, Y. Huang, H. Hou, X. Xie and C. Zhi, *Angew. Chem., Int. Ed.*, 2017, **56**, 9141.
197 R. Subadevi, M. Sivakumar, S. Rajendran, H.-C. Wuand and N.-L. Wu, *Ionics*, 2011, **18**, 283–289.
198 H. Du and J. Zhang, *Colloid Polym. Sci.*, 2009, **288**, 15–24.
199 H. N. Fard, G. B. Pour, M. N. Sarvi and P. Esmaili, *Ionics*, 2019, **25**, 2951–2963.
200 S. Petty-Weeks, J. J. Zupancic and J. R. Swedo, *Solid State Ionics*, 1988, **31**, 117–125.
201 S. Jha, S. Mehta, Y. Chen, L. Ma, P. Renner, D. Y. Parkinson and H. Liang, *ACS Sustainable Chem. Eng.*, 2019, **8**, 498–511.
202 P. Karthika, N. Rajalakshmi and K. S. Dhathathreyan, *ChemPhysChem*, 2013, **14**, 3822–3826.
203 X. Li, R. Liu, C. Xu, Y. Bai, X. Zhou, Y. Wang and G. Yuan, *Adv. Funct. Mater.*, 2018, **28**, 1800064.
204 X. Lv, G. Li, D. Li, F. Huang, W. Liu and Q. Wei, *J. Phys. Chem. Solids*, 2017, **110**, 202–210.
205 C. Meng, C. Liu, L. Chen, C. Hu and S. Fan, *Nano Lett.*, 2010, **10**, 4025–4031.
206 B. Yao, L. Yuan, X. Xiao, J. Zhang, Y. Qi, J. Zhou, J. Zhou, B. Hu and W. Chen, *Nano Energy*, 2013, **2**, 1071–1078.
207 L. Zhang, D. DeArmond, N. T. Alvarez, R. Malik, N. Oslin, C. McConnell, P. K. Adusei, Y. Y. Hsieh and V. Shanov, *Small*, 2017, **13**, 1603114.
208 A. Khosrozadeh, M. Xing and Q. Wang, *Appl. Energy*, 2015, **153**, 87–93.
209 Y. G. Zhu, Y. Wang, Y. Shi, J. I. Wong and H. Y. Yang, *Nano Energy*, 2014, **3**, 46–54.
210 P. Wu, S. Cheng, M. Yao, L. Yang, Y. Zhu, P. Liu, O. Xing, J. Zhou, M. Wang, H. Luo and M. Liu, *Adv. Funct. Mater.*, 2017, **27**, 1702160.
211 S.-I. Kim, J.-H. Kang, S.-W. Kim and J.-H. Jang, *Nano Energy*, 2017, **39**, 639–646.
212 Y. Jiang, C. Zhou and J. Liu, *Energy Storage Mater.*, 2018, **11**, 75–82.
213 C. Choi, J. A. Lee, A. Y. Choi, Y. T. Kim, X. Lepro, M. D. Lima, R. H. Baughman and S. J. Kim, *Adv. Mater.*, 2014, **26**, 2059–2065.
214 J. Chen, K. Fang, Q. Chen, J. Xu and C.-P. Wong, *Nano Energy*, 2018, **53**, 337–344.
215 Y. Yang, H. Fei, G. Ruan, C. Xiang and J. M. Tour, *Adv. Mater.*, 2014, **26**, 8163–8168.
216 K. Lu, B. Song, K. Li, J. Zhang and H. Ma, *J. Power Sources*, 2017, **370**, 98–105.
217 L. Zhang, P. Zhu, F. Zhou, W. Zeng, H. Su, G. Li, J. Gao, R. Sun and C. P. Wong, *ACS Nano*, 2016, **10**, 1273–1282.
218 Y. J. Kang, H. Chung and W. Kim, *Synth. Met.*, 2013, **166**, 40–44.
219 C. Wang, X. Wu, Y. Ma, G. Mu, Y. Li, C. Luo, H. Xu, Y. Zhang, J. Yang, X. Tang, J. Zhang, W. Bao and C. Duan, *J. Mater. Chem. A*, 2018, **6**, 8299–8306.
220 K. Sun, E. Feng, G. Zhao, H. Peng, G. Wei, Y. Lv and G. Ma, *ACS Sustainable Chem. Eng.*, 2018, **7**, 165–173.
221 L. Liu, Q. Dou, Y. Sun, Y. Lu, Q. Zhang, J. Meng, X. Zhang, S. Shi and X. Yan, *J. Mater. Chem. A*, 2019, **7**, 20398–20404.
222 L. Liu, Y. Yu, C. Yan, K. Li and Z. Zheng, *Nat. Commun.*, 2015, **6**, 7260.
223 G. Wang, X. Lu, Y. Ling, T. Zhai, H. Wang, Y. Tong and Y. Li, *ACS Nano*, 2012, **6**, 10296–10302.
224 Y. Shao, J. Li, Y. Li, H. Wang, Q. Zhang and R. B. Kaner, *Mater. Horiz.*, 2017, **4**, 1145–1150.
225 M. Wang, L. Fan, G. Qin, X. Hu, Y. Wang, C. Wang, J. Yang and Q. Chen, *J. Membr. Sci.*, 2020, **597**, 117740.
226 J. Yang, X. Yu, X. Sun, Q. Kang, L. Zhu, G. Qin, A. Zhou, G. Sun and Q. Chen, *ACS Appl. Mater. Interfaces*, 2020, **12**, 9736–9745.
227 S. B. Mitta, R. Harpalsinh, J. Kim, H. S. Park and S. H. Um, *Adv. Mater. Interfaces*, 2022, **9**, 70081.
228 X. Lu, G. Wang, T. Zhai, M. Yu, S. Xie, Y. Ling, C. Liang, Y. Tong and Y. Li, *Nano Lett.*, 2012, **12**, 5376–5381.
229 D. P. Dubal, N. R. Chodankar, D. H. Kim and P. Gomez-Romero, *Chem. Soc. Rev.*, 2018, **47**, 2065–2129.
230 R. Yi, R. Wang, J. Duan, Z. Fang, H. Li, Z. Chen, A. Zhou and Y. Sun, *Electrochim. Acta*, 2020, **338**, 135845.
231 J.-M. Yang and S.-A. Wang, *J. Membr. Sci.*, 2015, **477**, 49–57.
232 Y. Zhao, H. Ma, S. Huang, X. Zhang, M. Xia, Y. Tang and Z. F. Ma, *ACS Appl. Mater. Interfaces*, 2016, **8**, 22997–23005.
233 Y. Zhao, S. Huang, M. Xia, S. Rehman, S. Mu, Z. Kou, Z. Zhang, Z. Chen, F. Gao and Y. Hou, *Nano Energy*, 2016, **28**, 346–355.
234 Y.-F. Huang, P.-F. Wu, M.-Q. Zhang, W.-H. Ruan and E. P. Giannelis, *Electrochim. Acta*, 2014, **132**, 103–111.
235 G.-M. Hou, Y.-F. Huang, W.-H. Ruan, M.-Q. Zhang and M.-Z. Rong, *J. Solid State Electrochem.*, 2015, **20**, 1903–1911.
236 M. Ni, C. Ma, H. Huang, L. Han, X. Fu, Z. Yang, J. Li, L. Pan and M. Xu, *ACS Appl. Energy Mater.*, 2022, **5**, 6724–6733.
237 W. G. Moon, G. P. Kim, M. Lee, H. D. Song and J. Yi, *ACS Appl. Mater. Interfaces*, 2015, **7**, 3503–3511.
238 H. Peng, Y. Lv, G. Wei, J. Zhou, X. Gao, K. Sun, G. Ma and Z. Lei, *J. Power Sources*, 2019, **431**, 210–219.
239 Z. Song, H. Duan, D. Zhu, Y. Lv, W. Xiong, T. Cao, L. Li, M. Liu and L. Gan, *J. Mater. Chem. A*, 2019, **7**, 15801–15811.
240 Y. Matsuda, *J. Electrochem. Soc.*, 1993, **140**, L109.
241 S. Mondal, T. Yoshida, S. Maji, K. Ariga and M. Higuchi, *ACS Appl. Mater. Interfaces*, 2020, **12**, 58277–58286.
242 C. Zhong, Y. Deng, W. Hu, J. Qiao, L. Zhangd and J. Zhangd, *Chem. Soc. Rev.*, 2015, **44**, 7484–7539.
243 R. B. Rakhi, D. H. Nagaraju, P. Beaujuge and H. N. Alshareef, *Electrochim. Acta*, 2016, **220**, 601–608.
244 V. Vijayakumar, B. Anothumakkool, A. Torris A. T, S. B. Nair, M. V. Badiger and S. Ku- rungot, *J. Mater. Chem. A*, 2017, **5**, 8461–8476.

245 R. Na, Y. Liu, N. Lu, S. Zhang, F. Liu and G. Wang, *Chem. Eng. J.*, 2019, **374**, 738–747.
246 R. Na, N. Lu, S. Zhang, G. Huo, Y. Yang, C. Zhang, Y. Mu, Y. Luo and G. Wang, *Electrochim. Acta*, 2018, **290**, 262–272.
247 P. Kubisa, *Prog. Polym. Sci.*, 2009, **34**, 1333–1347.
248 C. Arbizzani, M. Biso, D. Cericola, M. Lazzari, F. Soavi and M. Mastragostino, *J. Power Sources*, 2008, **185**(2), 1575–1579.
249 V. Ruiz, T. Huynh, S. R. Sivakkumar and A. G. Pandolfo, *RSC Adv.*, 2012, **2**(13), 5591.
250 J. Feng, X. Sun, C. Wu, L. Peng, C. Lin, S. Hu, J. Yang and Y. Xie, *J. Am. Chem. Soc.*, 2011, **133**, 17832–17838.
251 H. T. Jeong, J. F. Du and Y. R. Kim, *ChemistrySelect*, 2017, **2**, 6057–6061.
252 X. Zhang, L. Wang, J. Peng, P. Cao, X. Cai, J. Li and M. Zhai, *Adv. Mater. Interfaces*, 2015, **2**, 1500267.
253 X. Tang, Y. H. Lui, A. R. Merhi, B. Chen, S. Ding, B. Zhang and S. Hu, *ACS Appl. Mater. Interfaces*, 2017, **9**, 44429–44440.
254 J. Wang, G. Chen and S. Song, *Electrochim. Acta*, 2020, **330**, 135322.
255 P. K. Adusei, S. N. Kanakaraj, S. Gbordzoe, K. Johnson, D. DeArmond, Y.-Y. Hsieh, Y. Fang, S. Mishra, N. Phan, N. T. Alvarez and V. Shanov, *Electrochim. Acta*, 2018, **312**, 411–423.
256 L. Yang, J. Hu, G. Lei and H. Liu, *Chem. Eng. J.*, 2014, **258**, 320–326.
257 X. Lyu, F. Su and M. Miao, *J. Power Sources*, 2016, **307**, 489–495.
258 P. Ahuja, R. K. Sharma and G. Singh, *J. Mater. Chem. A*, 2015, **3**, 4931–4937.
259 W. Liu, K. Wang, C. Li, X. Zhang, X. Sun, J. Han, X.-L. Wu, F. Li and Y. Ma, *J. Mater. Chem. A*, 2018, **6**, 24979–24987.
260 L. Feng, K. Wang, X. Zhang, X. Sun, C. Li, X. Ge and Y. Ma, *Adv. Funct. Mater.*, 2018, **28**, 1704463.
261 X. Deng, J. Li, S. Zhu, L. Ma and N. Zhao, *Energy Storage Mater.*, 2019, **23**, 491–498.
262 C. Yang, M. Sun, X. Wang and G. Wang, *ACS Sustainable Chem. Eng.*, 2015, **3**, 2067–2076.
263 J.-J. Zhu, L. Martinez-Soria and P. Gomez-Romero, *Nanomaterials*, 2022, **12**, 514.
264 Y. M. Kim, W. Y. Choi, J. H. Kwon, J. K. Lee and H. C. Moon, *Chem. Mater.*, 2021, **33**, 2683–2705.
265 H. Wang, Z. Wang, J. Yang, C. Xu, Q. Zhang and Z. Peng, *Macromol. Rapid Commun.*, 2018, **39**, 1800246.
266 K. Hashimoto, M. Hirasawa, H. Kokubo, R. Tamate, X. Li, M. Shibayama and M. Watanabe, *Macromolecules*, 2019, **52**, 8430–8439.
267 T. Kawazoe, K. Hashimoto, Y. Kitazawa, H. Kokubo and M. Watanabe, *Electrochim. Acta*, 2017, **235**, 287–294.
268 K. H. Lee, M. S. Kang, S. Zhang, Y. Gu, T. P. Lodge and C. D. Frisbie, *Adv. Mater.*, 2012, **24**, 4457–4462.
269 K. G. Cho, Y. K. Cho, J. H. Kim, H. Yoo, K. Hong and K. H. Lee, *ACS Appl. Mater. Interfaces*, 2020, **12**, 15464–15471.
270 H. Hwang, S. Y. Park, J. K. Kim, Y. M. Kim and H. C. Moon, *ACS Appl. Mater. Interfaces*, 2019, **11**, 4399–4407.
271 D. A. Kang, K. Kim, S. S. Karade, H. Kim and J. H. Kim, *Chem. Eng. J.*, 2020, **384**, 123308.
272 M. Taghavikish, S. Subianto, Y. Gu, X. Sun, X. S. Zhao and N. R. Choudhury, *Sci. Rep.*, 2018, **8**, 10918.
273 D. O. Ponkratov, E. I. Lozinskaya, P. S. Vlasov, P.-H. Aubert, C. Plesse, F. Vidal, Y. S. Vygodskii and A. S. Shaplov, *Electrochim. Acta*, 2018, **281**, 777–788.
274 H. Li, Z. Feng, K. Zhao, Z. Wang, J. Liu, J. Liu and H. Song, *Nanoscale*, 2019, **11**, 3689–3700.
275 K. Gopalsamy, Q. Yang, S. Cai, T. Huang, Z. Gao and C. Gao, *J. Energy Chem.*, 2019, **34**, 104–110.
276 Y. Yang, B. Cao, H. Li and H. Liu, *Chem. Eng. J.*, 2017, **330**, 753–756.
277 G. A. Tiruye, D. Muñoz-Torrero, J. Palma, M. Anderson and R. Marcilla, *J. Power Sources*, 2015, **279**, 472–480.
278 S. A. Alexandre, G. G. Silva, R. Santamaría, J. P. C. Trigueiro and R. L. Lavall, *Electrochim. Acta*, 2019, **299**, 789–799.
279 S. T. Senthilkumar, R. K. Selvan and J. S. Melo, *J. Mater. Chem. A*, 2013, **1**, 12386.
280 F. Gan, Y. Xu, H. Yang, Z. Ren and H. Du, *J. Appl. Polym. Sci.*, 2020, **137**, 48723.
281 L.-Q. Fan, J. Zhong, C.-Y. Zhang, J.-H. Wu and Y.-L. Wei, *Int. J. Hydrog. Energy*, 2016, **41**, 5725–5732.
282 G. Ma, E. Feng, K. Sun, H. Peng, J. Li and Z. Lei, *Electrochim. Acta*, 2014, **135**, 461–466.
283 K. Sun, F. Ran, G. Zhao, Y. Zhu, Y. Zheng, M. Ma, X. Zheng, G. Ma and Z. Lei, *RSC Adv.*, 2016, **6**, 55225–55232.
284 J. Zhou, Y. Yin, A. N. Mansour and X. Zhou, *J Solid State Electrochem.*, 2011, **14**, A25.
285 H. Yu, J. Wu, L. Fan, K. Xu, X. Zhong, Y. Lin and J. Lin, *Electrochim. Acta*, 2011, **56**, 6881–6886.
286 M. Kim and J. Kim, *Electrochim. Acta*, 2018, **260**, 921–931.
287 Z. Xun, Y. Liu, J. Gu, L. Liu and P. Huo, *J. Electrochem. Soc.*, 2019, **166**, A2300–A2312.
288 Y. Mo, W. Meng, Y. Xia and X. Du, *Polymers*, 2019, **11**, 1357.
289 C. Xia, M. Leng, W. Tao, Q. Wang, Y. Gao and Q. Zhang, *J. Mater. Sci.: Mater. Electron.*, 2019, **30**, 4427–4436.
290 Y. Park, H. Choi, D.-G. Lee, M.-C. Kim, N. A. T. Tran, Y. Cho, Y.-W. Lee and J. I. Sohn, *ACS Sustainable Chem. Eng.*, 2020, **8**, 2409–2415.
291 H. Yu, J. Wu, L. Fan, Y. Lin, K. Xu, Z. Tang, C. Cheng, S. Tang, J. Lin, M. Huang and Z. Lan, *J. Power Sources*, 2012, **198**, 402–407.
292 M. Kim, J. Yoo and J. Kim, *Dalton Trans.*, 2017, **46**, 6588–6600.
293 D. Yi ğit and M. Güllü, *J. Mater. Chem. A*, 2017, **5**, 609–618.
294 E. Feng, G. Ma, K. Sun, Q. Yang, H. Peng and Z. Lei, *RSC Adv.*, 2016, **6**, 75896–75904.
295 M. Kim, J. Yoo and J. Kim, *Chem. Eng. J.*, 2017, **324**, 93–103.
296 B. Jinisha, K. M. Anilkumar, M. Manoj, C. M. Ashraf, V. S. Pradeep and S. Jayalekshmi, *J. Solid State Electrochem.*, 2019, **23**, 3343–3353.
297 G. P. Shumakovich, O. V. Morozova, M. E. Khlupova, I. S. Vasil'eva, E. A. Zaitseva and A. I. Yaropolov, *RSC Adv.*, 2017, **7**, 34192–34196.
298 R. Xu, F. Guo, X. Cui, L. Zhang, K. Wang and J. Wei, *J. Mater. Chem. A*, 2015, **3**, 22353–22360.

299 Q.-M. Tu, L.-Q. Fan, F. Pan, J.-L. Huang, Y. Gu, J.-M. Lin, M.-L. Huang, Y.-F. Huang and J.-H. Wu, *Electrochim. Acta*, 2018, **268**, 562–568.
300 X. Li, J. Shao, S.-K. Kim, C. Yao, J. Wang, Y.-R. Miao, Q. Zheng, P. Sun, R. Zhang and P. V. Braun, *Nat. Commun.*, 2018, **9**, 2578.
301 Y. Jiang, C. Zhou and J. Liu, *Energy Storage Mater.*, 2018, **11**, 75–82.
302 K. Sun, E. Feng, G. Zhao, H. Peng, G. Wei, Y. Lv and G. Ma, *ACS Sustainable Chem. Eng.*, 2018, **7**, 165–173.
303 L. Liu, Q. Dou, Y. Sun, Y. Lu, Q. Zhang, J. Meng, X. Zhang, S. Shi and X. Yan, *J. Mater. Chem. A*, 2019, **7**, 20398–20404.
304 Q. Liu, J. Zhou, C. Song, X. Li, Z. Wang, J. Yang, J. Cheng, H. Li and B. Wang, *Energy Storage Mater.*, 2020, **24**, 495–503.
305 R. Na, N. Lu, S. Zhang, G. Huo, Y. Yang, C. Zhang, Y. Mu, Y. Luo and G. Wang, *Electrochim. Acta*, 2018, **290**, 262–272.
306 W. Liu, K. Wang, C. Li, X. Zhang, X. Sun, J. Han, X.-L. Wu, F. Li and Y. Ma, *J. Mater. Chem. A*, 2018, **6**, 24979–24987.
307 X. Zhang, M. Kar, T. C. Mendes, Y. Wu and D. R. MacFarlane, *Adv. Energy Mater.*, 2018, **8**, 1702702.
308 G. Ma, J. Li, K. Sun, H. Peng, J. Mu and Z. Lei, *J. Power Sources*, 2014, **256**, 281–287.
309 M. Kim and J. Kim, *Electrochim. Acta*, 2018, **260**, 921–931.
310 D. D. Potphode, L. Sinha and P. M. Shirage, *Appl. Surf. Sci.*, 2019, **469**, 162–172.
311 K. Wang, X. Zhang, C. Li, H. Zhang, X. Sun, N. Xu and Y. Ma, *J. Mater. Chem. A*, 2014, **2**, 19726–19732.
312 L. Liu, W. Weng, J. Zhang, X. Cheng, N. Liu, J. Yang and X. Ding, *J. Mater. Chem. A*, 2016, **4**, 12981–12986.
313 A. Brandt, S. Pohlmann, A. Varzi, A. Balducci and S. Passerini, *MRS Bull.*, 2013, **38**, 554–559.
314 S. Shahzad, A. Shah, E. Kowsari, F. J. Iftikhar, A. Nawab, B. Piro, M. S. Akhter, U. A Rana and Y. Zou, *Met. Sustainability*, 2019, **3**, 1800023.
315 S. Pan, M. Yao, J. Zhang, B. Li, C. Xing, X. Song, P. Su and H. Zhang, *Front. Chem.*, 2020, **8**, 261.
316 A. J. R. Rennie, N. Sanchez-Ramirez, R. M. Torresi and P. J. Ha, *J. Phys. Chem. Lett.*, 2013, **4**(17), 2970–2974.
317 H. Dai, G. Zhang, D. Rawach, C. Fu, C. Wang, X. Liu, M. Duboi, C. Lai and S. Sun, *Energy Storage Mater.*, 2021, **34**, 320–355.
318 L. Fagiolari, A. Lamberti, J. Amici, C. Francia, S. Bodoardo and F. Bella, *Energy Storage Mater.*, 2022, **51**, 400–434.

